Quantifying the Stimuli of Photorheological Fluids

by

Sarah Woodring Bates

B.S., Cornell University (2007)

Submitted to the Department of Mechanical Engineering
in partial fulfillment of the requirements for the degree of

Master of Science in Mechanical Engineering

at the

MASSACHUSETTS INSTITUTE OF TECHNOLOGY

February 2010

Author .....
Department of Mechanical Engineering
January 18, 2010

Certified by .....
Anette (Peko) Hosoi
Associate Professor
Thesis Supervisor

Certified by .....
Gareth H. McKinley
Professor
Thesis Supervisor

Accepted by .....
David E. Hardt
Chairman, Department Committee on Graduate Theses

Quantifying the Stimuli of Photorheological Fluids

by

Sarah Woodring Bates

Submitted to the Department of Mechanical Engineering
on January 18, 2010, in partial fulfillment of the
requirements for the degree of
Master of Science in Mechanical Engineering

Abstract

We develop a model to predict the dynamics of photorheological fluids and, more generally, photoresponsive fluids for monochromatic and polychromatic light sources. Derived from first principles, the model relates the irradiance of light source to the evolution of the concentration of a photoactive species within a sample. We show that the limiting time scale of the dynamics is the rate of photon delivery from the light source. Therefore, we recommend reporting the spectral irradiance of the light source and molar absorptivity, volume, area of the sample exposed to the beam, and concentration of the photoactive species as a standard minimum set of variables. Using the nondimensionalized time suggested by the model, we compare reaction rates of vastly different materials irradiated by very different light sources.

We validate our model using both published data from literature and our own rheological experiments. These datasets are shown to collapse onto characteristic curves when properly scaled. We extend the model to fluids with multiple photoactive components, so that we may study fluids that have a reversible transition between states accessible by changing the relative spectral irradiance during operation. We show that considering a light source as polychromatic is critical to determining the photostationary mole fraction as well as scaling results between different light sources.

We then use these metrics to determine whether photorheological fluids are appropriate for application onboard a small autonomous robot. We determine that the two candidate photoresponsive fluids, a micellar fluid and a nanoparticle-based fluid, are not appropriate for use in combination with commercial UV LEDs if the speed of transition is a constraint. However, we suggest features of a fluid ideal for this application and illustrate how techniques such as decreasing film thickness are effective in accelerating the reaction only for fluids with high initial absorbances. Finally, we suggest how the model aids research into microstructural dynamics of complex fluids.

Thesis Supervisor: Anette (Peko) Hosoi
Title: Associate Professor

Thesis Supervisor: Gareth H. McKinley
Title: Professor

Acknowledgments

I am so grateful to all those, near and far, who helped me complete this thesis. My advisors have been generous with their time and comments. Professor McKinley, thank you for improving my research while also deepening my ability to do research. Professor Hosoi, thank you for teaching me how to ask succinct research questions and showing me how to fit them within big pictures.

I also appreciate the technical assistance I received from Dr. Kooi at the ISN with determining the spectral power of my sources, and Dr. Vella and Dr. Mace from the Whitesides Group concerning my chemical synthesis quest.

To Team Peko and the NNF, thanks for pointing me in the right direction when I was looking for whatever I couldn't find. Thanks Tony for the many conversations about my favorite equation. I'm so glad that I got to have hot chocolate with Sungyon and do laps around various parts of MIT with Dawn. Randy, Vivek, and Philipp were great tour guides throughout my introduction to rheology. Many thanks to Matt, who found no less than three errant semicolons. I'd also like to acknowledge how much fun it is working with all of the members of the Squishbot team, both at MIT and at Boston Dynamics. Thank you Jeff, Ahmed, and Maria for making Tuesday Teleconferences fun. Also, I am grateful that Nadia is still sharing a desk with me despite the incident with the frogs.

It is with much love that I acknowledge my family. Mom and Dad, thank you for the phone calls, the emails, the visits. Mom, thank you for reminding me that we are very brave, and Dad, for telling me that not all things can be integrated. Abby, you are my sister whom I love and I will always be proud of you.

I also acknowledge the generous support of the Warren M. Rohsenow Fellowship and the DARPA DSO Chemical Robots program.

AMDG

Contents

List of Figures

List of Tables

Chapter 1

Introduction

Photorheological fluids, or fluids that change their flow properties in response to light, are interesting not only academically but also for their potential applications. With the increasing availability of light emitting diodes (LED) at new and smaller wavelengths, photoresponsive materials may make their way into a broad range of devices. This will only happen if researchers, designers, and manufacturers can systematically quantify the energy consumption and transition time of these materials in a variety of environments. In this thesis, we will propose a model describing the time evolution of the response of the material to light. We will see that this is an important step in determining the feasibility of a particular fluid for a specific application.

1.1 Complex Fluids

A fluid is defined as a material in which an applied stress gives rise to a constant strain rate as opposed to a solid where the same stress would lead to a constant strain. A familiar example of this definition is a Newtonian fluid:

$$\sigma = \eta\dot{\gamma} \tag{1.1}$$

1.1.1 Non-Newtonian Fluids

Many fluids can be described with the simple linear relation in 1.1. However, many fluid-like materials do not show this behavior and are therefore termed 'Non-Newtonian'. Non-Newtonian fluids often have a viscosity that depends on the applied stress or strain rate, yield stress fluids are an example of the former and shear thinning and shear thickening fluids of the latter. Yield stress fluids, like toothpaste and shaving cream, behave like solids when stressed below a certain stress, called the yield stress. Shear thinning fluids have a lower viscosity the higher the strain rate applied and vice versa for shear thickening fluids. Non-Newtonian fluids can also fall on the visco-elastic spectrum with some part of their stress response being related to the strain applied rather than the strain rate. Other complex fluids include thixotropic fluids whose microstructure changes over time, leading to a history dependent viscosity. These fluids offer a glimpse into the rich behavior of fluids beyond the simple behavior of the Newtonian fluid.

1.1.2 Active Fluids

In all of the examples above, the rheological properties of the fluid are fixed to the relevant dynamic conditions. We define active fluids as those fluids whose rheological properties are dependent on some external applied field. With these fluids, the experimentalist has more control over the response of the fluid even if the dynamic conditions like strain rate or applied stress are fixed. In this way, the fluid becomes a more 'engineerable' material for a given application.

These active fluids have found their way into many viable commercial products, such as hot glue guns. Car suspensions and clutches also take advantage of magnetorheological (MR) fluids and electroheological (ER) fluids. Application of a magnetic field or an electric field respectively causes the small particles suspended in these fluids to align and give structure to the fluid ([43], [45]). At high applied field strengths, both ER fluids and MR fluids behave more like solids below a yield stress. Thermorheological fluids, such as solder and hot glue, have a low melting temperature. When

heated, the internal temperature is raised and the viscosity of the fluid changes drastically. Another class of active fluid, photorheological (PR) fluids undergo a chemical reaction, upon the application of a particular spectrum of light, which changes the fluid on a molecular level leading to new rheological properties.

While these fluids all possess the same desirable nature, in situ tunable rheological properties, they are so different phenomenologically that they are difficult to compare for design purposes. Not only are the resulting rheological properties hard to compare (such as a change in yield stress versus a change in viscosity), but the required stimuli themselves are in distinct physical domains. If we consider designing a mechanism or sensor using an active fluid, then it may be that we wish to find a fluid that maximizes the difference between the two rheological states. Fig. 1-1 illustrates the magnitude of property changes for a variety of active materials.

Table 1.1: References for Figure 1-1

#	Reference
1	Tomatsu et al. [54]
2	Botella et al. [5]
3,4 8 -10,16	Ewoldt [44]
5	Haines et al. [24]
6	Wen et al. [60]
7	Alvarez-Lorenzo et al. [2]
11	MRF-140CG [14]
12	MRF-122EG[13]
13	Schmidt et al. [49]
14	Matsumoto et al. [37]
15	Steeman et al. [50]
17	Khan et al. [31]
18	Deshmukh et al. [17]
19	Ketner et al. [30]
20	Sakai et al. [46]
21	Dasgupta et al.[15]
22	Espin et al. [20]
23	Naciri et al. [39]
24,25	Verney et al. [56]
26,29	Cook et al. [12]
27,28	Jadzyn et al. [26]

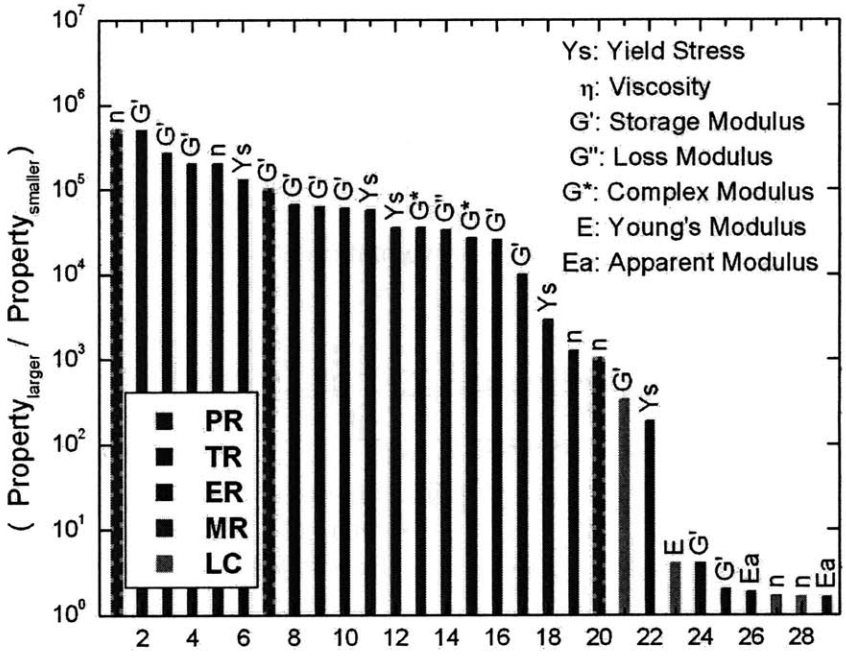

Figure 1-1: Active fluids span a range of changing material properties over many orders of magnitude. While photorheological fluids as a class of materials are not usually reversible, the three outlined in dotted green are reversible. Liquid Crystal (LC) materials are included for comparison. The references for these materials are included in Table 1.1.

There are many other relevant design considerations that are not captured by this figure. For instance, some materials go from a property possessing a smaller value to possessing a larger value with an applied field. Others show the reverse behavior. We consider the former a 'positive gain' material and the latter a 'negative gain' material. Choosing one or the other is an important application dependent decision. For instance, for a glue whose purpose it is to hold an object in place, we would want its resting state (zero field) to have a high yield stress. Only when we wish to move the object, do we want to apply a field and lower the yield stress. Therefore a negative gain material is most appropriate, so that we do not spend energy on maintaining the base state. This definition also assumes that we must continually apply energy to achieve one of the two rheological states. While this is true for the simplest mechanisms with TR, ER, or MR fluids (though permanent magnets [22], and capacitive circuits expand the stimuli possibilities), it is often not true for PR fluid.

1.1.3 Photorheological Fluids

Photorheological fluids change on a chemical level in response to light stimuli. The majority of PR fluids then stay in this new state for a long period of time until they relax to their more energetically favorable states (if at all). In this way, they act more like a switch than the other materials. If the application constrains the energy available, then this switching ability may be desirable. This is only desirable if the energy input required to switch is less than the energy required for a comparable material during the application lifetime. Upon first evaluation, PR fluids seem to require large amounts of power over large time scales to switch. However, as will be detailed in this thesis, the limited information that is presented in literature (often the wattage of a laboratory lamp) is not detailed enough to do an energy calculation that reflects realistic energy consumption. Determining what is a complete description of the light source will become a focus of this thesis.

1.2 Robotic Application

As we have mentioned, the evaluation of these fluids can be strongly application-dependent. Our application is in the field of robotics. Fluids are not often featured in mechanisms beyond fueling, cleaning or lubricating roles with the exception of hydraulic and underwater robots. As an active component, they find themselves under the same expectations as other components such as being task-appropriate, energy-efficient, lightweight, and robust. In the developing field of "Soft Robotics," where robots morph and deform, we imagine less traditional materials like foams and composites will be valued for their low moduli. If fluids could be manipulated successfully they also would lend themselves well to a robot which needed to be able to slither through tight spaces. Active fluids could play an important role in this class of robots.

1.2.1 SQUISHBot: a Soft Robot

Our team has been developing a robot, SQUISHBot, in response to the Defense Advanced Research Projects Agency (DARPA) ChemBot call for proposals [42]. Ideally, the ChemBot, approximately the size (but not necessarily the form-factor) of a regulation softball should demonstrate the ability to:

- travel a distance of 5 meters at a speed of 0.25 meters/minute;
- achieve a 10-fold reduction in its largest dimension; and
- traverse through a 1 cm opening of arbitrary geometry and reconstitute its original size and shape, in 15 seconds.

Obviously these requirements necessitate the development of a novel soft robot.

SQUISHBot is in part a next generation version of the Robosnail, first developed by Brian Chan [7]. This robot mimics the adhesive locomotion style of a snail with rigid sliders and a specially engineered yield stress fluid or slime [21]. Our team plans to incorporate the unique locomotion style of the Robosnail with tunable stiff-

ness composites to achieve deformability. Both this locomotion style and composite approach provide opportunities to incorporate active fluids.

1.2.2 Application Opportunities for Responsive Fluids

The slime played a central role in past instantiations of the Robosnail [8]. A large yield stress, while ideal for locomoting heavy robots up walls, would require a large pumping force and a large pump. In the past, the Robosnail did not have the need to be autonomous and so the slime was painted onto the surface by hand before placing the Robosnail on top of it. As the ChemBot must be autonomous, the slime has a new requirement of being pumpable. Unfortunately, the very property that would be optimal for locomotion is decidedly sub optimal for pumping. An active fluid with a switchable yield stress would be ideal as the fluid could be pumped when the slime has a low yield stress and used as an adhesive when the yield stress is large.

In tunable stiffness beams, the fluid plays a more structural role than in the active slime. SQUISHBot employs passively compliant of foams in combination with a single actuator, a spooler motor [10]. The foam contains an active fluid such as wax which either melts and leads to a compliant structure, or which hardens and maintains its shape upon loading [9].

1.2.3 Requirements and Relevant Characterization of Fluids

Both of these applications would benefit from a fluid with a large difference between rheological states. It would also be desirable for the fluids to move reversibly between states, although the slime application allows for a disposable fluid as a lesser substitute. Of most relevance are the constraints placed on the energy consumed by, and the cycle time of, these fluids. The velocity of the robot may well be limited by the timescale of these fluids moving between states. If the cycle time of the fluid is longer than a couple of minutes, the use of that fluid quickly becomes impractical. Related to this, the energy required to stimulate these active fluids must be small enough to allow for continued operation of the robot for the length of its required run. SQUISH-

Bot is a small battery powered robot. Therefore quantifying the energy requirements of these fluids is a primary task when determining the feasibility of using a specific fluid onboard a robot.

1.3 Photorheological Fluids

Photorheological fluids are used in a narrower set of applications than the other classes of active fluids such as UV curable glues. Despite this, they have definite advantages. While ER and MR fluids must often be sandwiched between two plates, PR fluids can be switched by a light source at a single location, possibly even physically removed from the fluid. PR and TR fluids are also generally isotropic. Due to the chemical nature of their property change, they can have the largest property changes that remain after the stimuli is removed as seen in Fig. 1-1. Long switching times and large energy demands may be prohibitive drawbacks. These disadvantages remain largely uncharacterized.

1.4 Problem Statement

In this thesis we will seek to quantify the time and energy required for a photoresponsive fluid to switch between two states. We will then apply this characterization to determine whether a few selected fluids are appropriate for robotic application given available light sources.

1.5 Thesis Outline

In chapter two, we will look at how molecules interact and absorb light. In chapter three, we will look at how quantifying the number of photons can be used as a metric to characterize energy consumption, light sources, reaction rates, and design efficiencies. In chapter four, we develop a framework for relating the number of photons to these quantities through fundamental relationships and experimentally measurable

quantities. In chapter five, we expand this model to analyze kinetics for situations involving monochromatic or polychromatic sources in conjunction with reversible or irreversible fluids. We also compare the models to data published in literature. In chapter six, we select three candidate materials for robotic application. In chapter seven, we describe a set of rheological experiments performed while irradiating the material with a polychromatic light source and discuss the results. In chapter eight, we conclude with a brief discussion about the feasibility of using these fluids in conjunction with commercially available UV LEDs onboard an autonomous robot.

Table 1.2: Frequently used variables

Variable	Value or Units	Definition
c	$3.00 \times 10^8 \frac{\text{m}}{\text{s}}$	speed of light in a vacuum
h	6.26×10^{-34} J s	Planck's constant
N_a	$6.022 \times 10^{23} \frac{1}{\text{mol}}$	Avagadro's Number
λ	m	wavelength of light
$I, I_i, I(\lambda)$	$\frac{\text{W}}{\text{sr nm}}$	radiant intensity prior to sample
I_t	$\frac{\text{W}}{\text{sr nm}}$	transmitted radiant intensity after sample
$I_{i\lambda}$	$\frac{\text{W}}{\text{sr}}$	incident radiant intensity of monochromatic light λ
$I_{t\lambda}$	$\frac{\text{W}}{\text{sr}}$	transmitted radiant intensity of monochromatic light λ
$I_{a\lambda}$	$\frac{\text{W}}{\text{sr}}$	absorbed radiant intensity of monochromatic light λ
$Ir, Ir_i, Ir(\lambda)$	$\frac{\text{W}}{\text{m}^2\text{nm}}$	spectral irradiance over an area prior to sample
$Ir_{i\lambda}$	$\frac{\text{W}}{\text{m}^2}$	incident irradiance of monochromatic light λ
$N_{photons}$	[ ]	number of photons
$N_{a\lambda}$	[ ]	number of photons of wavelengthλ absorbed
$N_{m\lambda}$	[ ]	number of molecules absorbing photons of wavelengthλ
E	J	energy
$E_{a\lambda}$	J	energy of absorbed photons of wavelength λ
$A(\lambda)$	[ ]	absorbance
A_λ	[ ]	absorbance given the incident light is wavelength λ
$\Phi, \Phi(\lambda)$	[ ]	quantum efficiency of material
Φ_λ	[ ]	quantum efficiency at wavelength λ
$\epsilon, \epsilon_X, \epsilon(\lambda)$	$\frac{\text{L}}{\text{mol cm}}$	molar absorptivity of material X
ϵ_λ	$\frac{\text{L}}{\text{mol cm}}$	molar absorptivity at wavelength λ
η	Pa s	viscosity
η_0	Pa s	zero shear rate viscosity
G'	Pa	storage modulus
G''	Pa	loss modulus
l	m	path length through a sample
Ω	sr	solid angle of beam
$Area_i$, A_i	m^2	incident area of beam
V	L	volume of a sample
t	s	time
t_{exp}	s	experimental time
τ	s	duration
$[S]$	$\frac{\text{mol}}{\text{L}}$	concentration of photoactive component
$[X]$	$\frac{\text{mol}}{\text{L}}$	concentration of X
$[X_0]$	$\frac{\text{mol}}{\text{L}}$	initial concentration of X
ϕ	[ ]	molar fraction
ω	$\frac{\text{rad}}{\text{s}}$	frequency of oscillation
$\dot{\gamma}$	$\frac{1}{\text{s}}$	strain rate

Chapter 2

Photon to Isomerization

In this chapter we describe the mechanisms behind photorheological fluids starting with how they absorb light. Absorption is a key step in stimulating photorheological fluids, and describing this step will lay the ground work for developing a metric that is useful for engineers and acceptable to chemists.

There are two different perspectives of importance when evaluating the stimuli of photorheological fluids. As an end user, the robotocist is interested in power requirements of the stimuli, time scales associated with the transition of states, material properties, and the lifetime of each state. While maximizing lifetimes and material advantages is a concern, he is probably interested in minimizing the transition speed and the power input to the lamp. To do this, the robotocist must match the light spectrum from a lamp to the spectrum that "activates" the fluid. For all intents and purposes, however, the robotocist wishes to treat the fluid as a black box.

The chemist however has a perspective informed by scientific inquiry rather than utility. The chemist seeks a deep understanding of the physics and chemistries of reaction and has already defined and characterized certain aspects of this process. However, these definitions can be unwieldy and often far removed from bulk characterizations useful to the engineer.

One of the goals of this thesis is to provide the engineer with the tools required to design with these sophisticated fluids. The tools however must be consistent with accepted chemistry paradigms. This criterion has the advantage of providing a frame-

work such that experiments in one field can be used and compared in another field.

Even though our application demands an engineering perspective, it may be easiest to start "at the beginning" with a chemical picture of the major actors in this reaction. All photorheological fluids are stimulated by light, so we begin with the nature of light.

2.1 Nature of Light

Modern conceptions of light include both the wave-like nature and particle-like nature of light. Einstein proposed this picture in support of Planck's suggestion that the energy of a light wave was quantized [19]. Light can be described as both having a wavelength (a wave property) and can be related to momentum through Planck's constant (a fundamental constant related to a particle or quantum phenomena). This special light particle, or photon, has a quantized energy:

$$E = \frac{hc}{\lambda} \tag{2.1}$$

where E is the energy of a photon, h is Planck's constant, c is the speed of light, and λ is the wavelength of the photon. Turro et al. [55] describes how the wave nature and the particle nature relate:

> "In this model, light is part of the electromagnetic field that is spread out and fills the entire universe; the wave can be considered to propagate through the universe "at the speed of light." When light is absorbed by a molecule, the "spread out" wave is suddenly "localized" in the small space occupied by the molecule."

Because we are interested both in emission and absorption, we encounter both natures in our study. As Turro summarizes, "Thus a photon behaves more like a wave when it is not strongly interacting with matter and more like a particle when it is strongly interacting with matter." When describing chemical reactions, this particle view of light will prove to be useful.

2.2 Interaction of Light with a Molecule

Since we are interested in the response of the fluid to light, a closer look at how light interacts with a molecule is warranted. To a molecule, the light wave is mostly an oscillating electromagnetic field that interacts with the electrons of a molecule.

$$F = eE + \frac{e\,(Hv)}{c} \tag{2.2}$$

Here F is the total force exerted on an electron, eE is the electrical force, $\frac{e(Hv)}{c}$ is the magnetic force, v is the velocity of an electron and c is the speed of light. Because the maximum speed of an electron is small compared to the speed of light, the magnetic component of the total force is small compared to the electrical component. The total field interacts with the molecule's electrons by exchanging energy through resonance.

For this process to happen, three conditions must be met:

1. $\delta E = h\nu$, the energy required for transition between the ground and promoted orbital must be equal to the energy of the incoming photon. This is a statement of energy conservation. It can be restated as Einstein's resonance condition: during a transition, the electric dipole moment of a cloud will resonate at frequency $\nu = \frac{E_1 - E_2}{h}$. This must equal the frequency of incoming electromagnetic radiation for a transition to occur.

2. Momentum must be conserved. There must be an exact match between the angular momentum gained or lost (captured by the creation or destruction of a node in the electron cloud, see Fig. 2-1) and the angular momentum of the photon.

3. The transition dipole moment created by the interaction of the electron with the electromagnetic field must be finite.

If these conditions are satisfied, the oscillating electrical field will reshape the electron distribution and cause it to oscillate between asymmetric shapes as the electron cloud is alternatively attracted and repelled by the wave. The nucleus does not resonate

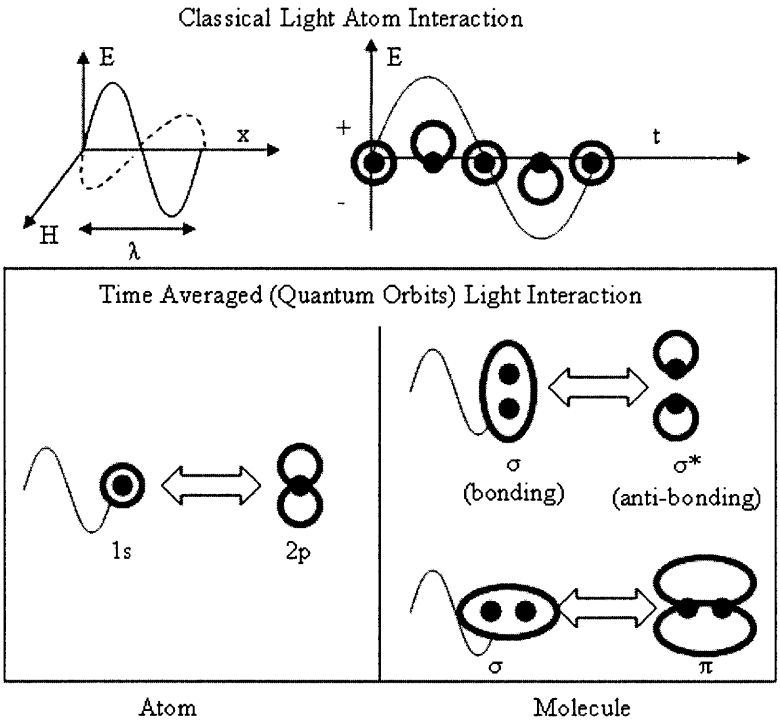

Figure 2-1: Illustration of classical and quantum views of the interaction of light with atoms and molecules. A photon's oscillating electric field interacts with the electrons in a molecule. The electron cloud oscillates between asymmetric shapes and, on average, looks like a promoted orbital. Here a He atom's 1s orbital is excited into the 2p orbital. The analogous molecular σ orbital being promoted to either a $\sigma*$ or π orbital is also shown.

with the same frequency as the electron cloud. The time average of this oscillation about the nucleus looks like a promoted orbital. Fig 2-1 details this process for a single He atom and for a simple molecule. For each photon absorbed by a material only one molecule is activated, a restatement of the resonance condition known as the Stark-Eistein law. In rare cases two photons can be absorbed to activate one molecule, however this occurs mostly in highly controlled laboratory settings.

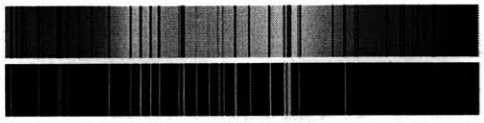

Figure 2-2: A representation of the absorption and emission spectrum of Mercury. The resonance condition implies that the absorption spectrum is the photonegative of the emission spectrum [41].

2.3 Absorption

Now that we understand the theoretical picture of light absorption, we discuss how to quantify this phenomenon in experiments. An experiment measuring the optical density of a sample is a standard way of measuring the absorbance of the sample. The intensity of the light falling on a sample and the intensity of the beam transmitted through the sample are measured. The log of this ratio is termed the optical density. The higher this number, the larger the amount of incident light absorbed. If we divide this number by the path length of the light, i.e. the thickness of the sample, and the molar concentration of absorbing molecules, we find the molar absorptivity. This is a fundamental molecular property and has units of area per mole (often reported $\frac{L}{mol\ cm}$). These relationships are characterized by the Beer-Lambert law in the following equation:

$$\epsilon = \frac{log(\frac{I_i}{I_t})}{l[S]} \tag{2.3}$$

In Eq. (2.3), [S] is the concentration of the absorbing species, the molar absorptivity is ϵ (also known as the molar extinction coefficient), the thickness of the sample is l, the incident intensity is I_i and I_t is the transmitted intensity.

One of the implications of this molecular picture of absorption is that the absorption must be wavelength (or frequency) dependent in order to satisfy the resonance condition. To communicate which wavelengths the molecule absorbs, we can plot the molar extinction coefficient (or its log, as the value varies widely) as a function of wavelength. This type of plot is called an absorption spectrum.

Given the resonance condition's limit on absorbable frequencies we would expect that the absorbance spectrum would only have a few fairly sharp peaks corresponding

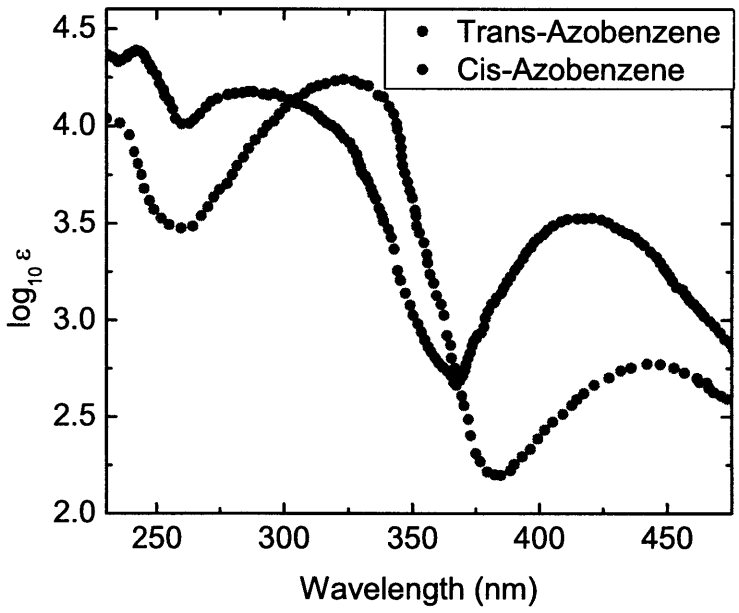

Figure 2-3: The absorption spectrum of the trans- and cis- isomers of Azobenzene. Note that the trans- isomer is more absorptive in the 300-350 nm region, where as the cis-azobenzene is more absorptive in the other wavelengths [53].

to the allowed wavelengths. This is the case for atomic spectra as the energy states are discrete. Fig. 2-2 illustrates the absorption spectrum of Mercury. However, the molecular absorption spectra have broader absorbance bands because of the many allowed rotations, vibrations, and collisions that can store energy. An absorption spectrum of a typical photorwsponsive compound, Azobenzene, is given in Fig. 2-3.

2.3.1 Result of Absorption

The first law of photochemistry, or the Grotthus-Draper law, states that a photon must be absorbed to cause a photochemical change. With this extra amount of energy, a variety of things can happen. The molecule may be more reactive or the new electron distribution can allow a trans-cis isomerization to occur. This step in the process can be characterized by a rate constant, describing the primary process or any secondary processes occurring if present. There are a variety of photomechanisms

each specific to the molecule, and reactants.

Not every absorbed photon leads to a reaction and is subsequently emitted. This phenomena can be quantified with the quantum efficiency (Φ) of the reaction. The quantum efficiency represents the probability that an absorbed photon of a particular wavelength effects a change in the molecule.

The following figure illustrates a few molecules and their uses before and after transition. Spiropyrans(a) are an example of a class of photochemicals called chromophores. These molecules can be found in automatically tinting indoor/outdoor glasses. This spiropyran can selectively bind Cu^{2+} or Co^{2+} when irradiated by visible or ultra violet light. Diarylethenes (b) can used as electrical switches and photocatalysts (d) can be used to break down volatile organic chemicals, change surface tensions, and alter a solution's pH. Of particular interest for our application are molecules that affect mechanical properties such as moduli, creeping behavior, and bulk deformation. This can be achieved with molecules that cleave crosslinks such as some photoinitiators (e), and molecules that reassemble into different configurations after having a conformal change in molecular geometry (c) typical with some photoisomerizations.

The variety of mechanisms provides a challenge for bridging the gap between engineer and chemist. Each one has a unique characterization, yet the engineer prefers to compare a bulk property. Individual chemical mechanisms are beyond the scope of this document and will be omitted in favor of a black box approach. To ensure validity, we will examine the mechanisms for select candidate fluids explored in a later section. We will use the fact that these diverse mechanisms all absorb photons to quantify whether a light source is appropriate for a fluid and to monitor the progress of a reaction. The fact that we can measure how easily a material absorbs photons leads to the success of the experimental framework suggested.

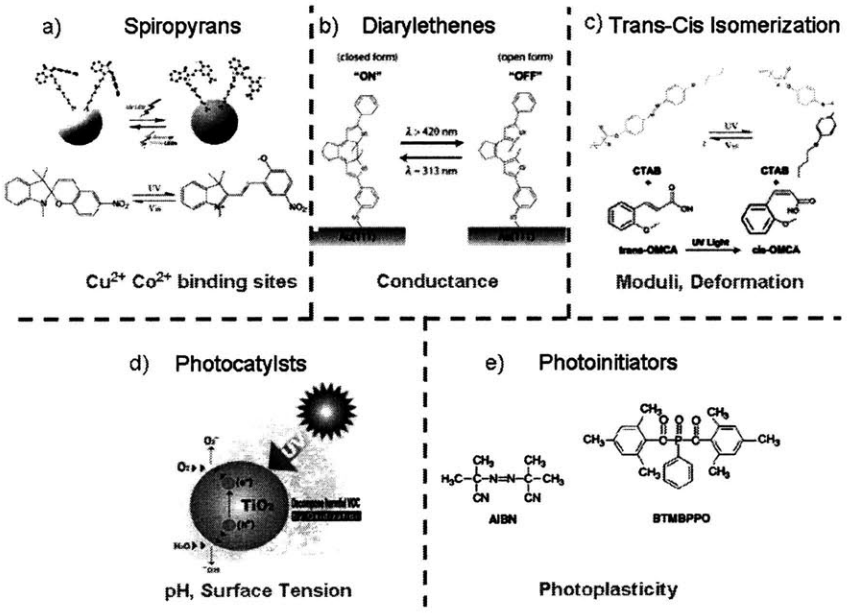

Figure 2-4: Five typical molecules or mechanisms, spiropyrans [48], [6], diarylethenes [29], photoisomerization [57] [30], photocatalysts [52] [23], and photoinitiators [12], are highlighted in this figure. Photomechanisms are diverse leading to a broad list of potential practical applications.

Chapter 3

Light as a Massless Reagent

Since cataloging all of the molecules and their reactions would be difficult even for an experienced photochemist, we take a different approach. All photoreactions consume a "massless reagent" – light. We wish to pick a metric that we can report that would allow an engineering comparison of the different photomechanisms for design purposes. Each mechanism, however, requires a different wavelength of light. We could report the most effective wavelength of light, the wavelengths used in experiment, the emission profile, the quantum efficiency, the absorbance spectrum, or a number of other quantities which are wavelength dependent. All of these variables characterize some part of the molecule or reaction, an ideal experiment, or a combination of both. When comparing stimuli of fairly different natures previously, we discussed active fluids in terms of an energy metric, specifically the energy consumption of each class of fluids. We will take the same approach here with the expectation that this will be easier as energy is directly related to the frequency of light and indirectly to the intensity of light. There are many energies available as metric candidates. We could report the energy per photon, the total energy absorbed by the material, the energy associated with the flux of photons from the beam, or the energy required to power the lamp. In this chapter, we lay the chemical ground work for the decision to use a metric related to the total energy absorbed by the material, a quantity that depends on the matching of the emission spectrum of the light source with the absorbance spectrum of the material.

3.1 Energy vs. Intensity: A Chemist's Perspective

The energy absorbed by a material as a metric is appealing from both the chemist's and engineer's perspective. For the engineer, the energy absorbed is closely related to the energy delivered by an external source. For the chemist, the energy absorbed can be used to count the number of absorbed photons :

$$N_{photons} = \frac{E_{Absorbed}}{\frac{hc}{\lambda_{absorbed}}} \tag{3.1}$$

The number of photons ($N_{photons}$) is proportional to the energy absorbed ($E_{absorbed}$) by the ratio of the wavelength of the photons (λ) to Planck's constant h and the speed of light (c). This ratio is the energy of a single photon.

While a chemist would argue that the most important energy is the energy per photon, from the argument above, we can see the experimental relevance of the absorbed energy. By focusing on the absorbed energy rather than total energy available, we avoid the ambiguity associated with the fact that red light may deliver to atoms which select photons by wavelength less "useful" energy than a less intense blue light despite being more energetic than blue light. After the historical misconceptions about the energy of a beam (intensity) versus the energy in a single photon, descriptions of the energy delivered by a beam have been de-emphasized in literature. However, a beam delivers a finite number of photons in finite time; a chemically relevant (and countable number) that impacts rates of reaction.

3.2 Reaction Rates

One mole of a single wavelength of photons is called an 'einstein' and carries varying amounts of energy. If these photons correspond to a low frequency as in the radio frequency (RF) range with wavelength 1 meter, the einstein carries 4 picojoules; if they correspond to a ultraviolet (UV) range wave with a 365 nm wavelength, 32 kilojoules. Experimental equipment can deliver photons at vastly different rates even for a given wavelength of light. A UV laser that delivers 5 Watts of 365 nm light

would take almost 2 hours to deliver an einstein of photons to the surface of the sample. UV LEDs, a recent technological advance, have a typical power output of 50μW, requiring over 20 years to deliver the same einstein of photons. Clearly this has chemical and engineering repercussions. In fact, this delivery mechanism generally represents the limiting timescale of an experimental setup involving a photoreaction.

The current practice of reporting times of transition between observable states is misleading if the power and the spectrum of the lamp are not also submitted. This follows from Stark-Einstein's law requiring one photon for each absorbing molecule. Therefore we can consider photons to be a limiting reactant. All of the other relevant time scales are significantly smaller than the hours and days represented by the delivery timescale. Fig 3-1 summarizes the relative event rates. The time scale governing absorption is less than 10 microseconds. The lifetime of a electronically excited organic molecule is bounded by fluorescence at 10^{-9} seconds and 10^{-5} seconds if it is a singlet state (spin forbidden transitions can be up to 10 seconds). Even in self assembling systems where active molecules must diffuse and assemble, the time constants related to diffusion (3ms) and assembly (hours) are much less than 20 years. The rate of reactions reported in literature would be highly dependent on the rate of photons delivered to the sample and subsequently absorbed. Therefore, there is a need for useful reporting standards for light sources.

3.3 Current Descriptions of Light Source

Scientists report experimentally accessible descriptions of their light sources. These descriptions are not standardized and provide scattered information about the light source. Examples of light source descriptions from literature and industry are provided in Table 3.1. While each paper has its own goal, scientists usually strive to provide complete descriptions of their apparatus so that future scientists may use the same data for related but different purposes. These scientists must be guided by a combination of importance of the description and experimental ease of obtaining that description, whether measured by cost, time, or specialized instruments required.

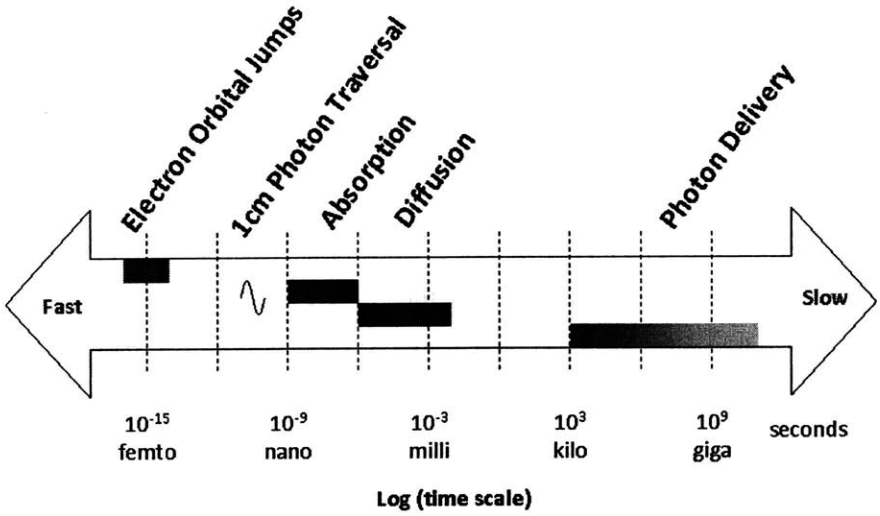

Figure 3-1: Time scales associated with photoreactions span many orders of magnitude. Note that the experimental task of delivering enough photons for a given reaction is often the limiting bottleneck. This figure is adapted from [55].

Therefore, sympathizing with this tradeoff, we wish to find a description of the light source that not only satisfies chemist and engineer but can also be attained with minimal additional effort compared to what is currently reported.

As we have seen from our chemical picture tour, what matters about the lamp is how many of the most absorbable photons can reach the sample. None of the descriptions in Table 3.1 summarizing published descriptions of optical setups can be used to recreate this metric. The bulb wattage is irrelevant except as a ballpark measure of relative intensity between laboratories. Both the lamp element and the wavelength range hint at the emission spectrum present at the sample, but are usually presented in a way which obscures the precise relative intensities. The irradiance and duration of cure tell us how strong and how long the cure was, while the experimental path length acknowledges an uncollimated light source. Unfortunately, the community has not captured a relevant metric with any of these descriptions.

	Bulb Wattage	Type of Lamp	Wavelength range	Irradiance	Duration of Cure	Path Length
Deshmukh et al.		✓	✓	✓	✓	
Ketner et al.	✓	✓	✓		✓	
Sakai et al.		✓	✓		✓	
Tomatsu et al.	✓	✓	✓			✓
Yan et al.	✓	✓			✓	
3M LC-1222 adhesive			✓		✓	

Table 3.1: Descriptions of optical setups are not standardized and vary between authors. This table presents five typical optical setup descriptions from literature, [17], [30], [46], [54], [61], and one industry data sheet, [1].

3.4 Quantifying Absorbable Energy Leads to Better Communication

Here we present absorbable energy as a standardizing characterization of a photon source. As mentioned previously we can obtain the number of photons of a given wavelength present in a beam. This holds for both monochromatic and polychromatic light sources as we can separate out the energy contributions from each wavelength. To do this, we must know the spectral composition of the beam. Fortunately, we can obtain the distribution of wavelengths of a beam with a spectrometer, or from the manufacturer. If we measure the total power (J/s) of the beam with a radiometer, we can now determine how many photons within a range of wavelengths are reaching the sample per second. The irradiance must be measured at the sample for incoherent sources. Alternatively, the path length can be used to calculate the incident energy on the sample using energy conservation. The initial intensity I_0 measured at some small distance from the source, lessens so that at some farther distance (r) the intensity has dropped to I;

$$\frac{I_0}{r_0} = \frac{I}{r} \tag{3.2}$$

To duplicate experiments for a given material, all of the variables put forward so far

would have to be replicated. If a lab cannot duplicate both the relative energies and distribution in wavelength of the source it can use the absorbing materials as reliable filters to compare results. When filters are used, the transmission can be calculated by convolving the filter specs with the measured emission spectrum. As we have seen, materials accept only very specific photons based on their absorbance spectrum. We can apply this absorbing material to our emission spectrum in the same fashion as with filters and calculate the delivered absorbable energy. This is now a single number that any scientist with the absorbance spectrum of the material can use to calculate the number of photons actually delivered. Any previously reported rates can be scaled with the size of the lamp and a radiometer easily recalibrates the metric during experimental testing. We can even compare these rates to other experiments with different photochemicals involved as desired by an engineer or designer. Engineers can then quantify the design tradeoffs associated with using different lamps with respect to rates of reaction, energy consumption, and source suitability for a particular material.

To summarize, where before it was a challenge to make meaningful comparisons outside of a single paper, we can now potentially compare rates of response and material behavior between experimental setups, cure conditions involving high and low power lamps, and even between different materials if we quantify the absorbed energy during our experiments.

3.4.1 Total Effective Dosage Model

The total absorbable dosage metric as a reporting metric for scaling light sources has been suggested in the literature [35]. In this and other studies, Martin uses this "total effective dosage model" to look at polymer degradation from the sun [34]. By using the total effective dosage model to appropriately scale his results with the intensity of his equipment, he shortens his trial time.

$$D_{total}(t) = \int_0^{\tau} \int_{\lambda_{min}}^{\lambda_{max}} E_0(\lambda, t)(1 - 10^{-A(\lambda,t)})\Phi(\lambda)d\lambda \; dt \tag{3.3}$$

Martin defines in [35] λ_{min} and λ_{max} as the minimum and maximum photolytically

effective wavelengths (units: nm), A(λ,t)as the absorbance of the sample at specified UV-visible wavelength and at time t, (units: dimensionless), $E_0(\lambda, t)$ as the incident spectral UV-visible radiation dose to which the polymeric material is exposed to at time t (units: J cm^{-2}) and $\phi(\lambda)$ as the spectral quantum yield, the damage at wavelength λ relative to a reference wavelength (dimensionless).

The total effective dosage,D_{total}, is defined contradictorily as both the total number of absorbed photons that contribute to the photodegradation of a material during an exposure period and as having units of Joules. This in addition to Eq. 3.3 being dimensionally inconsistent with either definition leads us to define our own model closely related to the one put forward by Martin et al.

$$\frac{E_A}{Area_i} = \int_{\lambda_{min}}^{\lambda_{max}} \int_0^{\tau} Ir_i(\lambda, t)(1 - 10^{-A(\lambda,t)})\Phi(\lambda)dt \; d\lambda \tag{3.4}$$

In our model, Eq. (3.4), $\frac{E_A}{Area_i}$ is the energy absorbed by the sample per unit area and we include Ir_i, the spectral irradiance hitting the sample in $\frac{\mathrm{W}}{\mathrm{cm}^2 \ \mathrm{nm}}$, instead of the radiation dose E_0. We will also expand this model to find the total number of absorbed photons. Because the Martin's definition is different than the one we propose, we spend the next chapter deriving the proposed model and accompanying metric.

Similar work employing dosage models has been successfully applied in photometry, radiometry, and nuclear science. A table of the units (Fig. 3-2) is included to define terms that may differ across fields. In this chapter we have suggested that the field is in need of a characterization for the stimuli of photorheological fluids and have suggested that a dosage metric founded on the absorption of light might be relevant.

Unit	Meaning	SI Unit	Notes
Einstein	Moles of Photons		
Radiant Energy	Energy	Joules (J)	
Radiant Power	Energy per time	Watts (W)	
Radiant Intensity	Power per Solid Angle	$W \cdot sr^{-1}$	
Irradiance	Power per Area	$W \cdot m^{-2}$	Incident on a Surface
Radiance	Power per Area per Solid Angle	$W \cdot sr^{-1} \cdot m^{-2}$	Emerging from surface
Radiant Emittance	Power per Area	$W \cdot m^{-2}$	Emitted from surface
Spectral Irradiance	Power per Area per Wavelength	$W \cdot m^{-2} \cdot nm^{-1}$	
Spectral Radiance	Radiance per Wavelength	$W \cdot sr^{-1} \cdot m^{-2} \cdot nm^{-1}$	
Power Spectrum	Power per Wavelength	$W \cdot nm^{-1}$	

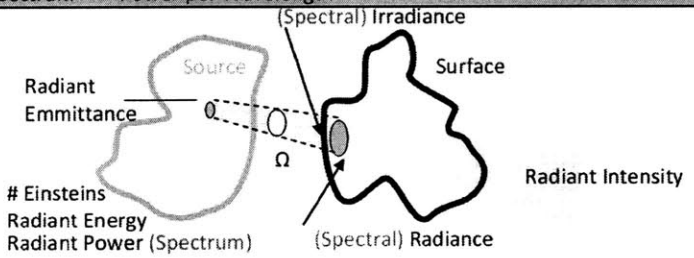

Figure 3-2: The study of light is at the heart of many disciplines including radiometry, astronomy, and spectrometry. This chart summarizes the definitions used in this document.

Chapter 4

Quantifying Photon Delivery in a Photochemical Reaction

In the following chapter we derive from first principles how measurable properties of a reaction (in the most general case, the concentration of a reactant of a reactant) are related to the photon source. As a result of our derivation we see that we can predict how our reaction will vary over a range of experimental conditions including the lamp irradiance, the initial concentration, and material properties.

4.1 Monochromatic Source

Let us return to the experimental embodiment of the Beer-Lambert Law which relates two measurable properties, radiant intensity and transmitted radiant intensity, to the absorbance or optical density of a sample:

$$A_\lambda = log_{10}\frac{I_{i\lambda}}{I_{t\lambda}}. \tag{4.1}$$

The radiant intensity, $I_{i\lambda}$, is incident on the surface from a monochromatic beam of wavelength λ, $I_{t\lambda}$ is the radiant intensity of a monochromatic beam of wavelength λ transmitted through the sample, and A_λ is the absorbance for a particular wavelength under experimental conditions. In most disciplines, the logarithm in the Beer-

Lambert law is base e. However in chemistry, for liquids and solids it is common to use base 10, which we adopt here. The absorbance is a combination of material properties, composition of the sample, and experimental parameters as previously discussed and is defined as

$$A_\lambda = \epsilon_\lambda l[S]. \tag{4.2}$$

Here ϵ_λ is the molar absorptivity for a particular wavelength of the material, $[S]$ is the concentration of the absorbing species, and l is the thickness of the sample.

Barring reflectance, we can rewrite Eq. (4.1) as a statement of energy conversion,

$$I_{i\lambda} - I_{t\lambda} = I_{a\lambda}. \tag{4.3}$$

The radiant intensity of a monochromatic beam of wavelength λ absorbed by the sample is $I_{a\lambda}$. While the incident and transmitted radiant intensities can be measured, the chemical reaction is related to the number of photons absorbed. This quantitative is captured by the absorbed radiant intensity given by Eq. (4.3).

We can solve for the ratio of absorbed radiant intensity to incident radiant intensity if we know the absorbance corresponding to our experimental setup. The absorbance of a sample is often measured by a UV-Vis spectrometer, which measures the absorbance through the Beer-lambert law. Combining Eq.(4.1) and Eq.(4.3), we find

$$\frac{I_{a\lambda}}{I_{i\lambda}} = 1 - 10^{-A_\lambda}. \tag{4.4}$$

If the sample thickness is small and the solid angle of the beam is small we can assume that the areas defined by the beam before and after the sample are approximately equal. This allows us to write the ratio of radiant intensities in Eq. (4.4) as a ratio of irradiances:

$$\frac{Ir_{a\lambda}}{Ir_{i\lambda}} = 1 - 10^{-A_\lambda}, \tag{4.5}$$

$$\text{if } 1 \ll 2l\sqrt{\frac{\Omega}{Area_i}}. \tag{4.6}$$

The solid angle describing the beam is Ω; the incident area defined by the beam's cross sectional area on an incident surface is $Area_i$; $Ir_{i\lambda}$ is the irradiance of a monochromatic beam of wavelength λ incident on a surface; $Ir_{a\lambda}$ is the effective absorbed irradiance or the power of the beam absorbed by the sample over $Area_i$. If we can measure $Ir_{i\lambda}$ and can assume that the energy is uniformly distributed across the beam, then we can infer the predicted number of photons the material is absorbing per second from the differential equation:

$$\frac{dN_{a\lambda}}{dt} = Ir_{i\lambda}(1 - 10^{-A_\lambda})Area_i\frac{\lambda}{hc}. \tag{4.7}$$

Here $\frac{dN_{a\lambda}}{dt}$ is the predicted number of photons per second of wavelength λ the material will absorb, h is Planck's constant, and c is the speed of light.

For an experiment of duration τ, we can now predict the energy delivered which is absorbed per unit area for a monochromatic beam of a known wavelength

$$\frac{E_{A\lambda}}{Area_i} = \int_0^\tau Ir_{i\lambda}(1 - 10^{-A_\lambda})dt. \tag{4.8}$$

This is related to the number of photons per area delivered during this time

$$\frac{N_{a\lambda}}{Area_i} = \int_0^\tau Ir_{i\lambda}(1 - 10^{-A_\lambda})\frac{\lambda}{hc}dt. \tag{4.9}$$

The quantum efficiency is the probability that a molecule undergoes a chemically significant change after absorbing a photon of a particular wavelength. With this, we can modify our metric to predict the number of molecules that will undergo chemically significant transitions after absorbing photons from a polychromatic beam:

$$\frac{N_{m\lambda}}{Area_i} = \int_0^\tau Ir_{i\lambda}(1 - 10^{-A_\lambda})\Phi_\lambda\frac{\lambda}{hc}dt, \tag{4.10}$$

where $N_{m\lambda}$ is the number of molecules affected by a beam of monochromatic light,

and $\Phi(\lambda)$ is the quantum efficiency. This means that we can predict the relevant concentrations of the affected molecules in our sample using

$$[S] = [S_0] - \frac{N_m}{N_A V} \tag{4.11}$$

$$[S'] = [S'_0] + \frac{N_m}{N_A V}. \tag{4.12}$$

Here $[S_0]$ is the original molar concentration of the untransitioned molecule, $[S'_0]$ is the original molar concentration of the transitioned molecule, $[S]$ is the new molar concentration of the untransitioned molecule, and $[S']$ is the new molar concentration of the transitioned molecule. The number of molecules transitioned is converted to a concentration by using Avagadro's Number, N_A, and the sample volume, V.

4.2 Polychromatic Light

To expand the monochromatic form to polychromatic light sources we need to address whether contributions from individual wavelengths are independent and additive. The "Addition Theorem" [47] requires that for a given effect which may be produced independently by several specific wavelengths of light, an equal effect can be produced by the combination of several of these wavelengths. Deviations from this theorem due to secondary photoreactions and photorecovery, are beyond the scope of this thesis and will not be addressed here.

We consider a polychromatic source to be a collection of monochromatic sources. Each of these monochromatic sources is a slice of a polychromatic source over a small wavelength range

$$Ir_{i\lambda} = Ir(\lambda)\Delta\lambda. \tag{4.13}$$

Note that photons are discrete entities with a continuously varying characteristic. The Addition Theorem supposes that the number of molecules transitioned is equal

to the sum of the number of molecules transitioned due to each wavelength

$$N_m \ f\left(\sum_{\lambda=\lambda_{min}}^{\lambda=\lambda_{max}} Ir_{i\lambda}\right) = \sum_{\lambda=\lambda_{min}}^{\lambda=\lambda_{max}} N_{m\lambda}. \tag{4.14}$$

By subsitituting Eq. (4.13) and Eq. (4.14) into Eq. (4.10) we find:

$$\frac{N_m}{Area_i} = \sum_{\lambda=\lambda_{min}}^{\lambda=\lambda_{max}} \left(\int_0^\tau Ir_i(\lambda)(1-10^{-A(\lambda)})\Phi(\lambda)\frac{\lambda}{hc}dt\right)\Delta\lambda. \tag{4.15}$$

Which in the limit of infinitessimaly small $\Delta\lambda$ becomes,

$$\frac{N_m}{Area_i} = \int_{\lambda_{min}}^{\lambda_{max}} \int_0^\tau Ir_i(\lambda)(1-10^{-A(\lambda)})\Phi(\lambda)\frac{\lambda}{hc}dt \ d\lambda. \tag{4.16}$$

Note that $Ir_i(\lambda,t)$ is the spectral irradiance and has units of $\frac{\mathrm{W}}{\mathrm{m}^2\ \mathrm{nm}}$. This expression captures the fact that both the molar absorptivity of a material and the radiant intensity, and therefore the irradiance delivered by a lamp (often called spectral irradiance), is wavelength dependent. As chemists are ultimately interested in the number of photons absorbed, we are not concerned with the difference between a 365 nm photon and a 366 nm photon if both are absorbed.

4.3 Time Dependence of Terms

In the previous section, we assumed that the terms were independent of time. However, the concentration of the absorbing molecules may be changing, as well as the molar absorptivity and quantum efficiency if a new species is introduced upon transition. In addition, mercury lamps are known to have a large power degradation and a subtle spectrum shift over time. This time dependence can be accounted for by modifying Eqs. (4.8) - (4.10) as

$$\frac{E_A}{Area_i} = \int_{\lambda_{min}}^{\lambda_{max}} \int_0^\tau Ir_i(\lambda,t)(1-10^{-\epsilon(\lambda,t)[S](t)l})dt \ d\lambda \tag{4.17}$$

$$\frac{N_a}{Area_i} = \int_{\lambda_{min}}^{\lambda_{max}} \int_0^\tau Ir_i(\lambda,t)(1-10^{-\epsilon(\lambda,t)[S](t)l})\frac{\lambda}{hc}dt \ d\lambda \tag{4.18}$$

$$\frac{N_m}{Area_i} = \int_{\lambda_{min}}^{\lambda_{max}} \int_0^{\tau} Ir_i(\lambda,t)(1-10^{-\epsilon(\lambda,t)[S](t)l})\Phi(\lambda,t)\frac{\lambda}{hc}dt\ d\lambda. \tag{4.19}$$

Finally by taking a time derivative of Eq. (4.19) and rearranging, we find the integro-differential form of our polychromatic evolution equation:

$$\frac{d[S]}{dt} = -\frac{A_i}{N_A V}\int_{\lambda_{min}}^{\lambda_{max}} Ir_i(\lambda,t)(1-10^{-\epsilon(\lambda,t)l[S](t)})\Phi(\lambda,t)\frac{\lambda}{hc}d\lambda. \tag{4.20}$$

For compactness $Area_i$ has been shortened to A_i.

4.3.1 Limiting Case: Time Independence

Let us consider first the case in which all of the quantities are time independent. This reduces Eq. (4.19) to a statement equivalent to an experimental observation termed the reciprocity law. For a given photoresponse, a material is said to follow the reciprocity law if the material response is constant with the product of irradiance multiplied by time [11]. If the material response is linear with the number of transitioned molecules, then the following equation is a statement of reciprocity:

$$\frac{N_m}{Area_i} = \tau\int_{\lambda_{min}}^{\lambda_{max}} Ir_i(\lambda)(1-10^{-\epsilon(\lambda)[S]l})\Phi(\lambda)\frac{\lambda}{hc}d\lambda \tag{4.21}$$

$$\frac{N_m}{Area_i} = \tau K\Big|_{f(\lambda)} \tag{4.22}$$

$$\tag{4.23}$$

where K is a constant for a given experimental setup and scales linearly with the irradiance of the source. This model suggests that the rate of photon delivery does not matter, but rather the absolute number of photons delivered. The reciprocity law most applies when there is the "right amount" of photons to molecules. If there are too few photons (much less than the number of absorbing molecules), we expect our absorbed energy to be an overestimate of reality as the photons could miss the few absorbers in space or some degradation process could prevent us from measuring a bulk response. On the other hand, if we flood the sample with a large number of photons then the material response should no longer be linear with time because

it has reached an upper limit. These two cases, illustrated in Fig (4-1), bound the application of the reciprocity law.

Some materials deviate from the reciprocity law, and are labeled as demonstrating reciprocity law failure [36]. For reference, Schawrzschild modified the reciprocity law by introducing the "Schawrzschild coefficient", p, which describes some reciprocity law failure responses: applicable to some materials.

$$Constant = \tau^{p} Ir. \tag{4.24}$$

These failures most often happen at either very low or very high irradiance levels. This could be explained by the limits previously described. Reciprocity law failure also has been observed with photographic materials where there are many absorbing reactions and a many step developing process. Metrics excluding the multi-step and time dependent reactions present may not be appropriate for these applications.

4.3.2 Limiting Case: Time Dependence

Where previous polymer degradation studies are not concerned with the absorbance changing with time (and therefore make the time independent approximation), our photoactive systems may change dramatically over time. For instance, an entire concentration of the absorbing species could permanently transition to some other non-absorbing state. This means that our metric at this point will become zero because the concentration, [S], is zero. This represents a large change over finite time. In another case, the photoactive species could transition between two states that have different absorption spectra and therefore absorb photons with a very different wavelength than initially. Past methodologies include using a negative quantum efficiency to represent the competing process called photorecovery [34], [28]. The use of a negative quantum efficiency is physically dubious. There may be better ways to account for competing reactions and large changes in the absorbance spectrum stemming from the introduction of a new species competing for photons. To do this, we explore reaction kinetics in the next chapter

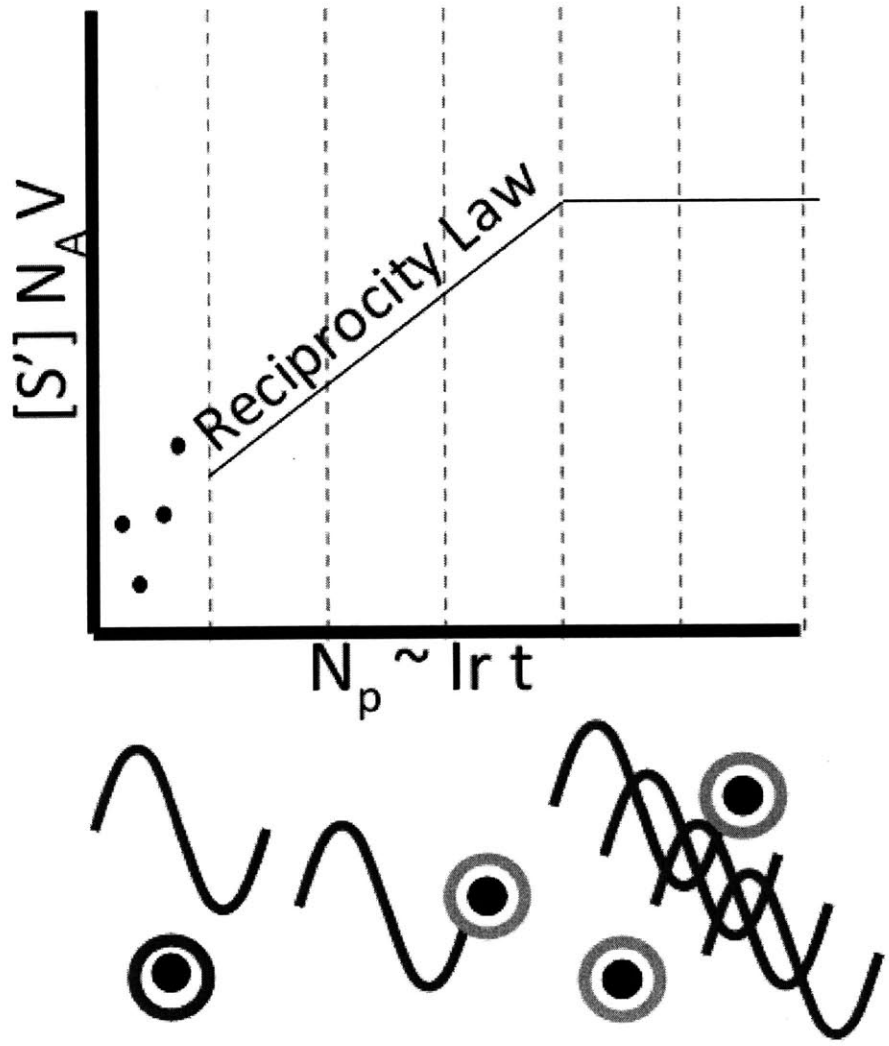

Figure 4-1: Regimes of application of the reciprocity law, with the number of converted molecules due to absorption on the y-axis and the number of photons delivered on the x-axis. Reciprocity failure is expected when there is either a small or large photon flux.

Chapter 5

Kinetics and Large Changes with Time

We wish to examine the rates of our reactions even when the original species concentration may become significantly depleted. Over the course of this chapter we use the differential form of the model we have developed to formulate a way to theoretically analyze rates of reactions whose limiting timescale is photon delivery. In practice, rate laws are empirical and experimental data is required to validate a particular rate law. Therefore we will compare literature data and, in a following chapter, our own data to our prediction. In the first part of this chapter, we examine fluids whose transitioned state does not absorb photons and therefore cannot return to its original state, leading to an irreversible transition. For fluids whose second species has an absorption spectrum that is larger than that of the original species, the transition may be reversible, especially if the emission spectrum is tuned to favor one species or the other (such as [54],[46]). In the second half of this chapter, we will address these reversible fluids. For both types of fluids, we examine the effect of monochromatic and polychromatic light.

5.1 Development of Kinetics within a Theoretical Framework

To construct the simplest rate law, we first examine the case where [S'] does not absorb photons and the reaction is irreversible:

$$S \underset{K_{rS}}{\overset{\alpha}{\rightleftharpoons}} S^* \overset{K_{dS}}{\rightarrow} S'. \tag{5.1}$$

Eq. (5.1) describes how the species S can become S' through the activated state of S*. The fact that not all S* become S' is reflected in a quantum efficiency that is not 1. If the quantum efficiency were 1, K_{rS} would be zero. The relationship between the rate constants and the quantum yield is given by

$$\Phi_S = \frac{K_{dS}}{K_{rS} + K_{dS}}. \tag{5.2}$$

5.1.1 Approximations

Historically, a number of estimates for the rate constant for the S to S* transition have been used ([59], [16], [62]). Zimmerman et al. [62] suggests, for instance, that the rate constant be taken as the rate of light absorption of each isomerization. Other chemists, such as in [16], suggest

$$\frac{d[S]}{dt} = -\alpha = -K[S]\epsilon_{S\lambda} Ir_\lambda \tag{5.3}$$

where K is a constant, $\epsilon_{S\lambda}$ is the molar absorption for the species S at a particular wave length, and $Ir_{i\lambda}$ is the irradiance of the wavelength in question.

Our model can be used to determine whether a zeroth order rate equation is appropriate and how this rate constant might be defined. We begin with the full polychromatic derivative with the concentration [S] explicitly written as

$$\frac{d[S]}{dt} = -\frac{A}{N_A V} \int_{\lambda_{min}}^{\lambda_{max}} Ir_i(\lambda)(1 - 10^{-\epsilon(\lambda) l [S]}) \frac{\lambda}{hc} \Phi(\lambda) d\lambda. \tag{5.4}$$

For a laser, i.e. a source with a dirac delta in spectral irradiance, this reduces to

$$\frac{d[S]}{dt} = -\frac{1}{N_A V}\frac{\lambda}{hc} A I r_{i\lambda}(1 - 10^{-\epsilon_\lambda l[S]})\Phi(\lambda). \tag{5.5}$$

If we make the approximation that the absorbance, $\epsilon(\lambda)l[S]$ in Eq. (5.4), is large then the rate equation reduces to a zeroth order rate law Eq. (5.6).

$$\frac{d[S]}{dt} = -\frac{A}{N_A V} I r_{i\lambda}\frac{\lambda}{hc}\Phi(\lambda). \tag{5.6}$$

Note how this reduces to Eq. (5.7) matching the currently accepted rate law and elaborating on the makeup of the constant in Eq. (5.3)

$$\frac{d[S]}{dt} = -\alpha = -CGMIr_{i\lambda}\lambda\Phi(\lambda). \tag{5.7}$$

Here C represents fundamental constants, G represents geometrical constants and M represents material constants. From Eq. (5.6), C equals $\frac{1}{N_A ch}$, G equals $\frac{A}{V}$, and M equals $\Phi(\lambda)$. We see that the source influences the rate of reaction both with irradiance and wavelength. For example two lasers with the same power but different wavelengths cause different rates of transformation from S to S'. The experimental manifestation of Beer's law suggests that this wavelength dependence is not a rate associated with the speed of absorption, but rather that the molar absorptivity captures an 'absorption efficiency' as a larger population of molecules is activated for a given number of photons. This efficiency is separate from a quantum efficiency and may be more recognizable if rewritten as the absorption cross section (σ) which is a measure of the probability of the absorption process,

$$\sigma = 2.303\frac{\varepsilon}{N_A} = 3.82 \times 10^{-21}\varepsilon. \tag{5.8}$$

When the concentration or absorbance becomes too small, the linear approximation

is no longer valid.

$$\text{If } 10^{-\epsilon_\lambda l[S]} \approx 1, \tag{5.9}$$

then we replace the exponential term with a first order Taylor Series approximation within the series' radius of convergence. This leads to the first order rate law

$$\frac{d[S]}{dt} = -\frac{A}{N_A V} I r_{i\lambda} ln(10) \epsilon_\lambda l[S] \frac{\lambda}{hc} \Phi(\lambda). \tag{5.10}$$

In the next section we will find that while these approximations are not necessary for the monochromatic source which has an explicit solution, they provide a solution pathway for more difficult problems like reversible fluids and polychromatic light sources.

5.1.2 Nondimensionalization of Monochromatic Case

Now that we have explored intuitively the rate of transition between S and S', we nondimensionalize Eq. (5.5) and evaluate it directly. We assume $\Phi = 1$, though it is easily re-inserted if desired. We define a nondimensional concentration $[\hat{S}]$ which is the familiar quantity known as the absorbance introduced earlier,

$$[\hat{S}] = \epsilon_\lambda [S] l. \tag{5.11}$$

Employing this definition, leads to the partially nondimentionalized equation:

$$\frac{d[\hat{S}]}{dt} = -\frac{A}{N_A V} (\epsilon_\lambda l) I r_{i\lambda} \frac{\lambda}{hc} (1 - 10^{-[\hat{S}]}). \tag{5.12}$$

Note that the expression $\frac{Al}{V}$ is defined as unity. We must now nondimentionalize time by a relevant experimental time scale. An appropriate nondimensionalization is suggested by grouping the remaining terms in Eq. (5.12):

$$\hat{t} = t_{exp} I r_{i\lambda} \frac{\lambda}{hc} \frac{\epsilon_\lambda}{N_A}. \tag{5.13}$$

We now can rewrite the fully nondimensionalized rate equation:

$$\frac{d[\hat{S}]}{d\hat{t}} = -(1 - 10^{-[\hat{S}]}). \tag{5.14}$$

Nondimensional Groups for Monochromatic Source Case

The two dimensionless numbers, $[\hat{S}]$ and $\hat{t}$, provide insight into the two factors that affect the rate at which the reaction progresses. $[\hat{S}]$ represents the number of "perfect absorbers" in the solution as it describes both how many absorbers are in an area, $[S]l$, and how efficiently they absorb, ϵ. The larger this number the longer $[\hat{S}]$ decreases at a constant rate. The time axis is scaled to reflect the fraction of the reaction that has taken place. If t is larger the reaction is closer to completion if it is smaller it is farther from completion. This is because $\hat{t}$ is directly related to the reaction coordinate: the longer (large t_{exp}) batches of photons (large $Ir_{1\lambda}\lambda$) are delivered to molecules that efficiently absorb them (large ϵ_λ), the more molecules that transition.

Characteristic Curve for Monochromatic Source Case

The nondimensional rate equation is a separable equation, and can be integrated by substitution yielding,

$$[\hat{S}] = log_{10}\left((10^{[\hat{S}]_0} - 1)10^{-\hat{t}} + 1\right). \tag{5.15}$$

Here $[\hat{S}]_0$ indicates the initial condition and $\hat{t}$ the scaled experimental timescale. Even though this equation is nondimensionalized, the dependent and independent variables are not normalized to 1. In fact, this equation represents a collection of curves as the solution depends on the initial concentration as shown in Fig. 5-1. Note that the zeroth order and first order approximations made in the previous section are captured by the characteristic curves. The solution may indeed be considered linear in $\hat{t}$ until $\hat{t} \approx log_{10}(10^{[\hat{S}_0]} - 1)$, when the linear solution predicts total conversion prematurely.

If we perform a variable substitution that collects both the initial absorbance ($\epsilon_\lambda[S_0]l$) and the time varying concentration into a single variable, we can collapse

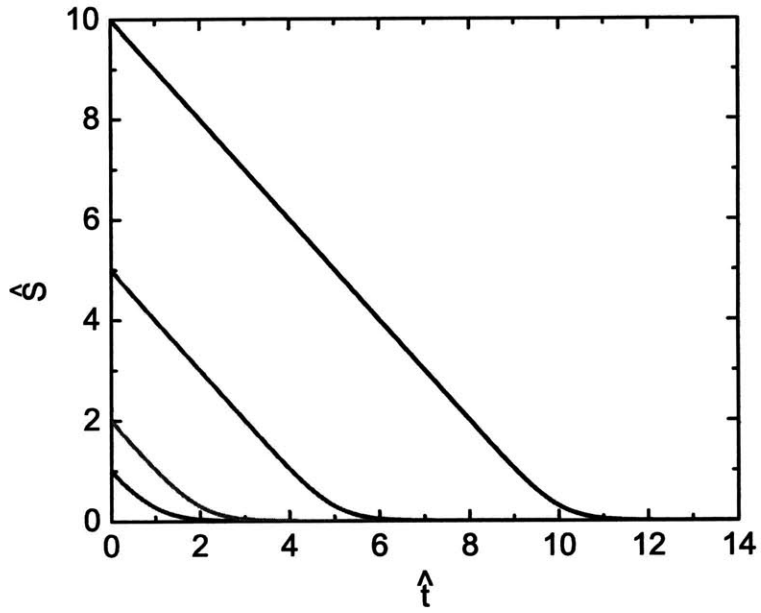

Figure 5-1: The evolution of $\hat{S}$ with $\hat{t}$ upon monochromatic irradiance depends on initial concentration $\hat{S}_0$. For small $\hat{t}$, $\hat{S}$ is decreasing linearly with $\hat{t}$, and for large $\hat{t}$ it decreases exponentially.

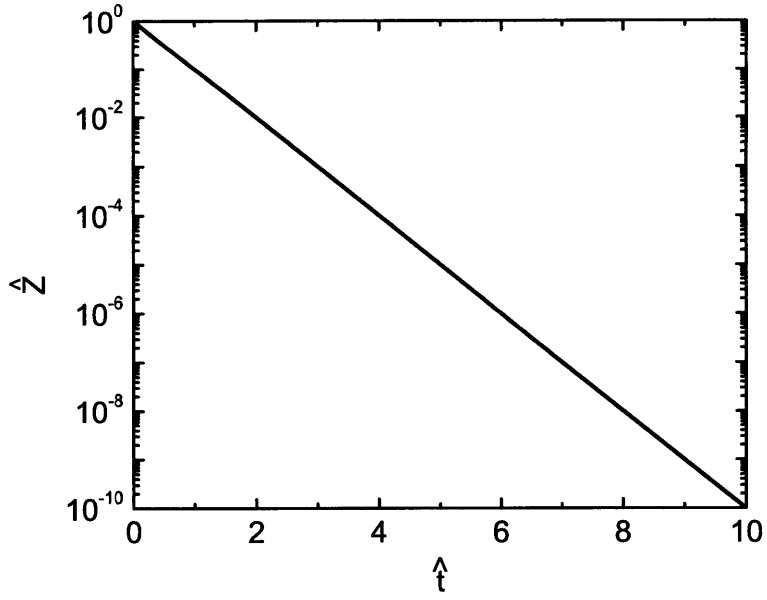

Figure 5-2: Evolution of $\hat{Z}$ with $\hat{t}$ upon monochromatic irradiance describes behavior of modeled photorheological fluids. The family of curves of $\hat{S}$ vs $\hat{t}$ seen in Fig. 5-1 collapse onto a single exponential curve.

this family of curves onto a single curve (Fig. 5-2). Let $\hat{Z} = \frac{10^{[\hat{S}]}-1}{10^{[\hat{S}]_0}-1}$ and substitute $\hat{Z}$ into Eq. (5.14). Solving leads to the single curve:

$$\hat{Z} = 10^{-\hat{t}}. \tag{5.16}$$

5.1.3 Validation through Analysis of Existing Literature

There is evidence that light reactions do have these types of characteristic shapes and evolutions. Early interest in the time evolution of photoresponsive materials originated in the photography and astronomy fields [58],[25],[27]. However the data required to generate the characteristic curve is often not reported. To normalize the data as suggested above, one needs not only molar absorptivity, wavelength of light, initial concentration (all routinely reported) but also the thickness of a given sample and the absolute irradiance of the light source at the sample. Some experimentalists

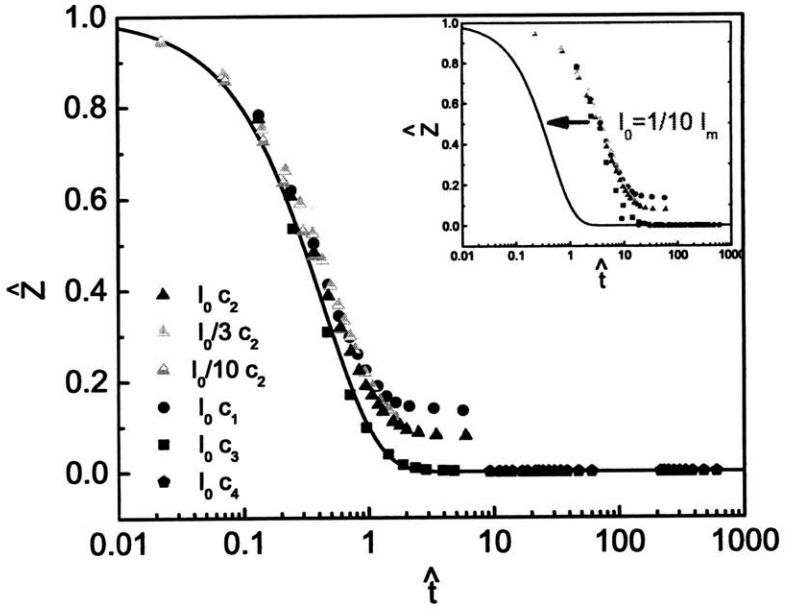

Figure 5-3: The metric is applied to the dataset [62] with a slight modification in the intensity ($I_0 = \frac{1}{10} I_m$). This is equivalent to $\Phi_{\lambda=313nm} = \frac{1}{10}$ as the quantum efficiency also linearly scales the intensity. The black line is the theoretical prediction The inset shows the $\hat{Z}$ vs $\hat{t}$ using the original parameters. See Table 5.1

only report relative intensities within an experiment while others are more careful to report absolute intensity in terms of photon fluxes.

To demonstrate the validity and usefulness of the above nondimensionalization, we will examine a dataset that reports most of the required quantities. This particular dataset reports measurements of azobenzene, a compound that is well documented through out literature. We have examined other published systems such as iodine in retinol ([3]), azobenzene in a polycarbonate film ([38]), and photoactivated CdSe nanocrystals ([40]), and found similar behavior, however since many of the required variables are unknown or unreported, we deem the analysis less convincing and proceed with the present case. Zimmerman et al. [62] report a time evolution study of several different concentrations of trans-isomer azobenzene irradiated at different intensities of monochromatic light. They also report the photostationary mole fraction, the ratio of converted isomer to original concentration, as a function of wavelength.

Using their reported experimental conditions, listed in Table 5.1, we nondimensionalize their data using the proposed scalings for Z* and t* values. Note that the area

Table 5.1: Experimental parameters from Zimmerman et al. [62]

Concentration ($\frac{\text{Mol}}{\text{L}}$)	Intensity (mW)
$c_1 = 10^{-5}$	$I_m = 2.99$
$c_2 = 2.5 \times 10^{-5}$	$I_m = 3.03$
$c_2 = 2.5 \times 10^{-5}$	$I_m = 0.91$
$c_2 = 2.5 \times 10^{-5}$	$I_m = 0.30$
$c_3 = 10^{-4}$	$I_m = 3.02$
$c_4 = 10^{-3}$	$I_m = 3.81$

$\lambda = 313\text{nm}\ \epsilon = 10^{4.4} \frac{L}{\text{mol cm}}\ l = 1.25cm\ A = 5cm^2$
A, l approximated from reported $V = 6.204\text{cm}^3$

and the thickness of the sample is not reported and we approximate these under the assumption that the sample is a cylinder of equal dimensions in radius and height. We then use this area to calcualte the irradiance from the measured intensity (originally reported in einsteins per minute).

In the inset of Fig. 5-3 we see that the nondimensionalization of the data does indeed cause the data to collapse onto a single curve. This is a strong indication that the nondimensionalization correctly accounts for varying concentrations, varying irradiations of light, and time dependence. When we compare this to the expected characteristic curve however, we see that the results are shifted by an order of magnitude in$\hat{t}$. Upon examining the definition of $\hat{t}$, we see the only opportunities for moving the data onto the prediction are in t_{exp}, and Ir_λ. Since the experiment was conducted over a time scale of minutes, it is unlikely an order of magnitude error was introduced in the time measurement. The irradiance however is a derived quantity from the given intensity measurement. We find that if we diminish the irradiance by a factor of ten, the data now lines up with the theoretical prediction (Fig. 5-3).

While relative intensity was determined in an experimentally rigorous way, the absolute intensity remains questionable. This difference between relative and absolute is consistent with the fact that the data points collapse on each other but not on the theoretically predicted curve. The absolute intensity was determined by the au-

thors using uranyl oxalate actinometry, a separate chemical reaction. Any difference between the two experiments, e.g. path length, or transmission of the quartz, would skew the irradiance values. Also, in our metric we assumed a quantum efficiency of 1. While the quantum efficiency is controversial and has been defined differently over the years, the azobenzene paper defines it as .44 at the indicated wavelength. A further reduction in intensity of .2 could easily occur particularly given that the light source was uncollimated and that intensity drops off as an inverse square law, making it particularly sensitive to small changes in path length. Also with such a thick sample the intensity at the bottom of the sample could be considerably less than the intensity at the top of the sample leading to a lower effective intensity. Lastly, the irradiance was calculated by dividing the intensity over the approximated area. If the area is larger than the 5 cm^2 assumed, the irradiance would be smaller. Of course, changing the area would also change the sample thickness as the volume is given. Nonetheless, we have shown that there exist reasonable values for A, l ,I_0, and Φ which would shift the experimental curve to the left leading to agreement with the theoretical prediction.

One may also question why the dataset follows the theory but then diverge beyond $\hat{t}$ =1. To understand this discrepancy, we move away from $\hat{t}$ and $\hat{Z}$ which are somewhat unintuitive and can mask the evolution of the concentration. In Fig.5-4, we see the molar fraction of the cis isomer rise with time. Our model predicts 100% conversion which is not reflected in the data (the data predicts somewhere around 80%). An irreversible fluid assumes that the entire population is eventually converted. In practice the cis isomer also absorbs and so can revert back to the trans-isomer. In addition, the cis-isomer can thermally isomerize back to the trans-isomer. There are a variety of approaches we can use to compare our predictions to the data despite this complication. In Fig. 5-5 (a), we simply scale the previous theory to .8 to reflect the observed photostationary mole fraction. In Fig. 5-5 (b), we try a more physically motivated method. For each concentration, we determine what fraction of the population is not absorbing photons and subtract this from the initial concentration. We then add that fraction of the population to the calculated concentration. This ap-

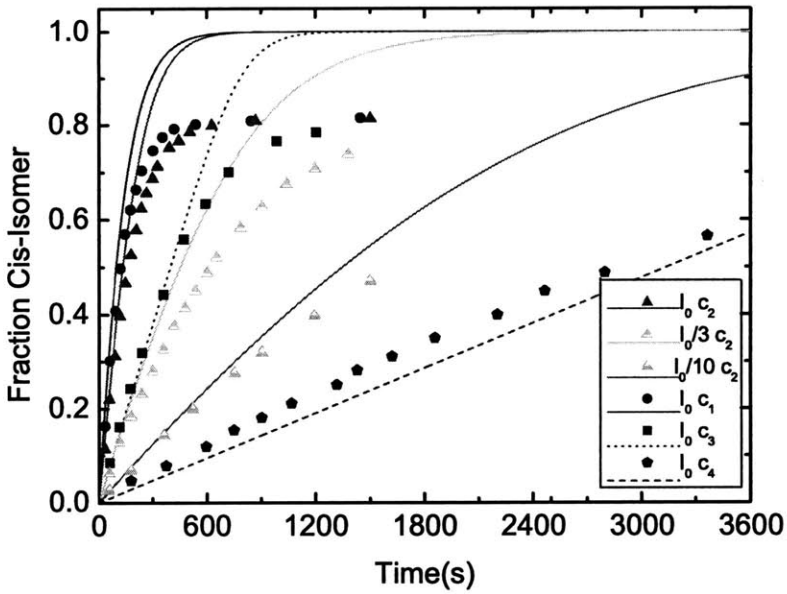

Figure 5-4: Theory over predicts the final photostationary mole fraction as it neglects absorption of Cis-Isomer and requisite Cis-trans isomerization. Points indicate experimental data [62]; lines are theoretical predictions.

proach, while better than the previous, is still chemically dubious. More appropriate corrections will be discusses in a later section, in which we develop a monochromatic solution for chemically reversible fluids.

At this point we have discussed a rather idealized case, where the source is monochromatic and the transitioned state has an absorption of zero. We briefly discuss an alternative approach in the next sections.

5.2 Extending Solutions to Polychromatic Light

Although the polychromatic form is the same as the monochromatic form with an additional integration over the wavelength, a closed form solution is no longer apparent for the differential equation. To demonstrate this we rewrite Eq. (5.4) as:

$$\frac{d[S]}{dt} = -\int_{\lambda_{min}}^{\lambda_{max}} f(\lambda)d\lambda + \int_{\lambda_{min}}^{\lambda_{max}} f(\lambda)10^{-[S]g(\lambda)}d\lambda \tag{5.17}$$

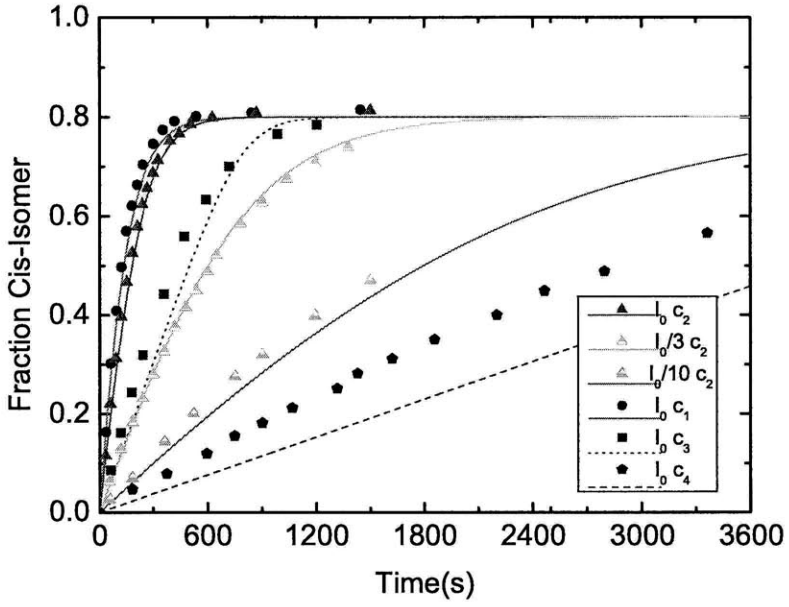

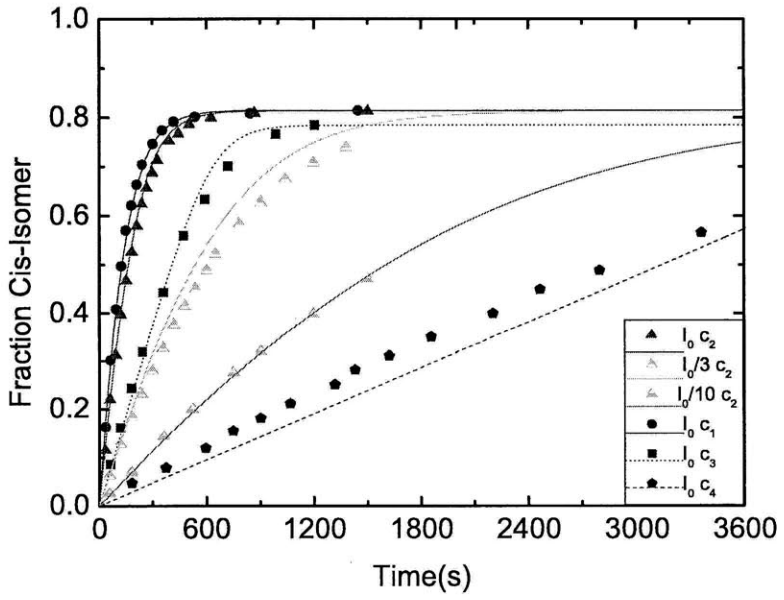

Figure 5-5: Comparison of experimental data [62] with two theoretical formulations. a) The monochromatic solution is simply scaled to 80% of original value. b) The initial concentration is modified to reflect the population which will not be converted.

We assume that researchers could evaluate both of the functions $f(\lambda) = \frac{A}{V}\frac{1}{N_A}Ir_i(\lambda)\frac{\lambda}{hc}$ and $g(\lambda) = \epsilon(\lambda)l$. Attempts to nondimensionalize this equation are thwarted by the fact that we cannot separate S from $g(\lambda)$ in the second integral. Because of this, the concentration evolution from a polychromatic source must be integrated numerically for an exact form. However, we can develop two approximate solutions: a linear solution appropriate for large absorbances and at short times, and a nonlinear solution comparable to the monochromatic solution for small absorbances.

First, because of its definite limits, the first integral is simply a constant

$$K = -\int_{\lambda_{min}}^{\lambda_{max}} f(\lambda)d\lambda \tag{5.18}$$

where

$$K \gg \int_{\lambda_{min}}^{\lambda_{max}} f(\lambda)(10^{-[S]})^{g(\lambda)}d\lambda. \tag{5.19}$$

At short times, the polychromatic form of the rate equation reduces to a zero-order system, linear with K; this is the short time polychromatic form of Eq. (5.6) .

Employing the initial concentration S_0 to nondimensionalize S, we find that short time solution can be approximated as Eq. (5.20) with dimensionless groups given by Eq. (5.21), and Eq. (5.22)

$$S' = -t' + 1 \tag{5.20}$$

$$S' = \frac{S}{S_0} \tag{5.21}$$

$$t' = \frac{t_{exp}A}{N_A chVS_0}\int_{\lambda_{min}}^{\lambda_{max}} Ir(\lambda)\lambda d\lambda. \tag{5.22}$$

Next we can evaluate at what concentration this assumption is no longer valid. First we define C as

$$C = \frac{\int_{\lambda_{min}}^{\lambda_{max}} f(\lambda)(10^{-[S]})^{g(\lambda)}d\lambda}{\int_{\lambda_{min}}^{\lambda_{max}} f(\lambda)d\lambda} \tag{5.23}$$

If C $\geq$ 1 the linear assumption is not appropriate and the full solution should be calculated numerically. During a one second interval, the linear approximation is

within 1% of the exact solution for absorbance functions larger than 5.

Next we consider the small absorbance limit. If the maximum absorbance is small ($\epsilon_{max} l[S_0] < .2$) we can take the first two terms of the Taylor series expansion for $10^{-\epsilon[S]\lambda} \approx 1 - ln(10)\epsilon(\lambda)l[S] + \frac{1}{2}\left(ln(10)\epsilon(\lambda)l\right)^2[S]^2$, and integrate the differential equation to get an analytical solution

$$\tilde{S} = \frac{10^{-\tilde{t}}}{1 - \frac{\beta_2 S_0}{\beta_1}(1 - 10^{-\tilde{t}})} \tag{5.24}$$

$$\frac{\beta_2 S_0}{\beta_1} = \frac{ln(10) l S_0}{2} \frac{\int_{\lambda_{min}}^{\lambda_{max}} Ir(\lambda)\lambda\epsilon(\lambda)^2 d\lambda}{\int_{\lambda_{min}}^{\lambda_{max}} Ir(\lambda)\lambda\epsilon(\lambda) d\lambda} \tag{5.25}$$

$$\tilde{S} = \frac{S}{S_0} \tag{5.26}$$

$$\tilde{t} = \frac{t_{exp}}{N_A c h} \int_{\lambda_{min}}^{\lambda_{max}} Ir(\lambda)\epsilon(\lambda)\lambda d\lambda. \tag{5.27}$$

Note that this solution has a singularity followed by nonsensical results if $\beta_2 > \beta_1$. This is to be expected when the two-term Taylor series is no longer sufficient.

The solutions to the monochromatic solution and polychromatic solution (large and small absorbance) are presented in Table 7.1. The approximations serve mostly to provide suggestions for relevant nondimensional groups that can be used to characterize an experimental set up. Note that the dimensional groups for t all look

Table 5.2: Dimensionless groups and solutions for irreversible fluids irradiated with a monochromatic source (1), a polychromatic source for a fluid in the large absorbance regime (2 a) and in the small absorbance regime (2 b)

Case	Solution	$\bar{S}$	$\bar{t}$
1	$[\hat{S}] = log_{10}\left((10^{[\hat{S}]_0} - 1)10^{-\hat{t}} + 1\right)$	$[\hat{S}] = \epsilon_\lambda [S] l$	$\hat{t} = t_{exp}\frac{Ir_{i\lambda}\epsilon_\lambda}{N_A}\frac{\lambda}{hc}$
$2(a)$:	$S' = -t' + 1$	$S' = \frac{S}{S_0}$	$t' = t_{exp}\frac{A}{V S_0}\frac{1}{N_a}\int_{\lambda_{min}}^{\lambda_{max}} Ir(\lambda)\frac{\lambda}{hc}d\lambda$
$2(b)$:	$\tilde{S} = \frac{10^{-\tilde{t}}}{1-\frac{\beta_2 S_0}{\beta_1}(1-10^{-\tilde{t}})}$	$\tilde{S} = \frac{S}{S_0}$	$\tilde{t} = t_{exp}\int_{\lambda_{min}}^{\lambda_{max}} \frac{Ir(\lambda)\epsilon(\lambda)}{N_A}\frac{\lambda}{hc}d\lambda$

similar to each other. In fact, $\tilde{t}$ reduces to $\hat{t}$ for monochromatic sources and the two are related to each other by a constant. It is understandable that case 2(a) looks slightly different, missing the molar absorptivity and the length scale, because in this

regime the fluid is not limited by the absorption of the fluid but by the delivery of photons. From this table we can see that a good recommendation for our metric is therefore the 2(b) case, $\tilde{t}$. However, for large absorbances and short times, t' may also be an acceptable choice. Nonetheless, to describe an experiment we recommend that researchers report the following minimum variables, $\epsilon(\lambda), Ir(\lambda), V, A, S_0$, so that they or another author can normalize the time scale. We have yet to find literature that appropriately reports experiments performed with a polychromatic source (though [11] may be considered a notable exception), therefore chapter 7, which describes our own experimental data, is in part used to validate this section.

5.3 Reversible Fluids

We have already encountered a fluid that requires us to extend slightly our theory to fluids which have two states that absorb UV light:

$$A \underset{K_{rA}}{\overset{\alpha}{\rightleftharpoons}} A^* \overset{K_{dS}}{\rightarrow} B \tag{5.28}$$

$$B \underset{K_{rB}}{\overset{\alpha}{\rightleftharpoons}} B^* \overset{K_{dS}}{\rightarrow} A. \tag{5.29}$$

We call this a reversible fluid and the bulk ϵ and Φ change in a way that is not obviously related to the time dependent concentration. Some trans-cis isomerizations are good examples of systems in which the when the resultant species ([B]) competes for photons with the original species ([A]). For the time being we will assume that all A* become B and all B* become A indicating a quantum efficiency of 1 for both reactions. This assumption need not be made and Φ may be added back into the formulation in addition to the reaction associated with K_{ds}.

Since our robotic application has a preference for reversible mechanisms we seek to formulate a rough prediction of the behavior of these fluids. This rough sketch is essential for understanding the feasibility of controlling a material property based on turning on and off different wavelengths of light. We will begin as before, first with the much simpler monochromatic case and then expanding the analysis to show that

once again reporting the spectra is essential to predicting the photostationary state.

5.3.1 Monochromatic Case

The rate of generation of the two species must be related to the concentrations of the two species absorbing photons. We assume these reactions are independent of each other:

$$\frac{d[A]}{dt} = -|f_a([A])| + |f_b([B])| \tag{5.30}$$

$$\frac{d[B]}{dt} = -|f_b([B])| + |f_a([A])| \tag{5.31}$$

We also assume that each of these functions are well described by our previous discussion:

$$\frac{d[A]}{dt} = -\frac{Area_i}{N_A V h c} I r_\lambda \lambda (1 - 10^{-\epsilon_A l[A]} - 1 + 10^{-\epsilon_B l[B]}), \tag{5.32}$$

for example. We consider the case in which initially there is only one species present so that we can relate the second species to the current concentration and the concentration of the first,

$$[B] = [A_0] - [A]. \tag{5.33}$$

Note that Eq. (5.32) and Eq. (5.32) are sufficient to generate a numerical analysis. We proceed with determining analytical approximations to gain insight into our model's application to reversible fluids. Using a first order Taylor series approximations for $10^{-\epsilon_A l[A]}$ and $10^{\epsilon_B l[A]}$ (requiring $\epsilon_A l[A] \ll 1$ and $\epsilon_B [A] l \ll 1$) on the combination of Eq. (5.32), and Eq. (5.33), we can write the differential equation for the concentration evolution of A (Eq. 5.34) as:

$$\frac{d[A]}{dt} = -\frac{Area_i}{N_A V h c} I r_\lambda \lambda ((K_0 - 1) + (\epsilon_A + K_0 \epsilon_B) ln(10) l[A]) \tag{5.34}$$

where

$$K_0 = 10^{-\epsilon_B l[A_0]} \tag{5.35}$$

The quantity K_0 is defined for convenience and to emphasize at this point that no requirements on the magnitude of K_0 have been made.

After applying appropriate initial conditions, integrating Eq. (5.34) and solving for A, we find:

$$[A] = [A_0]10^{-t(\frac{Area_i}{N_A V hc} l I r_\lambda \lambda(\epsilon_A + \epsilon_B * K_0)} + \frac{(K_0 - 1)[10^{-t\frac{Area_i}{N_A V hc} l I r_\lambda \lambda(\epsilon_A + \epsilon_B K_0)} - 1]}{(\epsilon_A + \epsilon_B K_0) ln(10) l}. \tag{5.36}$$

Approximating K as Taylor series $K_0 \approx 1 - ln(10)\epsilon_B A_0 l + O(ln(10)\epsilon_B A_0 l)^2$ we find

$$[A] = \left([A_0] - \frac{\epsilon_B [A_0]}{\epsilon_A + \epsilon_B - \epsilon_B^2 ln(10)[A_0] l}\right) 10^{-t\frac{Area_i \lambda}{N_A V hc} l I r_\lambda (\epsilon_A + \epsilon_B - ln(10)\epsilon_B^2 l A_0)} + ... + \frac{\epsilon_B [A_0]}{\epsilon_A + \epsilon_B - \epsilon_B^2 ln(10)[A_0] l}. \tag{5.37}$$

Defining dimensionless groups:

$$[\check{A}] = \left(1 - \frac{\epsilon_B}{\epsilon_A + \epsilon_B - \epsilon_B^2 ln(10)[A_0] l}\right) 10^{-\check{t}} + \frac{\epsilon_B}{\epsilon_A + \epsilon_B - \epsilon_B^2 ln(10)[A_0] l} \tag{5.38}$$

$$\check{t} = t_{exp} \frac{Area_i l}{V} \frac{I r_\lambda (\epsilon_A + \epsilon_B - ln(10)\epsilon_B^2 l[A_0])}{N_A} \frac{\lambda}{hc} \tag{5.39}$$

$$[\check{A}] = \frac{[A]}{[A_0]} \tag{5.40}$$

Note that Eq. (5.38) implies a similar form as the monochromatic form but decreasing at a slightly slower rate and implies a photostationary mole fraction dictated by a function involving the ratios of the two species' molar absorptivities. As the first order Taylor series approximations are not sufficient to fully describe the power series, we are not surprised by the singularities apparent in the denominators.

We have applied this to the azobenzene data discussed previously. The cis-isomer molar absorptivity (1000 $\frac{\text{L}}{\text{mol cm}}$) is reported in [62] as an order of magnitude different from the NIST webbook (11300 $\frac{\text{L}}{\text{mol cm}}$) [53]. Therefore we have a large fitting range

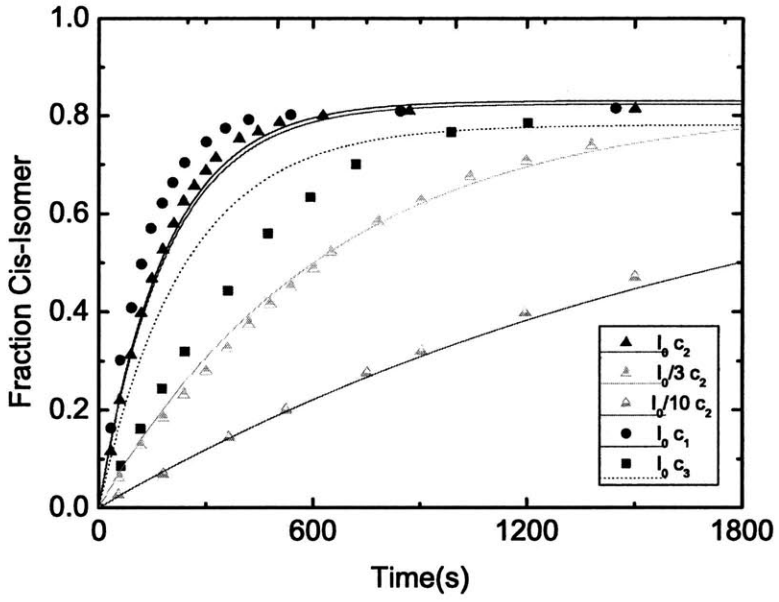

Figure 5-6: The reversible fluid monochromatic formulation is applied. Note that the $I_0 = 1/20 I_m$ and ϵ_b is $10^{3.7} \frac{\text{L}}{\text{mol cm}}$.

we could use. Fig. 5-6 uses a molar absorptivity of 5012 $\frac{\text{L}}{\text{mol cm}}$. Again, we must modify the intensity to be 1/20th of the reported intensity. Alternatively, we also find promising agreement with the data if we modify the thickness of the sample to be 1.5 mm and the area to 41 cm^2 (approximately a 3.6 cm radius) and use the reported quantum efficiency of .41.

We can also use this to determine the photostationary mole fraction:

$$\phi = \frac{\epsilon_B}{\epsilon_A + \epsilon_B - \epsilon_B^2 ln(10) A_0 l}. \tag{5.41}$$

This data is easy to collect and the aforementioned paper also reports the standing concentration. We can compare our prediction with their results as another check (See Table 5.3). The calculation used to generate this prediction uses only the reported experimental parameters and accepted physical constants. Our predicted mole fraction has not included the thermal isomerization of the cis-isomer to trans-isomer. Therefore the over-prediction is expected. The large disagreement for the 254 nm

Table 5.3: Comparison of experimentally observed [62], and predicted cis-isomer photostationary states

λ	Predicted Mole Fraction	Observed Mole Fraction
254	80%	8%
313	96%	81%
365	72%	40%
405	26%	15%
436	28%	14%
546	28%	18%
578	16%	5%

$[A_0] = 2.5 \times 10^{-5}$ M

wavelength may be related to the large molar absorptivity of the cis-isomer at that wavelength and the possible break down of the Taylor series approximation. This data as well as the 405 nm data should be analyzed numerically. In general, we see these results as being a satisfactory validation of our rough sketch.

5.3.2 Polychromatic Light Affects Photostationary State

Current wisdom in the chemistry community is that the standing concentration of a photoactive material is independent of the power spectrum delivered [16]. Eq. (5.41) supports this. In fact, there are four cases when the spectral power of the light source is not relevant to the standing concentration:

1. [B] does not absorb photons (ϵ does not change with time).
2. Light is monochromatic.
3. [A] and [B] have the same absorption and quantum efficiency spectrum.
4. Light has constant spectral intensity across all wavelengths absorbed by either [A] or [B].

However, when [A] and [B] have different absorbance spectra and the light is polychromatic over relevant portions of the absorbance spectral, the spectral power of the lamp can influence the final standing concentration. To begin, we can preform a

simple thought experiment. If a green light source is used to stimulate a mixture of species where one absorbs green light and the other blue, the species absorbing green will be most prevalent in the standing concentration. If however a blue light source is used, the concentration will be dominated by the other species. To express this mathematically, we can expand the monochromatic prediction to the polychromatic case in the same way we did for irreversible fluids.

$$\mathring{A} = \left(1 - \frac{\int_{\lambda_{min}}^{\lambda_{max}} Ir(\lambda)\lambda\epsilon_B d\lambda}{\int_{\lambda_{min}}^{\lambda_{max}} Ir(\lambda)\lambda\xi d\lambda}\right) 10^{-\mathring{t}} + \frac{\int_{\lambda_{min}}^{\lambda_{max}} Ir(\lambda)\lambda\epsilon_B d\lambda}{\int_{\lambda_{min}}^{\lambda_{max}} Ir(\lambda)\lambda\xi d\lambda} \tag{5.42}$$

$$\xi = (\epsilon_A + \epsilon_B - \epsilon_B^2 ln(10) A_0 l) \tag{5.43}$$

The relevant dimensional groups are:

$$\mathring{t} = \frac{t_{exp}}{N_A ch} \int_{\lambda_{min}}^{\lambda_{max}} Ir(\lambda)\lambda\xi d\lambda \tag{5.44}$$

$$\mathring{A} = \frac{A}{A_0} \tag{5.45}$$

Finally identifying the photostationary mole fraction is beneficial for comparison.

$$\phi = \frac{\int_{\lambda_{min}}^{\lambda_{max}} Ir(\lambda)\lambda\epsilon_B d\lambda}{\int_{\lambda_{min}}^{\lambda_{max}} Ir(\lambda)\lambda\xi d\lambda} \tag{5.46}$$

$$\mathring{A} = (1 - \phi)10^{-\mathring{t}} + \phi \tag{5.47}$$

This form is reminiscent of the procedure we applied to Fig. 5-5. Note that the photostationary concentration depends on the spectral irradiance.

In this chapter, we have developed approximations for the time evolution of concentrations for various situations including fluids stimulated by either monochromatic or polychromatic sources, and fluids where one or both species absorb. In the following chapters, we will use the nondimensional groups that are common to these solutions as a compact characterization for both experiments and lamp sources.

Chapter 6

Selection of Fluids

Having developed a framework to predict the speed of transition and power requirements of photoresponsive fluids, we select a few fluids to examine for application in our robot and as case studies for our framework. In this chapter we introduce three fluids, a micellar fluid, a nanoparticle fluid, and a hydrogel, which have various combinations of advantageous properties. We briefly mention the mechanisms behind the change in rheological properties and their possible contributions as robotic components.

6.1 Robotic Needs

Our robotic application requires a fluid that uses a low power commercial stimuli to switch rapidly, preferably reversibly, between rheological states that permit or prohibit a mechanical function. Therefore an optimal fluid would involve a photoactive ingredient with a high molar absorptivity of one state at one wavelength and another also large molar absorptivity at another wavelength. Ideally, the two states would require the transition of only a very small concentration of the photoactive ingredient and would have a large physical change in rheological properties.

Our biggest restriction on the fluids we can test is the ease with which we can synthesize them. Since the population of photorheological fluids is small, this is fairly limiting. We present three fluids that are synthesizable in the laboratory which

present different opportunities both for robotic application and scientific exploration. The micellar fluid is a fluid that starts with a viscosity of approximately 10 Pa.s which then decreases 1000 fold upon irradiation. The laponite fluid is a fluid that is easily pumpable until it is irradiated and then develops a yield stress. Both of these fluids represent one-way transitions and therefore are possibly appropriate for the active slime for the robot. Neither of these would satisfy the ideal case for a mechanism which is switchable. Therefore we include the reversible hydrogel as an example for feasibility studies. While we did not do experiments with this material, we can make some predictions that will help with understanding sizing of stimuli elements and speed of reaction. With this in mind we introduce our materials.

6.2 Materials

New research in photoresponsive chemistry is producing simpler recipes for photorheological fluids. Now engineers can perform 'kitchen chemistry' that limits the complexity of synthesis making photorheological fluids more readily available. Ketner et al. [30] addresses this and combines a cationic surfactant with a photoresponsive organic acid to form a surfactant/micellar solution with viscosity tunable by light. The same group has also developed a nanoparticle based light activated yield stress material. Given that a marked increase in PR fluids is expected from these papers, there is a need to coordinate stimuli descriptions for the purpose of comparing and contrasting such fluids. To further the description put forward in the previous chapter, we conduct experiments on two of these systems: the micellar solution and the laponite solution. For the purpose of our application we also discuss the possibility of using a reversible hydrogel system. The following chapter gives specifics on how each fluid works on a molecular level and how we prepared our materials for testing.

6.2.1 Photoresponsive Micellar Fluid

Ketner's photoresponsive micellar system combines cetyl trimethylammonium bromide (CTAB) with the photoresponsive molecule trans-ortho-methoxycinnamic acid

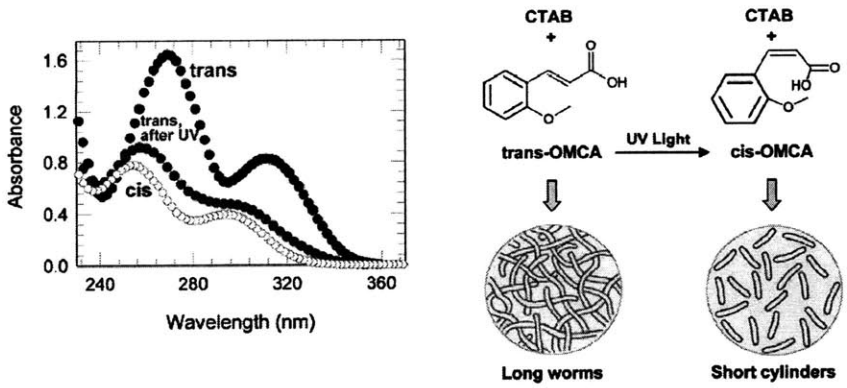

Figure 6-1: A) The absorbance of 1mM of OMCA measured with a Varian Cary 50 spectrophotometer (thickness approximated as 1 mm) B) The viscosity change seen after irradiation is hypothesized as being due to a change from long to short worm-like micelles. These figures are reproduced from [30].

(OMCA). The absorbance of OMCA is shown in Fig. 6-1. Unirradiated CTAB/OMCA mixtures form long wormlike micelles estimated as 3000 $\AA$ in length. Upon irradiation there is a dramatic reduction in the length of the micelles to less than 2% of their original length, estimated now to be 40 $\AA$. This change is effected by the photoisomerization of OMCA which changes the relative energy for various worm geometries and favors the formation of spherical endcaps over cylindrical body segments leading to shorter micelles. Long worms tangle more easily than short worms and therefore the bulk material has a higher viscosity. In this way the fluid changes from being a highly viscoelastic fluid with a zero shear viscosity of approximately 10 Pa.s to a thin water-like fluid with a viscosity $< .01$ Pa.s.

Preparation

OMCA was purchased from Sigma-Aldrich. CTAB was purchased from Aldrich Chemical Company. We used a magnetic stir bar and slight heat to aid the dissolution process. A 10M NaOH solution was used to neutralize the solution. Samples were left to sit for at least a day before testing. The following procedure was used to make suitable OMCA and CTAB solutions for testing.

1. Dissolve weighted amount of OMCA in de-ionized water

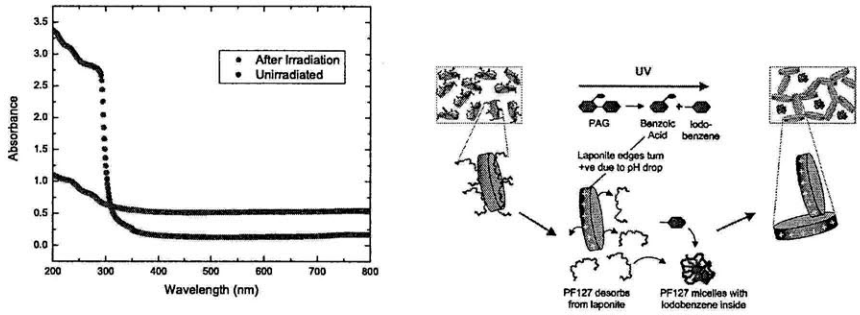

Figure 6-2: a) The absorbance of 13mM PAG, 5% Laponite, 6% PF127 measured with a Varian Cary 6000i spectrophotometer (thickness approximated as 1 cm) b) The appearance of a yield stress is thought to be from the formation of a "house of cards" network. Panel b is reproduced from [51]

2. Measure pH

3. Neutralize solution with NaOH

4. Dissolve weighted amount of CTAB in solution

5. Add NaOH till pH is between 9 and 11

Over the course of this research four batches of OMCA+CTAB solution were tested. These batches are listed in Table 6.1.

Table 6.1: Composition of four batches of OMCA+CTAB solutions prepared for experiments.

Label	OMCA (mM)	CTAB (mM)	pH
A	50.1	59.8	10
B	50.3	60.3	9
C	49.9	60.4	11
D	50.0	82.8	11

6.2.2 Photoresponsive Nanoparticle Based System

We also briefly examine a nanoparticle photoresponsive fluid, [51]. This fluid holds potential as it is very similar to previous slimes based on laponite. Pluronic F127

(PF127) sterically stabilizes dispersions of laponite when it is adsorbed onto the particle faces. This discourages the formation of the "house of cards" network which is thought to be responsible for the yield stress nature of laponite solutions. Upon absorption of UV light the chosen photo acid generator (PAG), diphenyl-iodium-2-carboxylate monohydrate, photolyzes into benzoic acid and iodobenzene. PF127 then forms micelles around iodobenzene and the benzoic acid gives rise to a positive charge on the laponite edges. The whole mixture gains a yield stress when a network forms due to the interactions between the positive edges and negative faces.

Preparation

Laponite was acquired from Southern Clay Products, PF127 from Sigma Aldrich, and PAG from TCI America. A 55 mL sample of 5% Laponite, 6% PF127, and 13mM PAG were dissolved in deionized water. The procedure involved dissolving Laponite into the water in mg amounts while being stirred with a magnetic stir bar and heated. A vortex mixer was then used for over an hour to disperse the particles. PF127 was then added and stirred. A large viscosity change was noted. Finally PAG was added and the solution was stirred overnight.

6.2.3 Photoresponsive Hydrogel

We also include a photoresponsive hydrogel as a promising reversible candidate material. The polymer chains of the hydrogel form an entangled network structure via hydrophobic associations of C12 side chains (Fig. 6-3 (a)). The system has a lower viscosity when α-cyclodextrin forms inclusion complexes with C12 side chains, preventing these hydrophobic associations, shown in Figure 6-3 (b). Because the α-cyclodextrin preferentially attaches to the trans isomer of 4,4-azodibenzoic acid, the hydrophobic associations can be blocked or unblocked depending on whether azodibenzoic acid is in its cis or trans isomer. Azodibenzoic acid (ADA) can be isomerised by photoirradiation, resulting in a photoresponsive system

The material is termed reversible because we can irradiate the sample with wave-

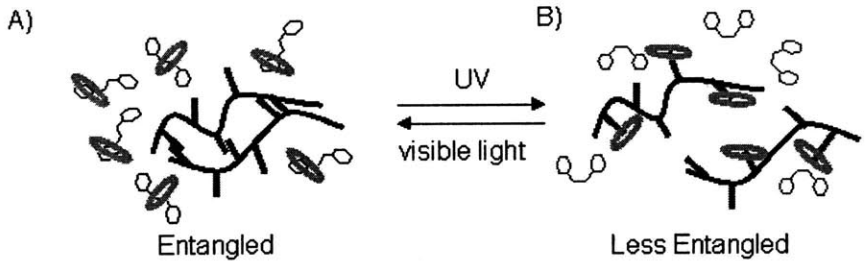

Figure 6-3: A multicomponent system described in [54] is photoresponsive due to α-cyclodextrin and the photoisomerizable azodibenzoic acid competing to bind with 'sticky' C12 sidechains on a poly-acrylic acid backbone

lengths less than 375 nm that will be absorbed by the trans-ADA, which then becomes quasi-cis, or we can irradiate it with violet/blue light that will be absorbed by the quasi-cis state which then becomes the trans isomer. This can be repeated a number of times to switch between the two viscosity states as seen in Fig. 6-4 (b).

Synthesis

While ADA and cyclodextrin can be purchased commercially, the hydrogel must be modified to include the C12 side chains. This is a simple synthesis procedure if the lab is equipped with standard chemical equipment. We have synthesized this material for future research. We have not done further experiments with this material due to the need for good environmental controls (e.g. light isolation) during in situ testing.

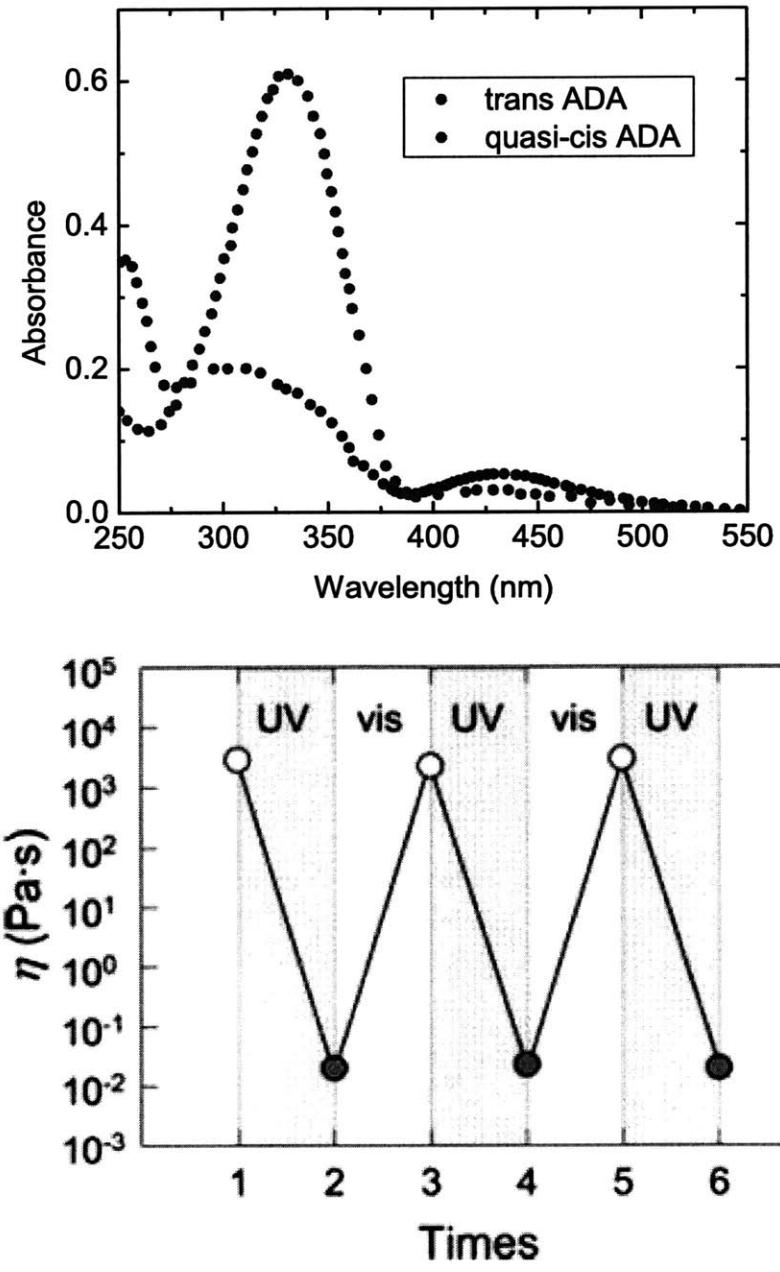

Figure 6-4: a) UV-vis absorption spectra of 2.5×10^{-5} M ADA collected by a Shimadzu UV-2500PC spectrophotometer using a 1 cm path length quartz cuvette. b) A ternary mixture of 5.0 g/L modified hydrogel, 10.0 g/L α-cyclodextrin, and 1.0 g/L azodibenzoic acid experiencing repetitive irradiations with UV (closed) and visible light (open) Both panels are reproduced from [54]

Chapter 7

Experiments and Polychromatic Behavior

Our aim in this chapter is two fold. Firstly, we wish to provide validation of the suitability of the material for robotics and secondly, to provide validation of the theory for polychromatic illumination developed in Chapter 5.

7.1 Optical Hardware

As we have suggested that a method for characterizing our light source is an important task, we begin by describing the UV lamp and related aspects of the experimental setup. The light delivery system consists of two pieces; (i) the lamp and its accessories, and the (ii)external hardware and optics, such as the UV rheometry fixture.

7.1.1 Experimental Setup

Light Source

There are many different applications utilizing UV light from forensics to sterilization. It is not surprising, therefore to find a broad range of mercury or xenon light sources on the market spanning UV lamps, LEDs, and lasers. All of these function in different ways and produce different colored spectra. For our purposes, the most important

selection criteria besides emitting in the UVA range is repeatable irradiances at the cure site. Not many lamps on the market allow intensity adjustments. Those that do are intended to counteract the degradation of the lamp bulb that leads to increasingly dimmer outputs. Because of this, most of the intensity adjustment features are manual and involve the user setting the output at a level that can be maintained throughout the curing process. For our experiments, we selected a UV lamp that features an automatic intensity adjustment feature, Fig. 7-1. The EXFO Omnicure S2000 is a lamp with a high pressure 200 watt mercury vapor short arc bulb and features "closed feedback technology" developed by EXFO. The EXFO lamp, with a standard 320-500nm filter installation, delivers a spectrum of UVA (315-400nm) and blue-green visible spectrum light detailed in Fig (7-2). This spectrum was collected using the Institute for Soldier Nanotechnologys Ocean Optics USB2000 Fiber Optic Spectrometer. The absolute spectral intensity was determined by calculating the area of the relative spectral intensity (arbitrary units) and normalizing it to the measured total irradiance.

The closed feedback technology of the EXFO Omnicure S2000 lamp was a key reason for the selection of this lamp. Over the lifetime of a lamp, the bulb degrades, notably 20% over the first 500 hours of use. To ameliorate this, the Omnicure S2000 has an adjustable iris that can be opened and closed to let more or less light through to the waveguide. This operation does not change the relative spectrum of the emitted light. This iris is controlled through a calibrated intensity sensor located close to the bulb. The user can therefore set an intensity less than the current maximum output and the output will remain within 2% of the commanded value. The entirety of the tests reported here were performed within the first 50 hours of lamp use. This lamp enables us to control the total irradiance present at the sample.

Waveguide

In conjunction with the S2000, we used a 5mm diameter liquid light guide (EXFO) which is 1 meter in length and suitable for signals within the wavelength range between 250 to 600 nm. A difference in measured irradiance between a straight waveguide and

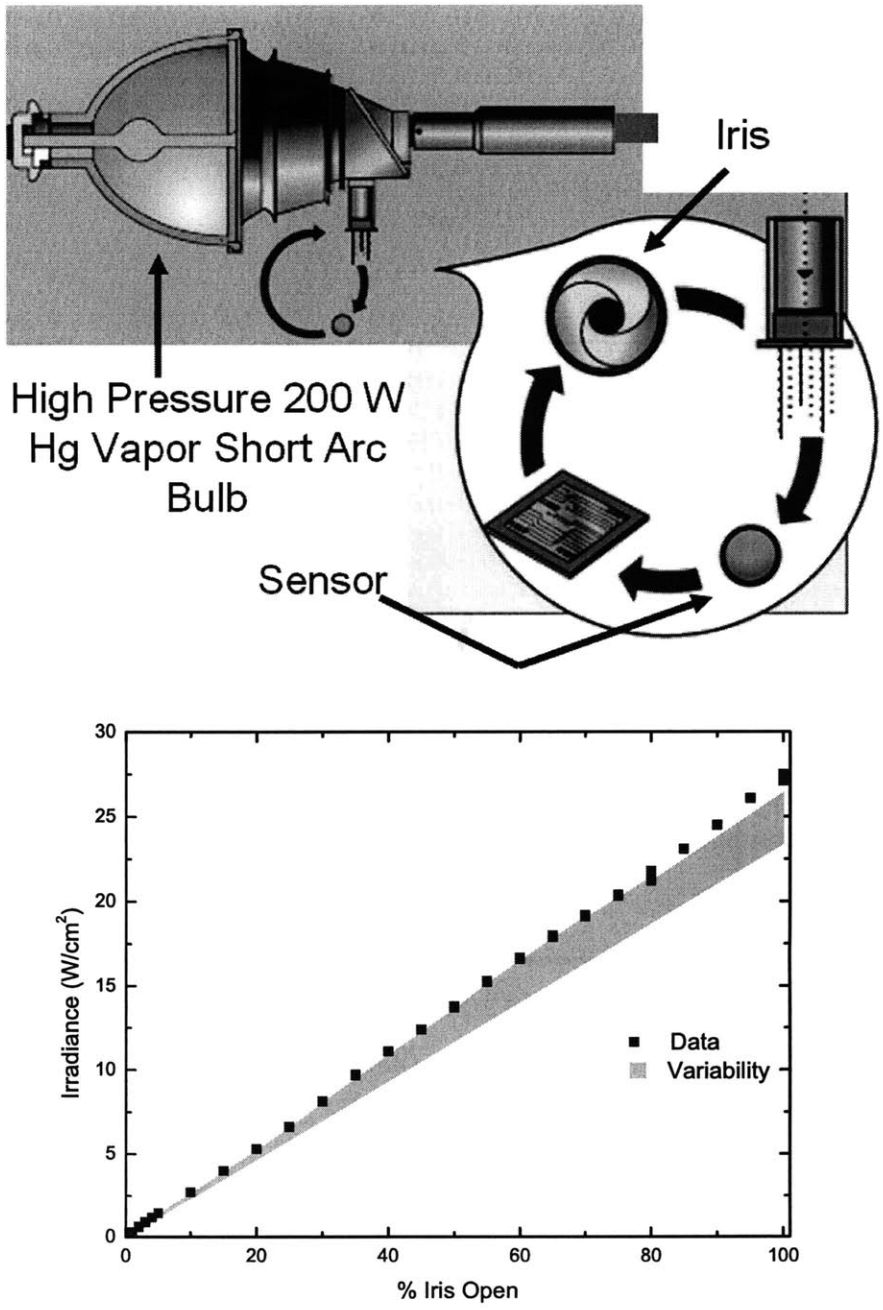

Figure 7-1: a) The EXFO S2000 lamp features a closed loop feedback system. A calibrated intensity sensor monitors the total intensity exiting the lamp while an iris opens and closes to produce the desired intensity. Panel adapted from [32]. b) We demonstrate that the irradiance is linear with the percent of the iris that is open, particularly at smaller desired irradiances.

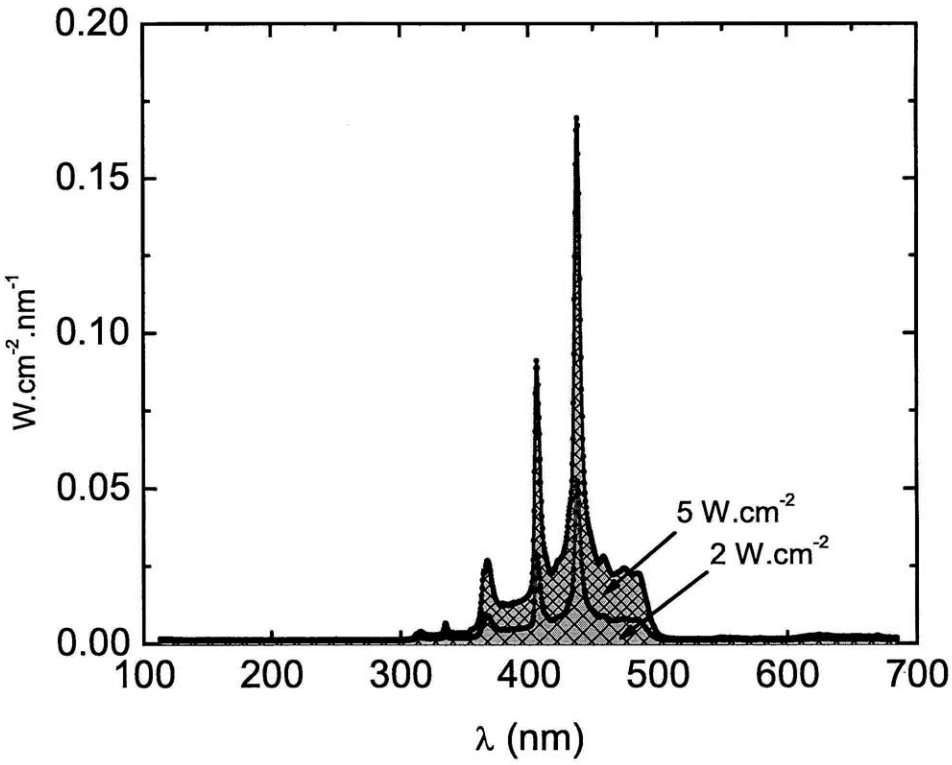

Figure 7-2: Comparison of spectral irradiance between two different total irradiance settings of the S2000 using the Ocean Optics USB2000 Fiber Optic Spectrometer. Note that the spectrum does not shift between the two tests despite the difference in total irradiance.

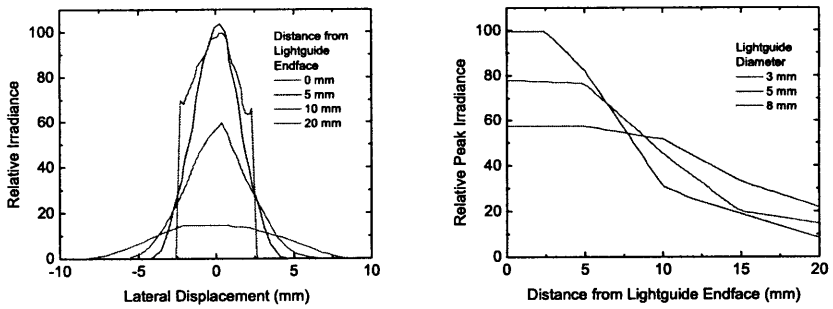

Figure 7-3: Uncollimated light sources exhibit variation in relative irradiance both across the cross-section of the beam (a) and along the path length (b). a) Illustrates the variation across the cross-section of a beam from a 5 mm diameter waveguide. b) Illustrates the variation in the peak irradiance from three waveguides with path lengths greater than 2 cm. Figures recreated from data supplied by the S2000 manufacturer [33]

a bent waveguide was noted during operation. Therefore, all subsequent tests were performed with the waveguide fully extended. The light emitted from the end of the waveguide is assumed to be incoherent, uncollimated (diverging) light. If desired, a collimator can be added to the end of the wave guide so that the emitted ray is effectively a parallel beam and can be focused. The manufacturing specifications in Fig 7-3 suggest that the energy of the beam is relatively evenly distributed across its cross section 2cm away from the end plate. Collimating the light may have other benefits such as lessening the peak irradiance decay shown in Fig 7-3 (b), but with a trade-off in reduced overall irradiance. As the path length of the light from waveguide to sample is larger than 2 cm, the experimental errors due to the lack of a collimator are likely smaller than those introduced by the long path length (> 10 cm).

ARES UV Fixture and Other Hardware

Neither the lamp nor waveguide can be easily adapted to include filters and since the intensity sensor of the lamp is calibrated with the manufacturer installed filter, replacing the filter is not an option.[1] A vertically adjustable stage (not pictured) is

[1]To test the wavelength dependence of the proposed theory one could use bandpass colored glass filters to manipulate the spectral distribution of the beam. A filter wheel may be used in conjunction with the described equipment to test the wavelength dependence of the above theory as shown in

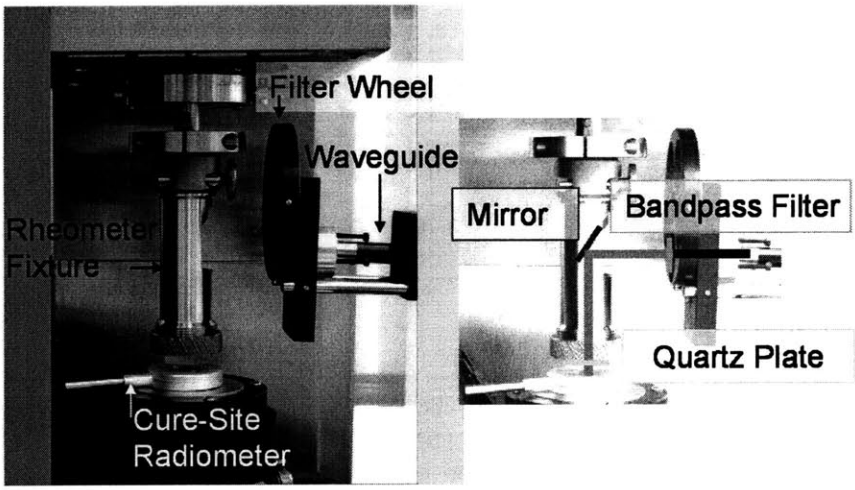

Figure 7-4: The beam from the lamp travels from the waveguide through open air to the ARES rheometer UV curing fixture where it is redirected by a mirror through a quartz plate and to the sample. We use two radiometers to measure the irradiance: one that measures the irradiance at the waveguide endface and one that measures the irradiance of the beam at the cure site.

used to fine tune the alignment of the waveguide with the latter optics. The next piece of equipment in the beam path is the ARES UV curing accessory. This fixture is a cylindrical tube with a window through which the beam passes. The beam enters the tube and hits a mirror placed at a 45 degree angle to the long axis of the cylinder. The light then travels down the tube to a quartz plate 1cm thick. Quartz has a transmission profile that has at least a 90% transmission in the range of UVA and UVB so we can expect the the spectrum to be unaltered upon exiting the fixture. The path length from endface of the waveguide to the mirror of the rheometer is approximately 5 cm and from mirror to the end of the quartz plate 5.5 cm. After this the material absorbs the beam according to the absorbance curves in Chapter 6.

7.1.2 Characterization

This detailed description of our optics should ideally collapse all this information into a single metric. Ultimately, we wish to report the relevant nondimensional time for the materials tested as discussed in a previous chapter. We make the approximation

Fig. 7-4. However in our setup the beam passes through the filter wheel without modification.

that the area of the sample is the same area as the quartz plate, and that the thickness of the sample is equal to the gap height. We also need to measure the irradiance of the beam at the cure site which is accomplished with two radiometers.

Radiometers

Certain radiometers may be more or less appropriate for certain sources. For instance, for noncollimated light sources measured irradiance may depend on the angle of incidence leading to results dependent on the orientation of the probe. Therefore an integrating sphere style detector is preferred over the flat pan detector style. Since the technology within both radiometers is proprietary, we focus on contrasting the specifications that the manufacturers provide and experimental data.

Table 7.1: Comparison of specifications of the Accu-Cal 50 radiometer and the R2000 Radiometer

Radiometer	λ range	Power Range	Resolution
Accu-Cal 50	320-395 nm	$1\frac{mW}{cm^2} - 40\frac{W}{cm^2}$	$1\frac{mW}{cm^2}$
Omnicure R2000	250-1000 nm	$5\frac{mW}{cm^2} - 60\frac{W}{cm^2}$	$5\frac{mW}{cm^2}$

Both radiometers have an accuracy of 5%-10%.

The R2000 is a radiometer that is sold in conjunction with the S2000 lamp and is meant to be used to calibrate the lamp to an absolute intensity. It also serves to measure the light irradiance emitted from the waveguide. The Accu-Cal 50 is a radiometer that is sold by Dymax. The advantage of the Accu-Cal is its slim wand like construction allowing for the evaluation of the irradiation right at the cure site. It also can be used in a manner similar to the R2000 by screwing the waveguide directly into the radiometer with the aid of a 5mm waveguide adapter. The two radiometers have different sensitivities and must be calibrated based on one another (Table 7.1).

Based on the reported wavelength range, the Accu-Cal measures 13.7% of the spectrum whereas the R2000 measures 96% of the spectrum. We are not told to what degree the Accu-Cal is sensitive to wavelengths outside of this wavelength range. Not only does the spectrum to which the R2000 is sensitive match the measured spectrum

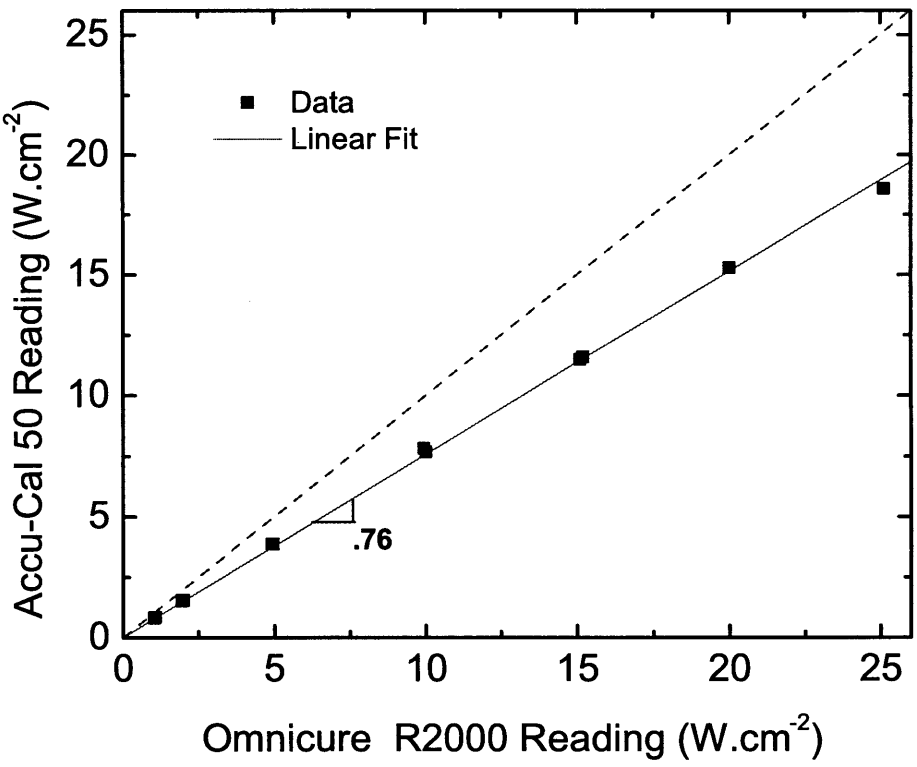

Figure 7-5: The radiometers systematically report different irradiances measured at the end of the waveguide. The ratio of the two radiometer measurements is constant over the operating range of the lamp.

of the lamp, the R2000 has been calibrated recently according to NIST standards. Therefore, we use the R2000 to calibrate the Accu-Cal. To do this we used the 5mm adapter to the waveguide and measured the irradiance for various settings with both the Accu-Cal and the R2000. Over this range, the R2000 consistently produced the lamp setting. The ratio between the two radiometer measurements, see Fig 7-5, is used to adjust the measurements from the Accu-Cal.

Compact Characterization

We can combine the spectral irradiance of the source, the absorbance profiles of the materials, and the experimental geometries imposed by the rheometer and sample volume to calculate t' and $\tilde{t}$ defined in chapter 5 for the two candidate fluids.

Table 7.2: Relevant time constants, t' and $\tilde{t}$, reported as experimental description given S2000 polychromatic source and candidate fluids

	Micellar Fluid	Nanoparticle Fluid
t'	$6.02 \times 10^{-6} t_{exp} \lvert Ir \rvert$	$2.12 \times 10^{-6} t_{exp} \lvert Ir \rvert$
$\tilde{t}$	$8.08 \times 10^{-5} t_{exp} \lvert Ir \rvert$	$1.47 \times 10^{-6} t_{exp} \lvert Ir \rvert$

7.2 Rheological Testing

The rheological measurements of the micellar candidate fluid are important for two reasons. Firstly, rheology is the primary way to evaluate whether a fluid is a good candidate for a robotic component. Secondly, they provide a means to validate the proposed model. In this context, the rheological data indicates the change in concentration of the photoresponsive components of the fluid with time. This is not a direct link between concentration and rheological measurements, because these fluids rely on a second or third reaction to bring about the rheological change, for instance a shortening of micelles [30], [18]. While this complexity is a hindrance, we may explore it in greater detail after the model is validated. For instance, by precisely controlling the concentration of a relevant species at a particular time, we can study both how the concentration impacts the rheology and on what time scale that change occurs.

Without our proposed framework, the experimentalist needed to mix up new samples to study concentration dependence. Now triggering the concentration in the same way as one triggers a high speed camera may be possible.

7.2.1 Rheometer

The majority of the tests were preformed using an Ares rheometer (TA Instruments), a strain controlled rheometer, with the parallel plate UV curing accessory described previously (Diameter D =20 mm, Gap $l = 500\mu$m). A Peltier plate kept the samples at a consistent temperature of 25^{o}C. Dynamic frequency spectra were obtained in the linear viscoelastic region according to a strain amplitude sweep performed at the beginning of the test. Most of the experiments involved performing a single shear flow test or oscillatory test over time while the sample was irradiated. Note that measuring the rheology of time-evolving materials during curing provides a unique challenge to rheologists. For instance, as the material changes, the chosen strain amplitude may no longer guarantee that the fluid is being tested in the linear regime. Moreover, a particular geometry/material combination that was appropriate at the beginning of the test may no longer be appropriate at the end of the test when the fluid has changed significantly. Knowledge of both the initial rheological state and the final rheological state must be applied whenever possible. Finally, because the curing process removes the ability to perform the traditional sweeps in frequency or strain rate, this data must be collected one point at a time and stitched together from several experiments, to obtain a more complete picture of the fluid.

7.2.2 Small-Amplitude Oscillatory Shear Flow

We briefly describe the collection of rheological data from small-amplitude oscillatory shear (SAOS). In SAOS, we use the rheometer to impose a small amplitude oscillation of the form:

$$\gamma = \gamma_0 \sin(\omega t), \tag{7.1}$$

where γ_0 is the strain amplitude and ω is the angular frequency of oscillation. If the shear strain amplitude, γ_0, is sufficiently small, then the shear stress will be linear in strain and strain rate [4]. We can therefore write

$$\tau_{xy} = -A(\omega)\gamma_0 sin(\omega t + \delta). \tag{7.2}$$

Here $A(\omega)$ is the amplitude of the stress and δ is the phase angle between the imposed strain and the measured stress. We can then separate this oscillating stress into the component that is in phase with the strain and the component that is in phase with the strain rate:

$$\tau_{xy} = -G'(\omega)\gamma_0 sin(\omega t) - G''(\omega)\gamma_0 cos(\omega t). \tag{7.3}$$

G'' scales the component of the response that is proportional with the strain rate and is sometimes called the 'loss modulus' for its similarity to a damper. In the same way, G' scales the component proportional to strain and is sometimes called the 'storage modulus.' We will also chose to relate these components together as a single component called the complex modulus,

$$|G^*| = \sqrt{G'^2 + G''^2} = A(\omega). \tag{7.4}$$

This complex modulus relates the stress to the strain. We can also write a complex viscosity that relates the stress to the strain rate. The relationship between the complex modulus and complex viscosity is as follows:

$$|\eta^*| = \frac{1}{\omega}|G^*|. \tag{7.5}$$

For some materials, one may relate the oscillatory data collected to how the fluid behaves under simple shear flow. To do this one may apply the Cox-Merz rule [4] which states that the complex viscosity can approximate the shear flow viscosity for

strain rates corresponding to the angular frequency ($\dot{\gamma}(\frac{1}{s}) = \omega(\frac{rad}{s})$),

$$|\eta|_{\dot{\gamma}} = |\eta^*|_{\omega}. \tag{7.6}$$

Due to the autocorrelation software employed by the Ares, data was reported every seven seconds.

7.2.3 Procedure

The material tested in this chapter is the photoresponsive micellar fluid described as batch D in Table 6.1, composed of 50mM OMCA and 83mM CTAB. Each test began by checking that the light system was well calibrated with both the R2000 radiometer and the Accu-Cal 50 radiometer. The light system was then aligned with the installed UV fixture. The cure site radiometer was used to take a measurement at the position where the sample would be loaded. The fixture was raised to accommodate the thick radiometer. Because this meant that the waveguide was no longer aligned squarely with the fixture window, the waveguide stage was adjusted, and both the first and maximum reading were recorded. The radiometer was then removed and a micro-pipette was used to load the ample. By cutting the excess fluid away with a razor blade, the sample was made to be flush with the upper plate. The waveguide and stage were then realigned. An experiment was performed usually involving UV irradiation at a specific irradiation and time. After testing, the sample was removed and the Peltier plate cleaned.

7.3 Results

In this section we report the results of our experiments. To begin, Fig. 7-6 details the rheology of the fluid in response to steady shear and oscillatory flows before irradiation takes place. The fluid is shear thinning, as it has a lower viscosity at higher rates, and is viscoelastic.

Fig. 7-7 shows the results of steady shear tests at three different strain rates at

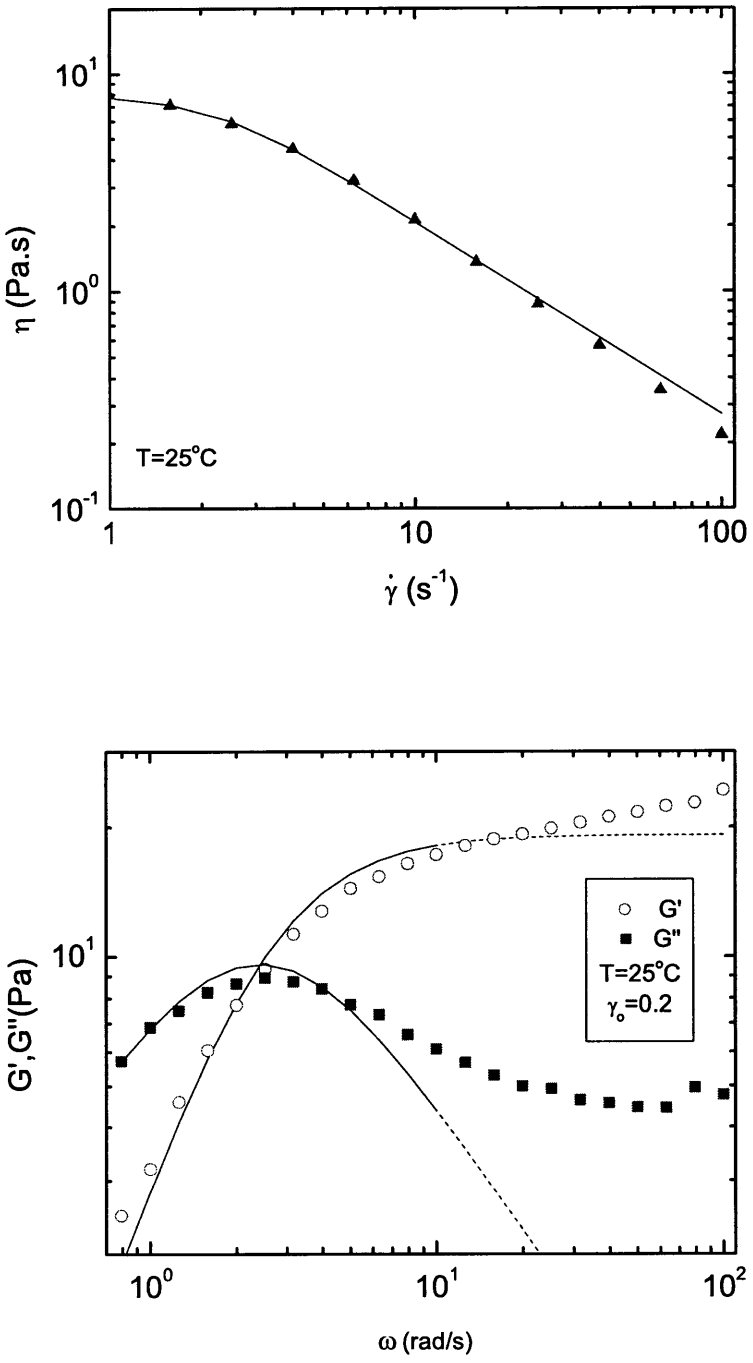

Figure 7-6: a) The steady shear viscosity as a function of shear rate before the sample (50 mM OMCA and 83mM CTAB) is irradiated, fitted with the Carreau Yasuada model: $\eta_0 = 8$Pa.s, $\lambda = 0.46$s, $a = 2.79$, $n = 0.042$. b) The dynamic moduli as a function of angular frequency of the unirradiated sample is fitted with the generalized Maxwell model: $\lambda = 0.41$s, $g_1 = 19.2$ Pa.

constant irradiation. We have demonstrated that we can control the irradiation and that our results are repeatable. The lower bound of the results are limited by the torque resolution of the rheometer, $T_{min} = 2\mu$N. Further analysis cannot be completed using the current experimental setup as a UV compatible geometry such as a quartz couette cell is not available.

To examine the effects of different irradiances on the evolution of rheology with time, we expose several samples to increasingly intense beams. Fig. 7-8 details the storage and loss modulus as a function of time for a fixed frequency of 30 rad/s at different irradiances. From this graph, we can see that the rheological properties are not necessarily linear with concentration as G'' rises despite a certain drop in concentration of the trans-isomer of the photoactive ingredient. The curves from each irradiance for a given modulus are similar with one another. We will later explore whether the model correctly predicts how to scale the time axis to have these curves collapse together.

7.3.1 Analysis

To compare the theoretical model with the experiments performed, we need to relate the rheological measurements to the concentration of the photoresponsive species. We did not perform any concentration studies of the rheology, however. Instead we will use published data of how the zero shear viscosity changes with concentration of a similar solution. We reproduce this data as Fig. 7-11 [30].

Possible Application of Constitutive Models

At low shear rates, the material imposes so little stress that the instrument cannot produce consistent measurements over time while the fluid cures. Therefore we did not collect how the zero shear viscosity changes as a function of time from our in-situ experiments. Instead, we relate oscillation data at moderate frequencies to a viscosity at corresponding shear rates through the complex viscosity, $\eta*$, as detailed previously. A range of models can be used to find the zero shear viscosity from

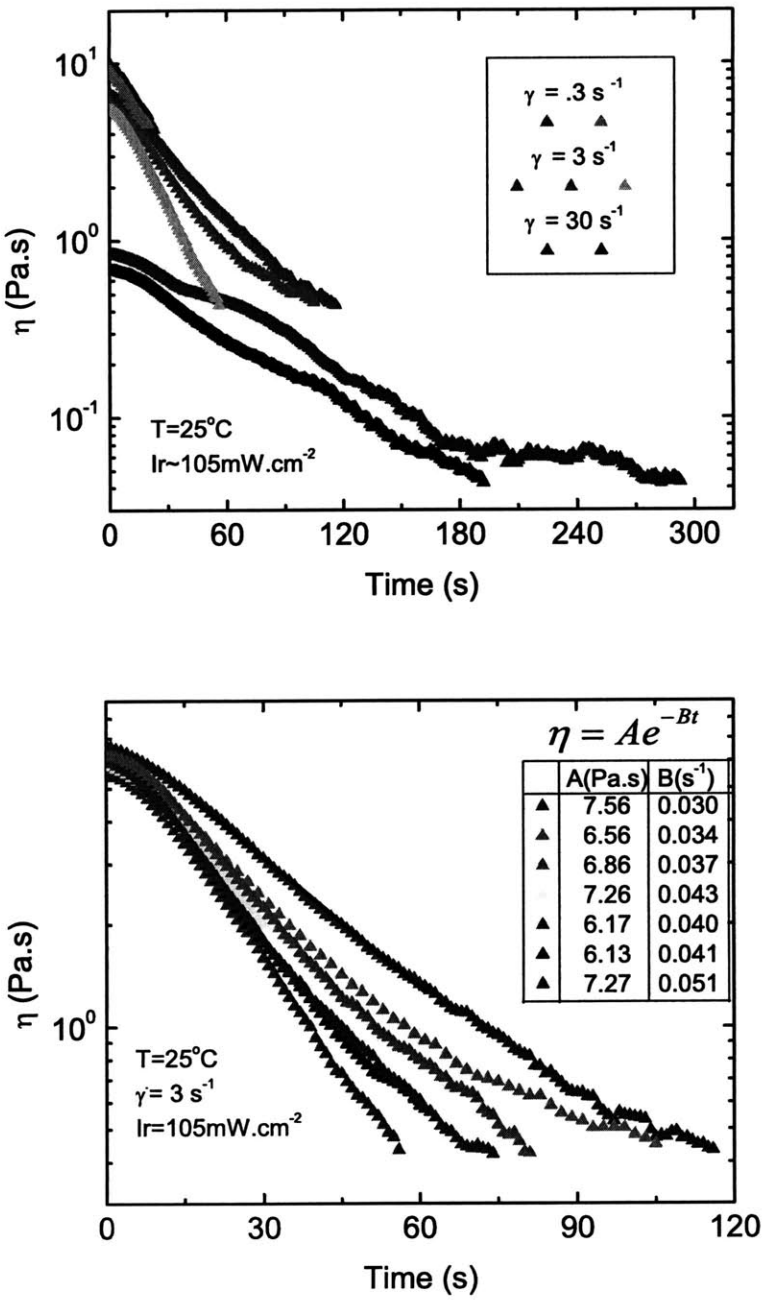

Figure 7-7: a) Time evolution of the steady shear viscosity at different strain rates for the 50mM OMCA + 83 mM CTAB solution during irradiation. b) Repetition of the steady shear test on this sample illustrates the reproducibility of data collected during irradiation. The time constants, have a mean ($\bar{B}$) of .0329 s^{-1} with a standard deviation of $6.8\times10^{-3}s^{-1}$ and the coefficients have a mean ($\bar{A}$) of 6.83 Pa.S with a standard deviation of 5.63 $\times10^{-1}$ Pa S.

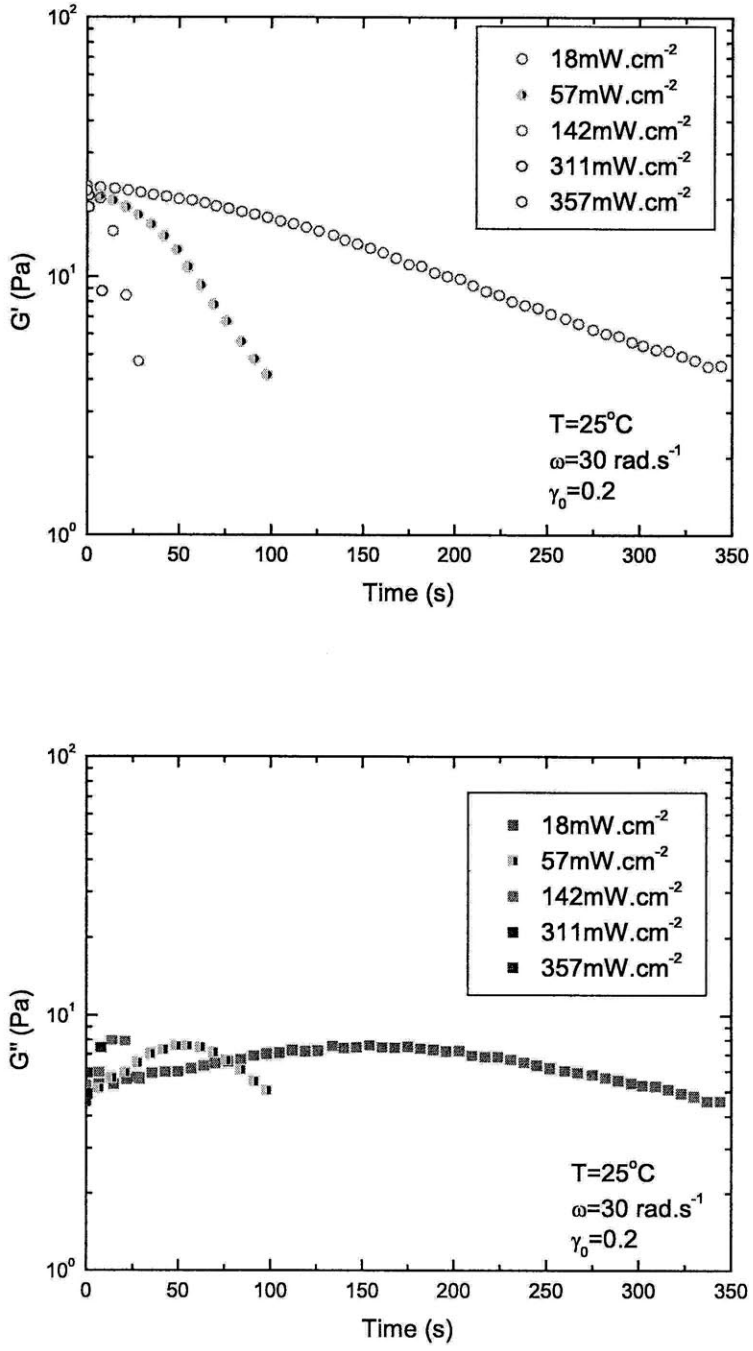

Figure 7-8: The moduli change over time as a 50 mM OMCA + 83 mM CTAB sample is irradiated. Here, each experiment corresponds to a different beam irradiance (measured at the cure site). Lower irradiances lead to longer times required to reach a desired modulus value, while higher irradiances require less time.

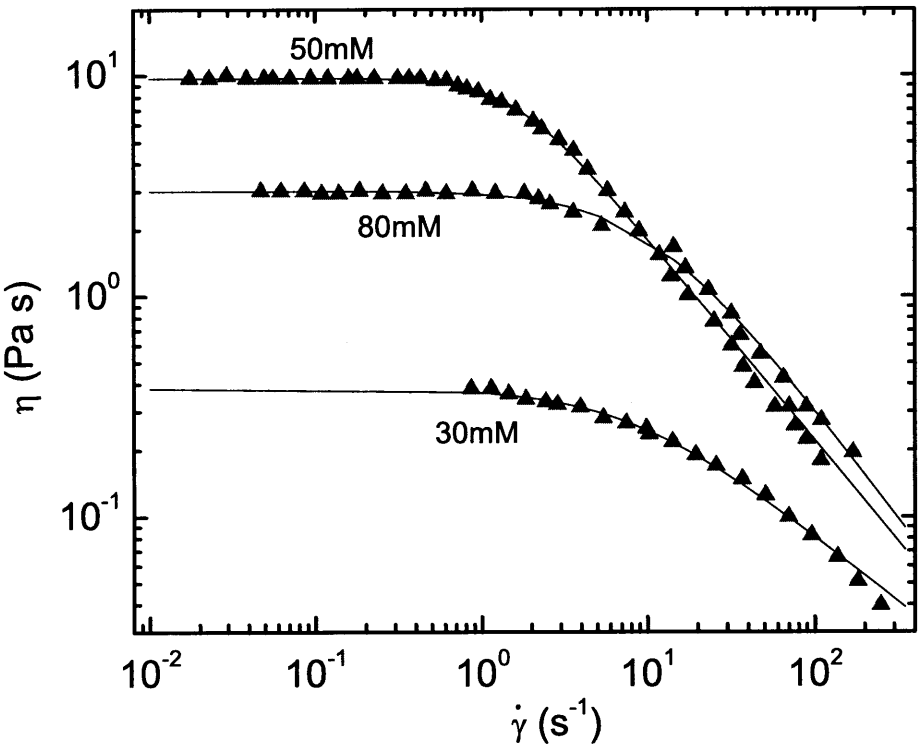

Figure 7-9: The shear viscosity as a function of strain rate for different weighted amounts of OMCA with 60 mM CTAB, re-plotted from Ketner et al [30]. The fit is to a simplified Carreau Yasuda model with the empirical constants listed in Table 7.3

the complex viscosity, if they are applicable, [4]. For instance, a simplified Carreau-Yasuada model might be fit to our data as we can assume that the viscosity approaches zero as we approach infinite shear rates:

$$\frac{\eta}{\eta_0} = [1 + (\lambda\dot{\gamma})^a]^{\frac{n-1}{a}}. \tag{7.7}$$

This model however involves three fitted parameters: a which describes the breadth of transition from Newtonian to power-law behavior, n which describes the power law exponent, and λ which determines the shear rate at which the transition occurs from the zero shear rate plateau to the power law region. The generalized Maxwell model

is also a possible model:

$$\underline{\underline{\tau_k}} + \lambda_k \frac{d\underline{\underline{\tau_k}}}{dt} = -\eta_k \underline{\underline{\dot{\gamma}}} \tag{7.8}$$

where $\eta_k = G_k \lambda_k$ The small amplitude oscillatory shear material functions satisfying the generalized Maxwell model are

$$G'(\omega) = \sum_{k=1}^{N} \frac{g_k \lambda_k \omega}{1 + \lambda_k^2 \omega^2}, \tag{7.9}$$

$$G''(\omega) = \sum_{k=1}^{N} \frac{g_k \lambda_k^2 \omega}{1 + \lambda_k^2 \omega^2}. \tag{7.10}$$

We truncate at k=1 as the first mode is sufficient to capture the low frequency dynamics. To determine whether either model can be used to predict the zero shear viscosity, we examine shear flow responses for different concentrations (Fig. 7-9) and oscillatory responses for tests with increasing exposure (Fig. 7-10). Tables 7.3 and 7.4 show that the fitting parameters for each data set vary with exposure and equivalently, concentration. Therefore these empirical models are inappropriate to apply to the data unless each concentration has been fitted separately.

Table 7.3: Fitting parameters for simplified Carreau Yasuda model of data shown in Fig. 7-9 of weighted amounts of OMCA and 60 mM CTAB

Concentration	η_0(Pa s)	λ (s)	a	n
80mM	3.01	0.10	1.27	0
50mM	9.72	0.62	2.02	0.04
30mM	0.38	0.12	1.12	0.35

Table 7.4: Fitting parameters for Maxwell model for data shown in Fig. 7-10 and the resulting zero shear viscosity. The sample is initially 50 mM OMCA + 60 mM CTAB and then undergoes irradiation for the time specified.

Exposure	g_1 (Pa)	λ_1 (s)	$\eta_0 = g_1\lambda_1$ (Pa s)
0 min	16.47	0.41	6.75
5 min	10.66	0.32	3.41
15 min	6.91	0.25	1.72

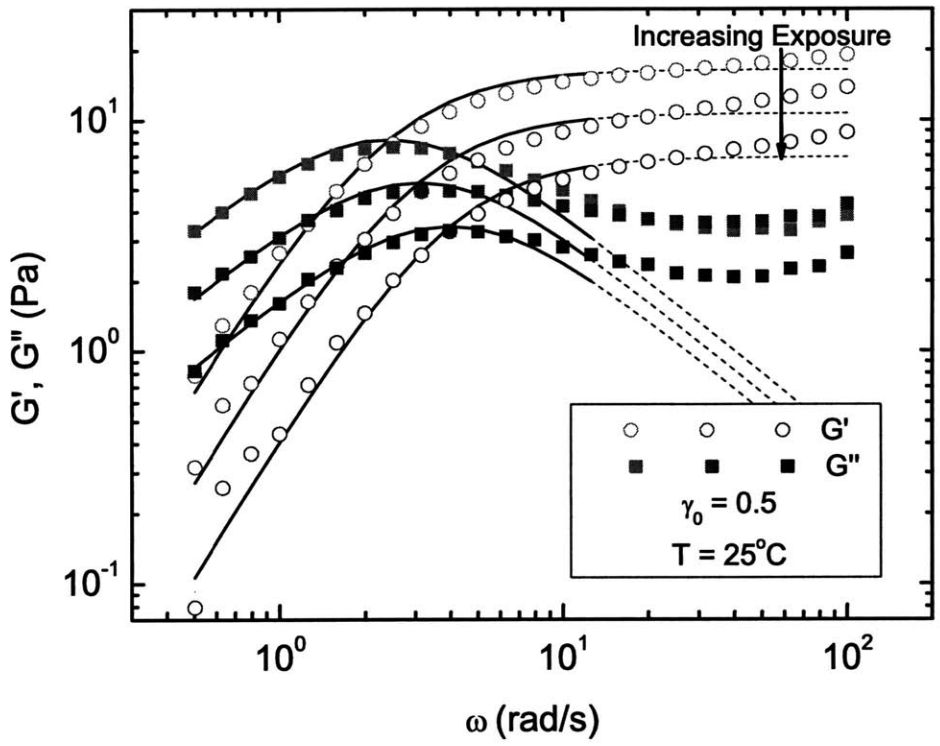

Figure 7-10: Exposure of 50 mM OMCA + 60 mM CTAB sample by an uncharacterized UV lamp for set periods of time. A Maxwell model is fit to each curve with parameters listed in Table 7.4.

Approximation of Viscosity as Zero Shear Viscosity

In order to use the concentration analysis completed by [30], we must find another way to determine the zero shear rate viscosity besides the application of the above models. In the future, we plan to measure the complex viscosity at the given frequency for varying concentrations therefore mapping what concentration is implied at a given material property. In the absence of this, we make the crude approximation of the viscosity at a corresponding strain rate to 30 rad/s is approximately equal to the zero shear viscosity. Our irradiation experiments, first introduced in Fig. 7-8 were carried out at this angular frequency and motivate this choice.

This is a coarse approximation as the fluid has already been identified as a shear thinning fluid. Using the empirical fit between zero shear viscosity and concentration in Fig.7-11, we estimate the final concentration of trans-OMCA of our samples during irradiation. We use this as a lower bound of our data. As an upper bound, we note that this method underpredicts the initial concentration given the measured complex viscosity. We take the difference between this predicted initial concentration and the known initial concentration and use this as a correction to achieve the upper bound. The error bars described are illustrated in Fig 7-12 for the final points of the SAOS experiments in Fig. 7-8. We take the average of the bounds in concentration to choose the scale with which to compare our concentration and our complex viscosity measurements in Fig 7-13. This scaling implies that $\eta* = (.005)10^{44.29[\mathrm{OMCA_{trans}}]}$ and is used again in Fig. 7-17.

We note that the shear flow experiments taken at a strain rate of 3 s^{-1} in Fig. 7-7, provide a better estimate of the evolution of the zero shear rate viscosity, although we do not have the experiments at various irradiance for this experimental condition. Again using the empirical relation derived from [30], we similarly relate viscosity to concentration in Fig. 7-15 by the relationship $\eta = (1.23 \times 10^{-3})10^{76.27[\mathrm{OMCA_{trans}}]}$.

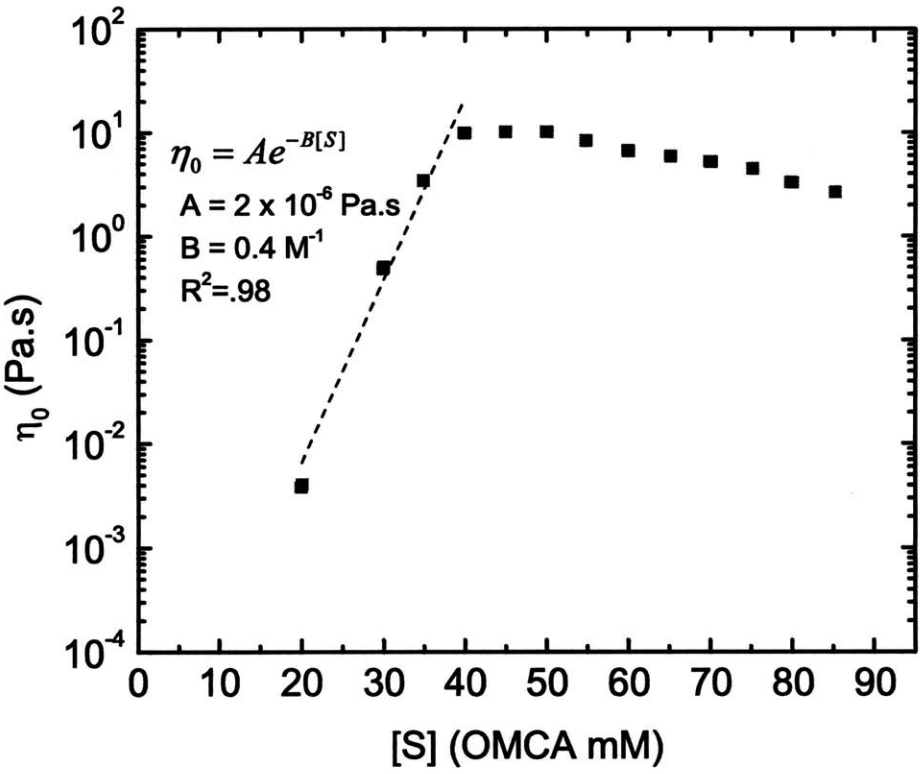

Figure 7-11: Data describing the relationship between weighted amounts of trans-OMCA + 60 mM CTAB concentration and zero shear viscosity reported in Ketner et al [30]. Using an exponential fit, we approximate a relationship between the concentration of the OMCA and the viscosity to be used in our comparisons between experiment and theory.

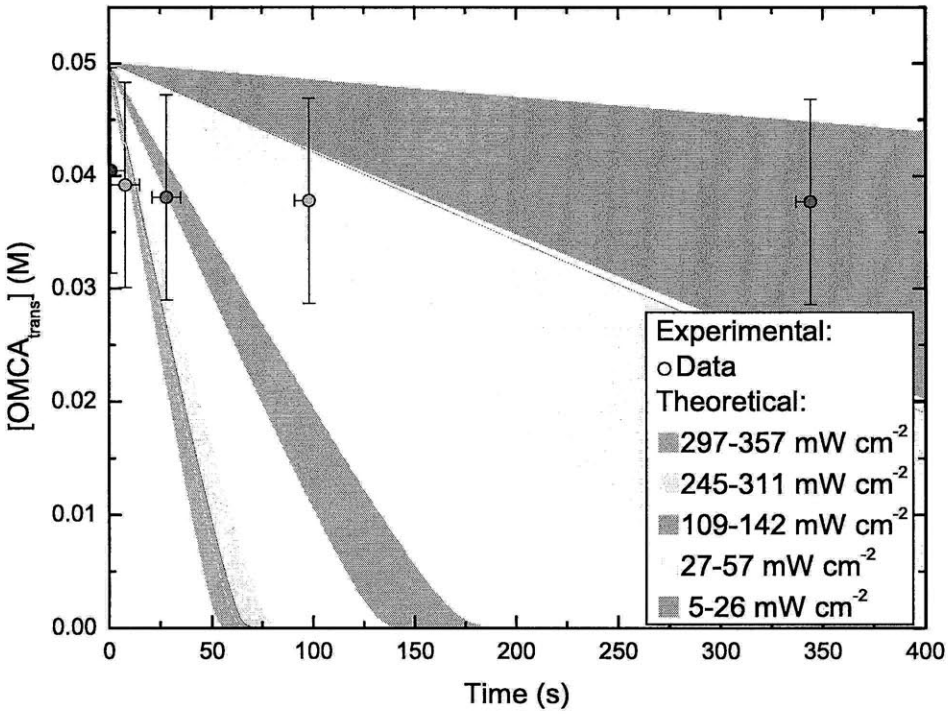

Figure 7-12: Estimation of final concentration of OMCA from the rheological data taken and relationship derived from Fig. 7-11. This is then compared to our model's prediction of the concentration given the experimental conditions.

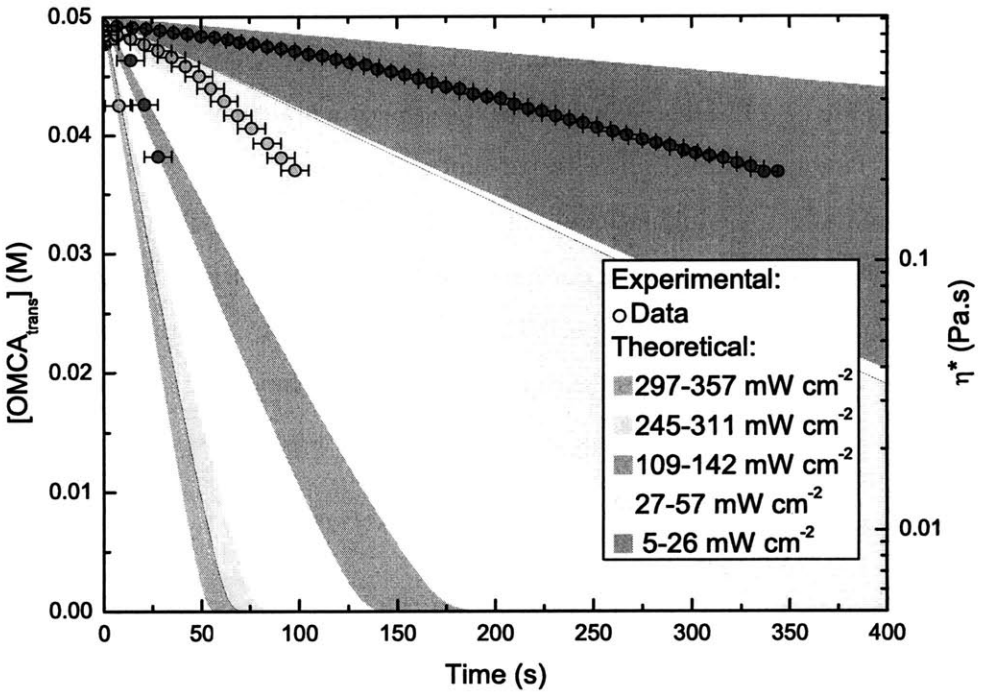

Figure 7-13: Comparison of complex viscosity, $\eta*$, experimental data with theoretical prediction. The concentration and complex viscosity axis have been scaled to reflect the empirical relationship between concentration and $\eta*$.

Comparison between prediction and experiment

The colored swaths in Fig. 7-12 and Fig. 7-13 were generated using a standard numerical solver applied to the nonlinear differential equation, Eq. (5.4). We used the first and the maximum irradiance measurements recorded by the radiometer as bounds for the irradiance for each trial, with the exception of the lowest irradiance test where the error tolerances of the radiometer and the maximum measurement were used. These swaths are in reasonable agreement with the experimentally measured complex viscosities. After noting that the experimental data fall in the linear portion of the evolution of the concentration, we choose to scale the moduli in Fig 7-8 linearly by t' as in Fig. 7-14. The regions where the experimental curves do not overlap may be because the data acquisition software captures a measurement only every 7 seconds. This would affect the higher irradiance trials predominately which is reflected in Fig. 7-14. The agreement between curves indicate the suitability of the t' scaling as well as the repeatability of the experiment. These figures in addition to Fig. 7-13 are taken as validation of the polychromatic form of our model.

7.4 Limitations and Extensions

In this section we provide a brief set of examples of the rich exploration that can be done with in-situ photorheological testing in conjunction with the concentration data predicted by our model. Specifically we present 'dose' experiments and a comparative study of irradiation with a temperature ramp as a means of studying micelle dynamics.

7.4.1 Dose Experiments

Beyond validation, the in situ tests can provide a window into the chemical and microstructural dynamics of a fluid. In addition to the time evolution experiments, we also irradiated the sample for specific lengths of time and recorded the material response after the light source was turned off. By conducting these 'dose' experiments, we investigate the validity of assuming that the chemical dynamics of the photore-

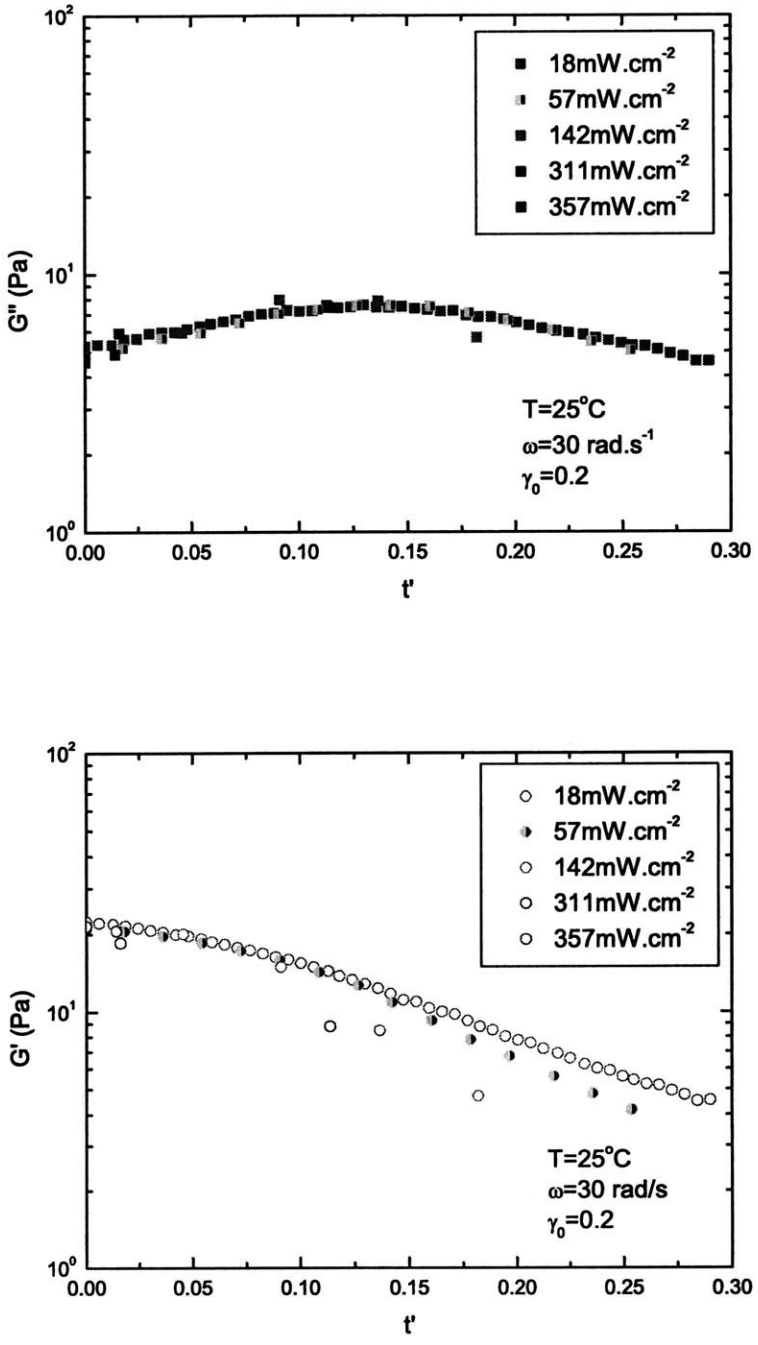

Figure 7-14: The evolution of moduli during irradiation with time axis scaled to t'. In contrast to Fig. 7-8, the data has collapsed onto characteristic curves.

sponsive species are either the only or the limiting dynamics with respect to material response. In Fig. 7-15, Fig 7-16, and Fig 7-17, we see a significant recovery upon the interruption of irradiation. This may be due to the concentration of the trans-OMCA increasing, or the re-assembly of worm like micelles. The cause of the recovery remains an open question for future research. These experimental results limit the application of our model by showing that the sample has dynamics that our model cannot predict: although we note the ability of the model to describe the material response before the source is turned off. On the other hand, these results uncover an opportunity to study chemical and microstructural dynamics. Assuming that the model presented here is correct, the rheologist can study the dynamics of the worm-like micelle lengthening and shortening upon the introduction of a concentration of cis-OMCA.

7.4.2 Temperature Sweep versus Irradiation

Comparing the evolution of dynamic moduli over time during irradiation (for a total duration of 100 s) and that of a temperature sweep, as in Fig. 7-18, we suggest that the process the micelles go through during irradiation could be similar to the process they go through when heated, i.e. the micelles shortening. The graphs are so similar in fact, we initially worried that our experiments might be examining how UV irradiation heats the sample rather studying a photochemical reaction. We used three procedures to ensure that that was not the case. First we used an IR thermometer to verify the Peltier plate and the quartz plate were at 25^{o}C. A thermal camera was then used to image the sample and the rheometer. We found that over a 10 minute time span the region of interest did not change more than half a degree. Finally, we performed similar tests on an 83 mM CTAB +50mM of NaSal (Sodium Salicylate) sample which forms a similar fluid to the CTAB+OMCA solution, though it is not photoresponsive. We performed irradiation and a temperature ramp during shear flow experiments. If the UV light was causing the fluid to heat up, we would have seen this fluid behave as if it were responsive to light. This was not the case as the rheological properties of the sample remained constant throughout the test. Therefore, the temperature

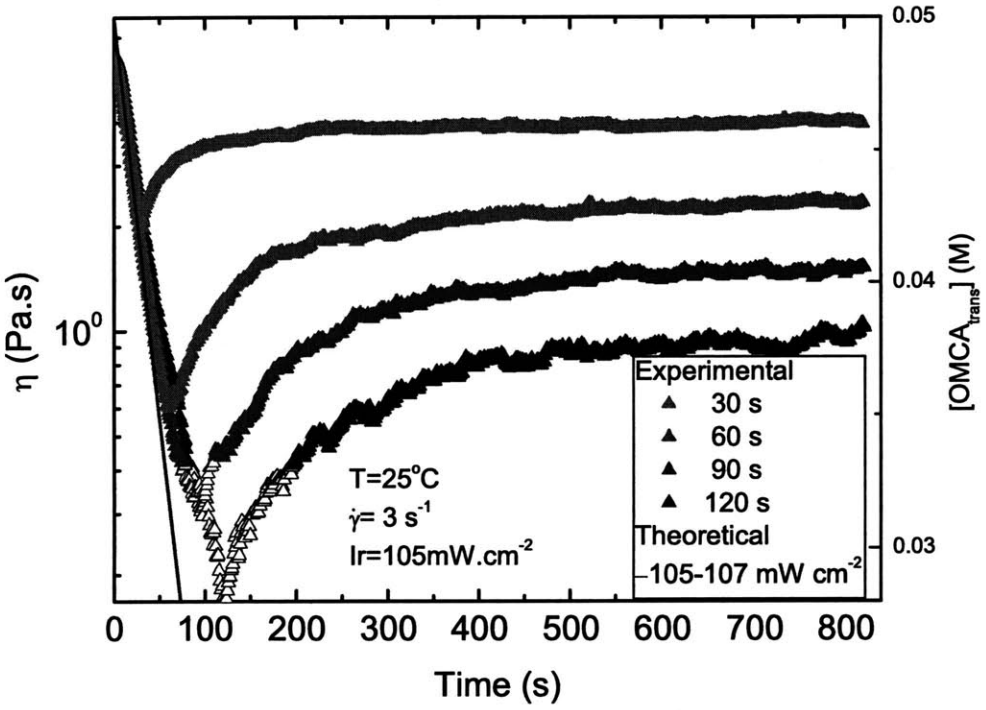

Figure 7-15: After doses of irradiation, the sample recovers. Open triangles indicate that the measurements were taken despite being below the stated torque resolution of the ARES rheometer. The initial evolution of the viscosity is compared with the theoretical prediction of the concentration.

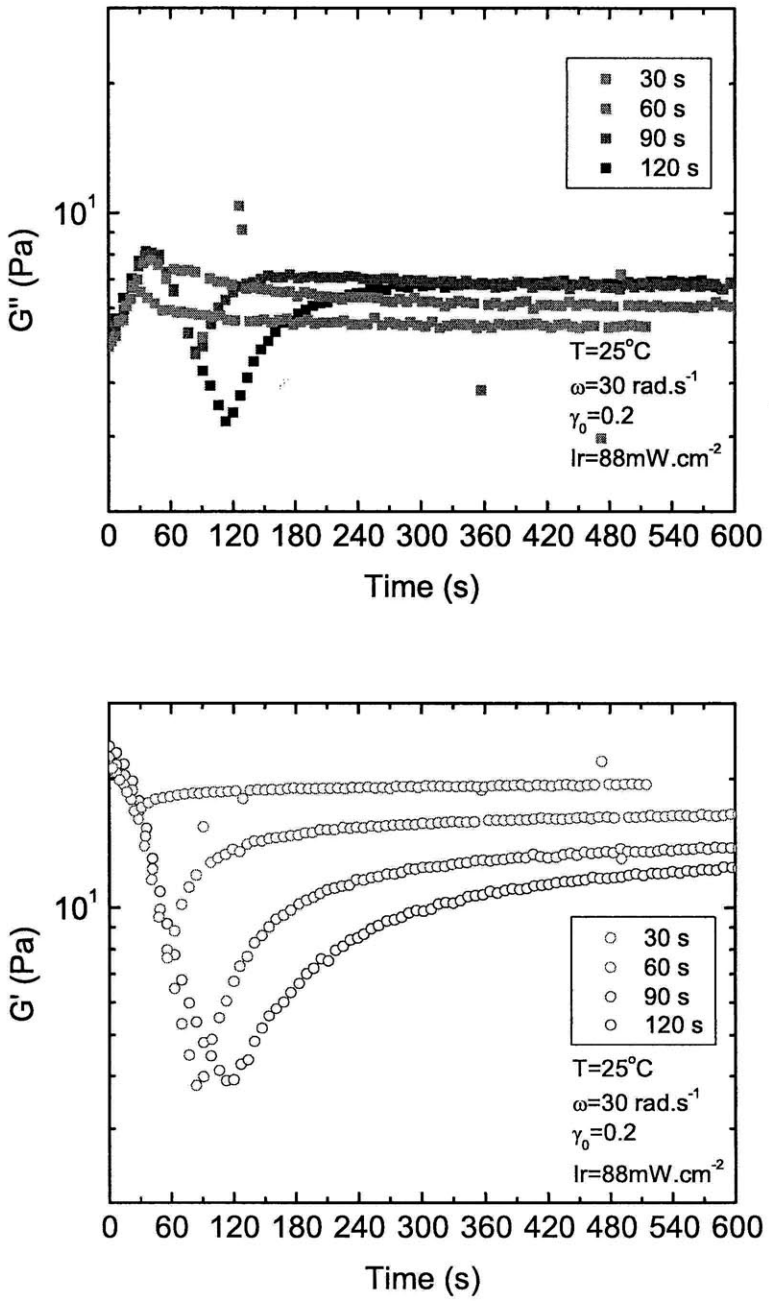

Figure 7-16: The moduli are examined after doses of irradiation are delivered. After the irradiation is stopped, the sample partially recovers.

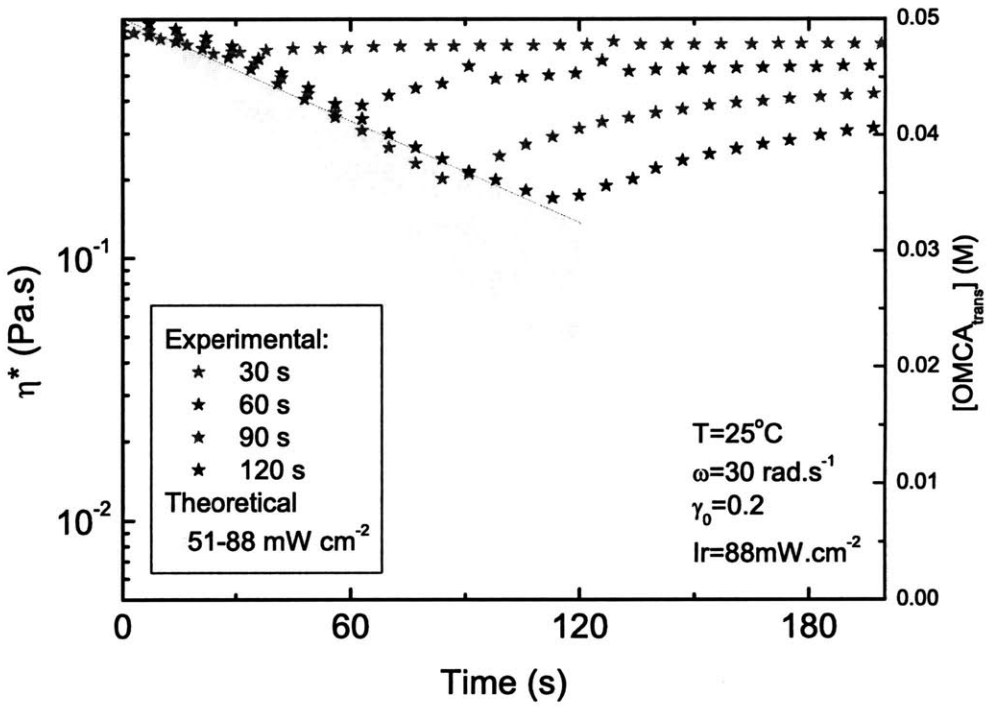

Figure 7-17: The measurement of complex viscosity from the dose experiments is compared to the theoretical prediction of concentration through the process described in section 7.3.1.

response and the exposure response did not superimpose, and we see this to be a feature of the photoresponsive micellar system only. This may also provide evidence that the dynamics seen in the UV dose experiments are related to the lengthening and shortening of the micelles on an experimentally relevant timescale.

7.5 Summary

We have validated our model with experimental results using a polychromatic light source. We have demonstrated how we can compactly and comprehensively describe our setup in a way that other groups can replicate our results even if they do not have the same light source. Now that we have an ability to predict the concentration of the photoactive component during a rheology experiment, we have explored possible avenues of research into microstructural dynamics of a sample given the knowledge of how the concentration of an internal species changes.

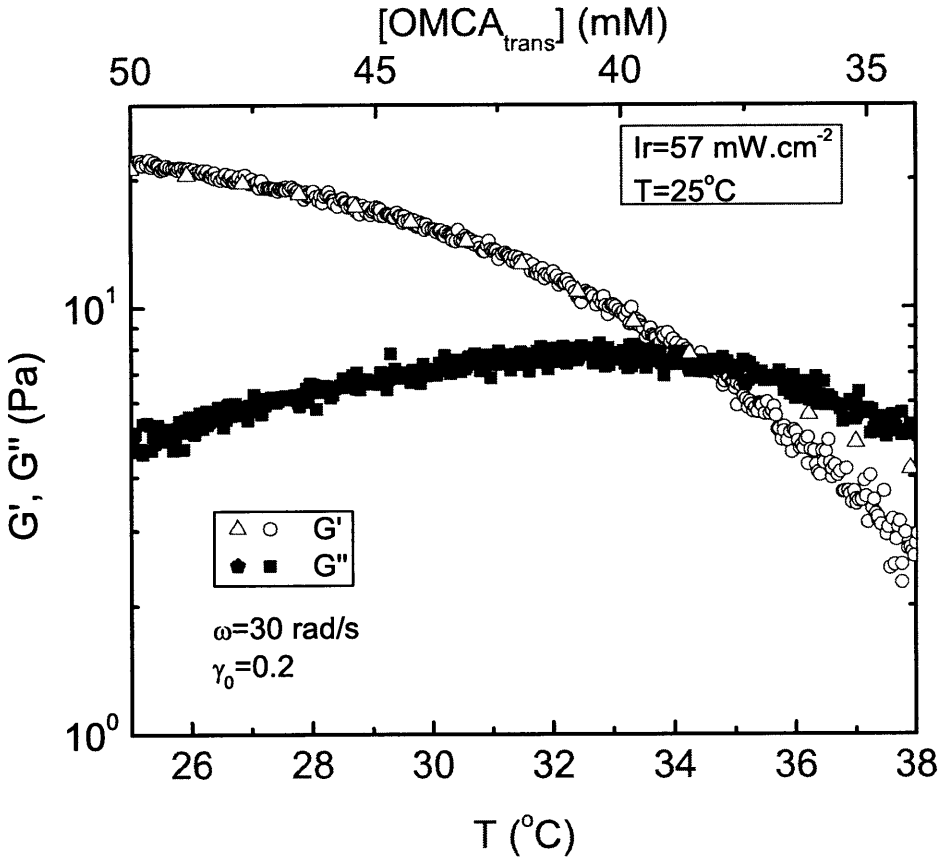

Figure 7-18: Comparison of dynamic moduli of a 50 OMCA + 83 CTAB sample undergoing a temperature ramp without irradiation (bottom axis) and under irradiation causing the concentration at constant temperature of trans-OMCA to decrease (top axis). The scaling of the two axis is 1.23 mM per °C. During the 100 second interval of irradiation the absorbed energy was calculated to be approximately 1 J.

Chapter 8

Robot Application

In this final chapter we discuss how these findings impact potential robotic applications. We also suggest desirable features of a photoresponsive fluid for material scientists and chemists who wish to develop fluids more appropriate for our application.

8.1 Feasibility of Current Photoresponsive Fluids for Autonomous Robots

While in previous chapters we focused on a lab scale UV lamp, we now evaluate light sources appropriate for robotics. Fig 8-1 shows the spectral power for a FOX UV LED. This UV LED has a total intensity of $50\mu W$ and a corresponding irradiance of approximately $29\frac{W}{m^2}$.

Table 8.1: Relevant time constants, t' and $\tilde{t}$, of $8\mu L$ of micellar fluid irradiated with LED compared to 160 μL of nanoparticle fluid irradiated with S2000.

	Micellar Fluid LED	Micellar Fluid S2000	Nanoparticle Fluid LED	Nanoparticle Fluid S2000
t'	$1.34 \times 10^{-4} t_{exp}$	$9.49 \times 10^{-3} t_{exp}$	$1.45 \times 10^{-4} t_{exp}$	$3.34 \times 10^{-3} t_{exp}$
$\tilde{t}$	$5.6 \times 10^{-4} t_{exp}$	$1.27 \times 10^{-1} t_{exp}$	$1.07 \times 10^{-5} t_{exp}$	$2.32 \times 10^{-3} t_{exp}$

Using our compact notation we can adequately describe the conditions of our

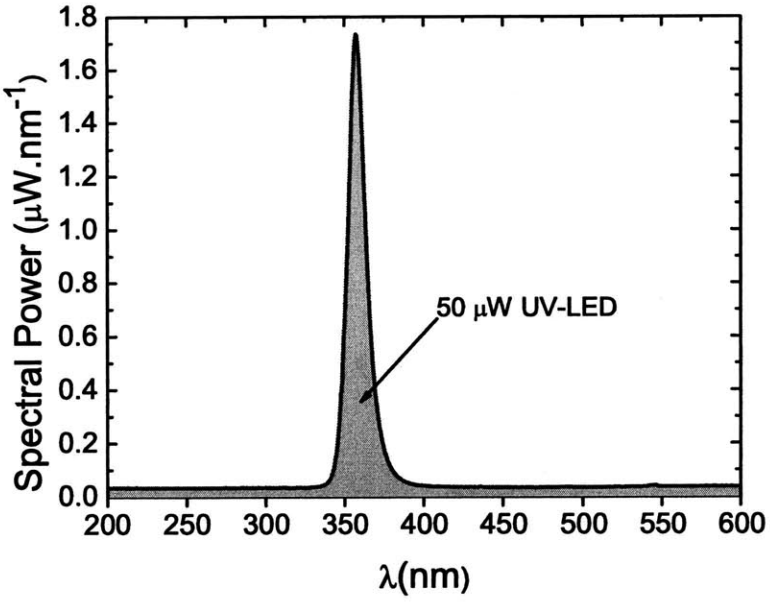

Figure 8-1: Spectral power of a UV-LED (FOX) measured by the Ocean Optics USB2000 Fiber Optic Spectrometer.

experiment in Table 8.1. We have duplicated Table 7.2 within this table with the average lamp irradiance $1.6\frac{kW}{m^2}$ used in the irradiation studies presented in chapter 7 to aid comparison. Note that we are comparing, different volumes of different concentrations of materials with different absorption spectra irradiated with different light sources with different relative spectral intensities and overall irradiances. Prior to this work, the author does not know of a similar technique to compare vastly different photoactive materials irradiated with a broad spectrum of light sources.

We present the calculated switching times of two of our candidate fluids achieved with the characterized UV LED in 8-2. The long switching times (hours) suggested by Fig 8-2, lead us to conclude that even with small volumes of fluid with an ideal $\Phi = 1$, photoreological fluids are not feasible with an autonomous robot equipped with LEDs.

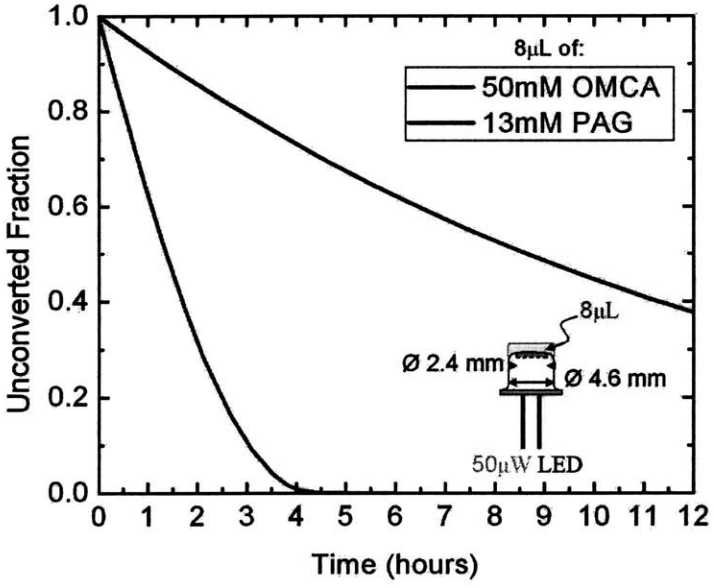

Figure 8-2: The evolution of the material composition during irradiation from an LED for two candidate fluids with a photoactive species concentration of 50 mM OMCA and 13 mM PAG respectively. Note that both fluids require hours of irradiation to convert half of the photoactive species.

8.2 Designing Future Photoresponsive Fluids for Fast Switching Times

While the photoresponsive fluids examined here are inappropriate for autonomous applications that require swift transitions between states, we explore in this section the attributes that would be desirable if we had the ability to design a photoresponsive fluid. We also present when and how tuning the experimental conditions will impact the speed of reaction for a given fluid.

There exist a large number of mechanisms that lead to the rheology and the change in rheology of a material, and an even larger number of mechanisms involved in any observable change such as physical, mechanical, optical changes. It is impossible to describe how best to tune the fluid for speed without knowing how the addition or reduction of a particular component interacts with the rest of the fluid. In particular, for the model introduced, there is a large difference if the property of interest is dependent on the absolute molar concentration of the photoactive species that are in a particular form (for instance the molar concentration of cis-isomer) or if it is dependent on the percentage of the photoactive species that are in a particular form (for instance the ratio of cis-isomer to trans-isomer). Which quantity is more relevant will depend on the nature of the dynamic balance between the photoactive species and other chemically significant components in the material.

Firstly, the ideal photorheological fluid would have a large physical change with the introduction of either a small amount (moles or molar) of the activated species or a small percent change in concentration of the activated photoresponsive species. For example the transition would be complete when 1% of the trans-isomer transitions to its cis-isomer form. Another example would be that the transition is complete when 1 mM of the cis-isomer is present. The application of this fluid would center around this transition by considering this concentration or percent concentration as an operating point.

How fast this transition occurs depends on the magnitude of the absorbance of the fluid. To begin, we assume that the transition depends on the absolute number of

moles or concentration of the photoactive fluid. There are two regimes of response of any photoresponsive fluid, a regime where the concentration decreases linearly and a regime where the concentration decreases exponentially (as originally noted in Table 7.1). Because the time constant of the exponential decay is very small, the same absolute increase in concentration will take longer in the exponential regime than in the linear regime. Ideally both the initial and final states of the fluid would place the operation of the fluid in the linear regime. To do this both states must have an average absorbance, i.e. product of the concentration, molar absorptivity, and thickness of the sample, above 5, as discussed in Section 5.2. Given a typical molar absorptivity of 640 $\frac{\text{L}}{\text{mol cm}}$ at 365 nm for trans-azobenzene and a sample thickness of 1 mm, both states should have a concentration of photoactive species greater than 80mM. The time constant within this linear regime, t', then is adversely affected by large volumes and positively affected by large surface areas. Keeping in mind the requirement of a large absorbance for this regime, increasing the ratio of the area to the volume, e.g. making the fluid film thinner, will speed the reaction.

Alternatively we could assume that the transition depends on the percent increase of the activated species. If the initial concentration in the fluid is small, a demanded increase in the percent concentration of the activated species translates to a very small absolute change in concentration. Therefore, even though the time constant of exponential decay is very small, the same percent increase in concentration will take a shorter amount of time in the exponential regime than in the linear regime as the absolute change in concentration is small enough to offset the slower response. Whether desired or mandated by a low molar absorptivity or low photoactive species concentration, the fluid may evolve in the slower exponential regime. The response of the fluid can be quickened predominantly by increasing $\tilde{t}$ within this regime. Seeking a large molar absorptivity is the only factor besides a well matched source with a large irradiance that is controllable that will speed the reaction. In this regime, the smaller the initial absorbance the less the thickness of the film impacts the speed of the reaction.

For the special case of a monochromatic light source and an interest in 95% conver-

sion of the photoactive species, we may use the monochromatic curve, Eq. (5.15), to derive two helpful representative decay times. For solutions with initial absorbances above 1.05, 95% of the photoactive solution is converted at

$$t'_{95} = 0.05\frac{S_0 l N_A}{Ir}\frac{hc}{\lambda}. \tag{8.1}$$

For solutions with initial absorbances below unity, 95% of the photoactive solution (with an error of at most 3% at absorbances close to unity) is converted at

$$\tilde{t}_{95} = 0.0223\frac{N_A}{Ir\epsilon_\lambda}\frac{hc}{\lambda}. \tag{8.2}$$

We can therefore summarize the discussion with Table 8.2 describing what parameters affect the speed of reaction for a fluid given the initial absorbance of the fluid.

Table 8.2: Parameters which tune how quickly the sample reaches 95% conversion

for: $S_0\epsilon_\lambda l < 1$ $\tilde{t}_{95} = 0.0223\frac{N_A}{Ir\epsilon_\lambda}\frac{hc}{\lambda}$	for: $S_0\epsilon_\lambda l > 1.0256$ $t'_{95} = 0.05\frac{S_0 l N_A}{Ir}\frac{hc}{\lambda}$
• doubling Ir halves $\tilde{t}_{95}$ • doubling ϵ_λ halves $\tilde{t}_{95}$	• doubling Ir halves t'_{95} • halving S_0 halves t'_{95} • halving l halves t'_{95}

The above description is most intuitive for the monochromatic light source, but should also provide guidance for a polychromatic source as well. Of course in either case we have assumed that the light source is well matched to the absorbance spectrum of the fluid. Ideally the emission spectrum of the lamp would overlap entirely with the absorbance spectrum of the fluid, including having its peak at a wavelength that is also a strongly absorbed wavelength. Given that most commercially available LEDs have wavelengths greater than 350 nm, the fluid should also be strongly absorbing above 350 nm. We have also assumed throughout that the area of the sample and that of the incident beam is the same, that thickness and opacity of the solution is such that the irradiance at the middle of the sample is the same as at the top of the

sample, as well as that the quantum efficiency of the fluid is maximized.

We have already discussed some of the criteria concerning the more complicated reversible photorheological fluids. The criteria on the molar absorptivity of the two species and the spectral irradiance of the source in order for the fluid to have a reversible transition between states is of first importance, followed by the ratio in Eq. (5.46) describing the photostationary concentration. The dynamics are complicated enough that a recommendation for tuning the dimensionless time related to a reversible fluid and a polychromatic source,$\mathring{t}$, is not made beyond stating its definition.

8.3 Summary of Governing Equations and Other Relevant Quantities

We recommend reporting the spectral irradiance of the light source and molar absorptivity, volume, area of the sample exposed to the beam, and concentration of the photoactive species as a standard minimum set of variables. With these quantities a broad range of relevant quantities can be calculated such as the energy the sample has absorbed and the number of molecules that transition as a result of this process (Table 8.3). We have put forward a model, presented in Chapters 2 through 5, that can be used to predict how a photoactive species evolves under the irradiation of a variety of sources with time. This is summarized in Table 8.4 for fluids where each molecule transitions after absorbing a photon. We then developed an exact solution for the concentration as a function of time for the monochromatic source and irreversible fluid case and approximations for this in regimes defined by the absorbance of the fluid , summarized in Table 8.5 for the fluids with only one photoactive component and in Table 8.3 for fluids with two absorbing species. These results are intended to aid in comparison of the responses of photoresponsive fluid and guide application specific design decisions.

Table 8.3: The energy absorbed and the number of molecules converted during an exposure period

$$\frac{E_A}{Area_i} = \int_{\lambda_{min}}^{\lambda_{max}} \int_0^{\tau} Ir_i(\lambda,t)(1-10^{-\epsilon(\lambda,t)[S](t)l})dt\ d\lambda$$
$$\frac{N_m}{Area_i} = \int_{\lambda_{min}}^{\lambda_{max}} \int_0^{\tau} Ir_i(\lambda,t)(1-10^{-\epsilon(\lambda,t)[S](t)l})\Phi(\lambda,t)\frac{\lambda}{hc}dt\ d\lambda$$

Table 8.4: Summary of governing equations for irreversible and reversible fluids for monochromatic and polychromatic sources (Φ=1)

Species	Light Source	Differential Equation
[S]	Monochromatic	$\frac{d[S]}{dt} = -\frac{Area_i}{N_A V} Ir_{i\lambda}(1-10^{-\epsilon_\lambda l[S]})\frac{\lambda}{hc}d\lambda$
[S]	Polychromatic	$\frac{d[S]}{dt} = -\frac{Area_i}{N_A V}\int_{\lambda_{min}}^{\lambda_{max}} Ir_i(\lambda)(1-10^{-\epsilon(\lambda)l[S](t)})\frac{\lambda}{hc}d\lambda$
[A], [B]	Monochromatic	$\frac{d[A]}{dt} = -\frac{Area_i}{N_A Vhc} Ir_\lambda\lambda(-10^{-\epsilon_{A\lambda}l[A]} + 10^{-\epsilon_{B\lambda}l[B]})$
[A], [B]	Polychromatic	$\frac{d[A]}{dt} = -\frac{Area_i}{N_A Vhc}\int_{\lambda_{min}}^{\lambda_{max}} Ir_\lambda\lambda(-10^{-\epsilon_A(\lambda)l[A]} + 10^{-\epsilon_B(\lambda)l[B]})d\lambda$

Table 8.5: Summary of solutions and dimensionless numbers for illumination of irreversible fluids (Φ=1)

Monochromatic	$[\hat{S}] = log_{10}\left((10^{[\hat{S}]_0} - 1)10^{-\hat{t}} + 1\right)$	$[\hat{S}] = \epsilon_\lambda [S] l$		$\hat{t} = t_{exp} \frac{Ir_{i\lambda}\epsilon_\lambda}{N_A} \frac{\lambda}{hc}$
Polychromatic:				
$\epsilon_\lambda [S] l \gg 1$	$S' = -t' + 1$	$S' = \frac{S}{S_0}$	$t' = t_{exp} \frac{Area_i}{VS_0} \frac{1}{N_A} \int_{\lambda_{min}}^{\lambda_{max}} Ir(\lambda) \frac{\lambda}{hc} d\lambda$	
$\epsilon_\lambda [S] l \ll 1$	$\tilde{S} = \frac{10^{-\tilde{t}}}{1 - \frac{\beta_2 S_0}{\beta_1}(1 - 10^{-\tilde{t}})}$	$\tilde{S} = \frac{S}{S_0}$	$\tilde{t} = t_{exp} \int_{\lambda_{min}}^{\lambda_{max}} \frac{Ir(\lambda)\epsilon(\lambda)}{N_A} \frac{\lambda}{hc} d\lambda$	
	$\frac{\beta_2 S_0}{\beta_1} = \frac{ln(10) l S_0}{2} \frac{\int_{\lambda_{min}}^{\lambda_{max}} Ir(\lambda)\lambda\epsilon(\lambda)^2 d\lambda}{\int_{\lambda_{min}}^{\lambda_{max}} Ir(\lambda)\lambda\epsilon(\lambda) d\lambda}$			

Table 8.6: Summary of approximate solutions and dimensionless numbers in the limit of small absorbances for illumination of reversible fluids (Φ=1)

Monochromatic:	$[\breve{A}] = (1 - \phi_\lambda)\, 10^{-\breve{t}} + \phi_\lambda$	$[\breve{A}] = \frac{[A]}{[A_0]}$	$\breve{t} = t_{exp} \frac{Ir_\lambda \xi_\lambda}{N_A} \frac{\lambda}{hc}$	$\phi_\lambda = \frac{\epsilon_{B\lambda}}{\xi_\lambda}$
	$\xi_\lambda = \epsilon_{A\lambda} + \epsilon_{B\lambda} - (\epsilon_{B\lambda})^2 ln(10) A_0 l$			
Polychromatic:	$[\mathring{A}] = (1 - \phi(\lambda))10^{-\mathring{t}} + \phi(\lambda)$	$[\mathring{A}] = \frac{A}{A_0}$	$\mathring{t} = t_{exp} \int_{\lambda_{min}}^{\lambda_{max}} \frac{Ir(\lambda)\xi(\lambda)}{N_A} \frac{\lambda}{hc} d\lambda$	$\phi(\lambda) = \frac{\int_{\lambda_{min}}^{\lambda_{max}} Ir(\lambda)\epsilon_B(\lambda)\lambda d\lambda}{\int_{\lambda_{min}}^{\lambda_{max}} Ir(\lambda)\xi(\lambda)\lambda d\lambda}$
	$\xi(\lambda) = \epsilon_A(\lambda) + \epsilon_B(\lambda) - (\epsilon_B(\lambda))^2 ln(10) A_0 l$			

8.4 Conclusion

The goal of this thesis was to determine if photorheological fluids are appropriate for our robotic application. Since the engineering tools necessary to answer this question were not apparent, we developed models and metrics to describe the chemical dynamics and quantify relevant parameters effecting the speed of the rheological transition. Our metric is applicable to lamp characterization, predicting rate equations, and comparing between very different photorheological fluids. We have shown that our metric describes published data for monochromatic sources, and experimental data obtained from polychromatic sources. We recommend that the metric is further examined for the broad cases of reversible fluids and fluids where two species have comparable molar absorptivities. On the robotics side, we determined that, given current technology and materials, photorheological fluids are not feasible for small scale autonomous robots where the stimulus input is based on a typical UV LED. In the meantime, we recommend the continued use of energy metrics such as the expression in Table 8.3 to find and optimize other active fluids. We note that given the increased interest in photorheological fluids for a variety of applications and the manufacturing trend towards increased intensity of LEDs and lower wavelength, new materials may become available making it necessary to revisit this design decision. We have also provided a description of what attributes a new fluid would need to be desirable for this application. To aid swift adoption of new materials and technology, we encourage researchers to report the spectral characterization of their source and responses using the methods put forward in this thesis. Finally, we recommend the continued support of innovative robotics programs that push scientists to look at their problems in new ways.

Bibliography

[1] 3M. 3M light cure adhesive LC-1222, October, 2008. http://multimedia.3m.com/mws/mediawebserver?66666UuZjcFSLX TtmxMXo8TcEVuQEcuZgVs6E666666- Accessed: January 1 2010.

[2] C. Alvarez-Lorenzo, S. Deshmukh, L. Bromberg, T. A. Hatton, I. Sandez-Macho, and A. Concheiro. Temperature- and light-responsive blends of pluronic f127 and poly(n,n-dimethylacrylamide-co-methacryloyloxyazobenzene). *Langmuir*, 23(23):11475–11481, 2007.

[3] N.R. Baumgartner and P.E. Blatz. Wavelength dependency of the rate of iodine catalyzed photoisomerization of retinol and retinal. *Photochemistry and Photobiology*, 54(5):805–810, 1991.

[4] R. B. Bird, Armstrong R. C., and Hassager O. *Dynamics of Polymeric Liquids*, volume Volume 1 Fluid Mechanics. John Wiley & Sons, New York, 1987.

[5] A. Botella, J. Dupuy, A. Roche, H. Sautereau, and V Verney. Photo-rheometry/NIR spectrometry: An in situ technique for monitoring conversion and viscoelastic properties during photopolymerization. *Macromolecular Rapid Communications*, 25(12):1155–1158, 2004. 10.1002/marc.200400087.

[6] R. Byrne, S. Stitzel, and D. Diamond. Photo-regenerable surface with potential for optical sensing. *Journal of Materials Chemistry*, 16:1332, 2006.

[7] B. Chan, N. J. Balmforth, and A. E. Hosoi. Building a better snail: Lubrication and adhesive locomotion. *Physics of Fluids*, 17(11):113101, 2005.

[8] B. Chan, S. Ji, C. Koveal, and A. E. Hosoi. Mechanical devices for snail-like locomotion. *Journal of Intelligent Material Systems and Structures*, 18(2):111–116, 2007.

[9] N. Cheng, A. Gopinath, L. Wang, K. Iagnemma, and A Hosoi. Multi-scale studies of wax-cellular solid composites for controllable stiffness robotic elements". In *Materials Research Society Fall Meeting*, Boston, MA, 2009.

[10] N. Cheng, G. Ishigami, S. Hawthorne, H. Chen, M. Hansen, M Telleria, R. Playter, and K. Iagnemma. Design and analysis of a soft mobile robot composed of multiple thermally activated joints driven by a single actuator. In *Pro-*

ceedings of the 2010 IEEE International Conference on Robotics and Automation, Anchorage AK, 2010.

[11] J. Chin, T. Nguyen, E. Byrd, and J. Martin. Validation of the reciprocity law for coating photodegradation. *Journal of Coatings Technology and Research*, 2(7):499–508, 2005. 10.1007/s11998-005-0009-7.

[12] W. Cook, S. Chausson, F. Chen, L. Pluart, C. Bowman, and T. Scott. Photopolymerization kinetics, photorheology and photoplasticity of thiol-ene-allylic sulfide networks. *Polymer International*, 57(3):469–478, 2008. 10.1002/pi.2357.

[13] LORD Corporation. Lord technical data, MRF-122EG magneto-rheological fluid, 2008. http://www.lordfulfillment.com/upload/DS7027 Accessed: January 1 2010.

[14] LORD Corporation. Lord technical data, MRF-140CG magneto-rheological fluid, 2008. http://www.lordfulfillment.com/upload/DS7012 Accessed: January 1 2010.

[15] D. Dasgupta, S. Manna, A. Garai, A. Dawn, C. Rochas, J. M. Guenet, and A. K. Nandi. Morphology, structure, rheology, and thermodynamics of piezoelectric poly(vinylidene fluoride)-ethylene carbonate thermoreversible gel. *Macromolecules*, 41(3):779–787, 2008.

[16] S. Deshmukh, L. Bromberg, K. Smith, and Hatton TA. Photoresponsive behavior of amphiphilic copolymers of azobenzene and n,n-dimethylacrylamide in aqueous solutions. *Langmuir*, 25(6):3450–3466, 2009.

[17] S. Deshmukh and G. H. McKinley. Rheological behaviour of magnetorheological suspensions under shear, creep,and large amplitude oscillatory shear (LAOS) flow. In The Korean Society of Rheology, editor, *Proceedings XIVth International Congress on Rheology*, Seoul, Korea, 2004.

[18] C. A. Dreiss. Wormlike micelles: where do we stand? recent developments, linear rheology and scattering techniques. *Soft Matter*, 3(8):956–970, 2007. 10.1039/b705775j.

[19] A. Einstein. Uber einen die erzeugung and verwandlung des lichtes betreffenden heuristischen gesichtspunkt. *Annalen der Physik*, 6:132–148, 1905. English translation: "On a heuristic point of view about the creation and conversion of light".

[20] M. J. Espin, A. V. Delgado, and L. Rejon. Electrorheologial properties of hematite/silicone oil suspensions under DC fields. *Journal of Non-Newtonian Fluid Mechanics*, 125(1):1–10, 2005.

[21] R. H. Ewoldt, C. Clasen, A. E. Hosoi, and G. H. McKinley. Rheological fingerprinting of gastropod pedal mucus and synthetic complex fluids for biomimicking adhesive locomotion. *Soft Matter*, 3(5):634–643, 2007. 10.1039/b615546d.

[22] R. H. Ewoldt, G. H. McKinley, and A. E . Hosoi. Controllable adhesion using field responsive fluids. In *Bulletin of the American Physical Society*, volume 53(15), 2008.

[23] Greenmillennium. Titanium dioxide, January 1 2010. www.greenmillennium.com/tio2intro.htm.

[24] L. A. Haines, K. Rajagopal, B. Ozbas, D. A. Salick, D. J. Pochan, and J. P. Schneider. Light-activated hydrogel formation via the triggered folding and self-assembly of a designed peptide. *J. Am. Chem. Soc.*, 127(48):17025–17029, 2005.

[25] J Halm. Determination of fundamental photographic magnitudes. *Monthly Notices of the Royal Astronomical Society*, 75:150–177, 1915.

[26] J. Jadzyn and G. Czezhowski. The shear viscosity minimum of freely flowing nematic liquid crystals. *Journal of Physics: Condensed matter*, 13(12):l261–L265, 2001.

[27] L.A. Jones, V.C. Hall, and R.M. Briggs. On the relation between time and intensity in photographic exposure. *Journal of the Optical Society of America*, 12(4):321–348, 1926.

[28] G. Kampf, K Sommer, and E. Zirgiebl. Studies in accelerated weathering: Part 1. determination of the activation spectrum of photodegradation in polymers. *Progress in Organic Coatings*, 69, 1991.

[29] N. Katsonis, T. Kudernac, M. Walko, S. J. van der Molen, B. J van Wees, and B. L Feringa. Reversible conductance switching of single diarylethenes on a gold surface. *Advanced Materials*, 18(11):1397–1400, 2006. 10.1002/adma.200600210.

[30] A. M. Ketner, R. Kumar, T. S. Davies, P. W. Elder, and S. R. Raghavan. A simple class of photorheological fluids: Surfactant solutions with viscosity tunable by light. *J. Am. Chem. Soc.*, 129(6):1553–1559, 2007.

[31] S. A. Khan, I. M. Plitz, and R. A. Frantz. In situ technique for monitoring the gelation of UV curable polymers. *Rheologica Acta*, 31(2):151–160, 1992. 10.1007/BF00373237.

[32] EXFO Life Sciences & Industrial Division. Omnicure S2000 product literature, 2010. http://www.exfo-omnicure.com/products-s2000.php, Accessed: January 1 2010.

[33] EXFO Life Sciences & Industrial Division. Peak irradiance fall-off and near field beam profiles, 2010. http://www.uvabcs.com/lightguides-nearfield.php Accessed: January 1 2010.

[34] J. W. Martin. Quantitative characterization of spectral ultraviolet radiation-induced photodegradation in coating systmes exposed in the laboratory and the field. *Progress in Organic Coatings*, 23:49–70, 1993.

[35] J. W. Martin, T. Nguyen, E. Byrd, B. Dickens, and N. Embree. Relating laboratory and outdoor exposures of acrylic melamine coatings - i. cumulative damage model and laboratory exposure apparatus. *Polymer Degradation and Stability*, 75:193–210, 2002. [1] doi:10.1016/S0141-3910(01)00218-X.

[36] J.W. Martin, J.W Chin, and T Nguyen. Reciprocity law experiments in polymeric photodegradation: a critical review. *Progress in Organic Coatings*, 47:282, 2003.

[37] S. Matsumoto, S. Yamaguchi, S. Ueno, H. Komatsu, Ikeda M., K. Ishizuka, Y. Iko, Tabata K., S. Aoki, H.and Ito, and I. Noji, H.and Hamachi. Photo gel-sol/sol-gel transition and its patterning of a supramolecular hydrogel as stimuli-responsive biomaterials. *Chemistry - A European Journal*, 14(13):3977–3986, 2008. 10.1002/chem.200701904.

[38] I. Mita, K. Horie, and K. Hirao. Photochemistry in polymer solids. 9. photoisomerization of azobenzene in a polycarbonate film. *Macromolecules*, 22:558–563, 1989.

[39] J. Naciri, A. Srinivasan, H. Jeon, N. Nikolov, P. Keller, and B. R. Ratna. Nematic elastomer fiber actuator. *Macromolecules*, 36(22):8499–8505, 2003.

[40] A.Y. Nazzal, L. Qu, X. Peng, and M Xiao. Photoactivated CdSe nanocrystals as nanosensors for gases. *Nano Letters*, 3(6):819–822, 2003.

[41] University of Oregon Department of Physics. Absorption and emission spectra for elements - java physics book, January 1, 2010. http://jersey.uoregon.edu/vlab/elements/Elements.html.

[42] Defense Sciences Office. Defense sciences research and technology special focus area: Chemical robots. solicitation number baa07-21, July 2 2008. http://www.darpa.mil/dso/solicitations/baa07-21mod2.html Accessed: January 1st 2010.

[43] M. Parthasarathy and D.J. Klingenberg. Electrorheology: Mechanisms and models. *Materials Science and Engineering: R: Reports*, 17(2):57–103, 1996.

[44] Ewoldt R. Thermo-rheological materials: activation timescale and energy requirements, September 29 2008.

[45] PJ Rankin, JM Ginder, and DJ Klingenberg. Electro and magneto rheology. *Current Opinion in Colloid and Interface Science*, 3(4):373–381, 1998.

[46] H. Sakai, Y. Orihara, H. Kodashima, A. Matsumura, T. Ohkubo, K. Tsuchiya, and M. Abe. Photoinduced reversible change of fluid viscosity. *J. Am. Chem. Soc.*, 127(39):13454–13455, 2005.

[47] RM Sayre, RL Olson, and MA Everett. Quantitative studies on erythema. *Journal of Investigative Dermatology*, 46, 1966.

[48] S. Scarmagnani, Z. Walsh, N. Alhashimy, A Radu, B. Paull, M. Macka, and D. Diamond. Beads-based system for optical sensing using spiropyran photoswitches. In *Proceedings of the 29th Annual International Conference of the IEEE EMBS*, 2007.

[49] L. Schmidt, Y. Leterrier, JM Vesin, M Wilhelm, and JE Mnson. Photorheology of fast UV-curing multifunctional acrylates. *Macromolecular Materials and Engineering*, 290(11):1115–1124, 2005. 10.1002/mame.200500229.

[50] P. A. M. Steeman, A. A. Dias, D. Wienke, and T. Zwartkruis. Polymerization and network formation of UV-curable systems monitored by hyphenated real-time dynamic mechanical analysis and near-infrared spectroscopy. *Macromolecules*, 37(18):7001–7007, 2004.

[51] K. Sun, R Kumar, D Falvey, and S Raghavan. Photogelling colloidal disperisons based on light-activated assembly of nanoparticles. *Journal of American Chemical Society*, 131(20):7135–7141, 2009.

[52] M. Takeuchi, K. Sakamoto, G. Martra, S. Coluccia, and M. Anpo. Mechanism of photoinduced superhydrophilicity on the TiO_2 photocatalyst surface. *J. Phys. Chem. B*, 109(32):15422–15428, 2005.

[53] V. Talrose, E.B. Stern, A.A Goncharova, N.A. Messineva, N.V. Trusora, and M.V. Efimkiva. "UV/visible spectra" in NIST chemistry webbook. In *NIST Standard Reference Database Number 69*. NIST, January 1 2010.

[54] I. Tomatsu, A. Hashidzume, and A. Harada. Photoresponsive hydrogel system using molecular recognition of α-cyclodextrin. *Macromolecules*, 38(12):5223–5227, 2005.

[55] N. J. Turro, V Ramamurthy, and J. C. Sciano. *Principles of molecular photochemistry: an introduction.* University Science Books, 2008.

[56] V. Verney and S. Commereuc. Molecular evolution of polymers through photoageing: A new UV in situ viscoelastic technique. *Macromolecular Rapid Communications*, 26(11):868–873, 2005. 10.1002/marc.200500073.

[57] E. Verplogen. *Morphology and self-assembly behavior of side chain liquid crystalline block copolymers.* PhD thesis, MA, 2008.

[58] R.J. Wallace and H.B Lemon. Studies in sensitometry. iii on the evaluation of the reciprocity law, basic fog and preliminary exposure. *Astrophysical Journal*, 29:146, 1908.

[59] C.E. Wayne and Wayne R.P. *Photochemistry.* Oxford chemistry primers; 39. Oxford University Press, 1996.

[60] W. Wen, Xi. Huang, S. Yang, K. Lu, and P. Sheng. The giant electrorheological effect in suspensions of nanoparticles. *Nat Mater*, 2(11):727–730, 2003. 1476-1122 10.1038/nmat993 10.1038/nmat993.

[61] B. Yan, J. Tao, C. Pang, Z. Zheng, Z. Shen, C. H. A. Huan, and T. Yu. Reversible UV-light-induced ultrahydrophobic-to-ultrahydrophilic transition in an α-Fe_2O_3 nanoflakes film. *Langmuir*, 24(19):10569–10571, 2008.

[62] G. Zimmerman, LY Chow, and UJ Paik. The photochemical isomerization of azobenzene. *Journal of the American Chemical Society*, 80(14):3528–3531, 1958. doi: 10.1021/ja01547a010 0002-7863 doi: 10.1021/ja01547a010.